Natural gas to methanol process flowsheet improvement via integration of ITM oxygen technology

Phumzile Fankomo (2404321)

Master of Science in Chemical Engineering by Research

A dissertation submitted to the Faculty of Engineering and the Built Environment, University of the Witwatersrand, Johannesburg, in fulfilment of the requirements for the degree Master of Science in Chemical Engineering.

Supervised by

Dr. Isabella L. Greeff and Dr. Saeideh Babaee

18 February 2023

As the candidate's supervisor, I agree to the submission of this dissertation:

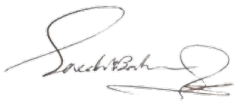

_____ 21 Feb 2023

Dr. Saeideh Babaee **Date**

Declaration of Dissertation Authorship

I, Phumzile Precious Fankomo, student number: 2404321, hereby declare the following:

I am aware that plagiarism (the use of someone else's work without their permission and/or without acknowledging the original source) is wrong.

I confirm that the research work submitted is my own, except where I have indicated otherwise, in which case, I have followed the required conventions in referencing the work and findings of others.

I understand that the University of the Witwatersrand may take disciplinary action against me if I did not satisfactorily adhere to the above declarations.

Signed at Johannesburg on this 18th day of February 2023

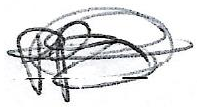

_____

Phumzile Fankomo (student)

Student No.: 2404321

Acknowledgements

I acknowledge and convey my personal thanks to the following persons and institutions for their support and contributions to this work.

- Dr. Isabella Greeff for her leadership and guidance throughout all the stages of this project,
- My aunt Yvonne Mahlake for her love and support,
- My mother Sarah Mahlake for having taught me the skill of perseverance and consistency,
- Adonis Siwela for motivational support,
- Christopher Buchanan for technical discussions and report review,
- The University of the Witwatersrand for the honour and opportunity to perform this research in the institution and to obtain my MSc Chemical Engineering qualification.

Abstract

Current industrial gas-to-liquids (GTL) processes suffer high energy penalties and associated carbon emissions caused by inefficient energy utilization and recovery. With the increasing demand for methanol and stricter regulations requiring reduced carbon intensity, there is a need to improve efficiencies of the existing process. This study analysed the existing large-scale natural gas to methanol flow sheet and investigated development of a new and improved flow sheet. In a conventional natural gas to methanol process, the air compressors in the cryogenic air separation unit (ASU) as well as the syngas compressor in the methanol synthesis unit are the most energy intensive and contribute significantly to the energy cost of large-scale syngas manufacture. The conventional autothermal reformer (ATR) process contributes the largest exergy losses as a result of the large temperature driving force used in the syngas cooler.

The novel ion transport membrane (ITM) oxygen technology has the potential to replace the cryogenic air separation and reduce the large power demands associated with oxygen production. Its high temperature operation makes it suitable for process integration with syngas production. Integration of this ITM oxygen technology into a natural gas to methanol flow sheet was investigated. The pinch analysis method was used to evaluate flow sheet minimum energy requirements and identify opportunities for process heat integration to reduce utility requirements. Exergy analysis was conducted to identify areas of large exergy destruction and opportunities for improvement and, to quantify and compare exergy losses of the flow sheet cases. Power cycles were integrated to efficiently recover and convert process heat to power. Performance of the power cycles was measured by the cycles' thermal efficiencies. The overall plant and process efficiency as well as the specific

gas efficiency were evaluated to assess and compare energy efficiency of the process flow sheet cases.

Replacing the cryogenic ASU with ITM and integrating ITM oxygen into the ATR process is a more efficient method to recover the high temperature syngas heat with reduced exergy losses. The ITM oxygen unit integrated with power cycles resulted in 47% more power production compared to the conventional case A. The exergy analysis results showed a decrease in overall exergy losses by 26% in this new flow sheet. The ITM oxygen power cycle was found to produce enough power to drive its own compressors and with excess power of 28 MW, whereas the cryogenic ASU in the conventional case has a power demand of 33 MW. This work shows that lower cost production of oxygen may be the feasible solution to reduce the high costs of large-scale syngas manufacture. The ITM oxygen presents such opportunities by substituting the energy intensive cryogenic ASU and combining oxygen, syngas and power production into a single thermally integrated unit.

The methanol loop was found to have sufficient process heat for combined heat and power production. The Rankine medium pressure (MP) steam cycle produced enough power to drive the syngas compressor. Configuring the methanol process into a power production cycle results in an increase in the flow sheet excess power production by 68% compared to the conventional case. However, reduced methanol production rate caused by lower flash pressures as well as reduced process heat for feed preheat are the main challenges to consider. The specific gas efficiency improved by 6% while carbon dioxide emissions decreased by 40%.

The overall thermal efficiencies of the cases were not optimized as this was not part of the study objectives. A further study can be conducted to investigate improving the thermal efficiencies of the power cycles in each case by performing a sensitivity analysis to impact parameters such as turbine and compressor inlet temperature and

pressure ratio. The specific parameters to assess can be determined from the air-standard model equation for a Brayton power cycle. The thermal efficiency improvement can result in higher power production and reduced equipment duties which is a benefit to both capital and operating costs.

Table of Contents

List of Figures

List of Tables

List of Symbols

Symbol	Description	Units
Q_H	Heat transfer at low temperature	MW
η	Thermal efficiency	%
Q_C	Heat transfer at low temperature	MW
W_{NET}	Net work done	MW
P	Pressure	kPa
k	Specific heat ratio	-
R	Universal gas constant	8.314 J/mol.K
n	Number of moles	mol
e_f	Specific exergy	kJ/kg
h	Specific enthalpy	kJ/kg
h_0	Specific enthalpy at reference state	kJ/kg
T_0	Temperature at reference state	K
s	Entropy	kJ/kg.K
s_0	Entropy at reference state	kJ/kg.K
V	Velocity	m/s
g	Acceleration due to gravity	9.81 m/s^2
z	Elevation	m
e^{ch}	Exergy flowrate for a chemical reaction	J/kg
E_d	Exergy destruction	MW
E_q	Exergy transfer accompanying heat transfer	MW
E_w	Exergy transfer accompanying work	MW
ΔT_{min}	Minimum heat transfer temperature approach	°C

List of acronyms and abbreviations

Acronym or Abbreviation	Description
ASU	Air separation unit
ITM	Ion transport membrane
ATR	Autothermal reformer
GTL	Gas-to-liquids
SMR	Steam-methane reformer
POX	Partial oxidation
HER	Heat exchange reformer
H_2/CO	Hydrogen to CO ratio
DME	Dimethyl ether
WHB	Waste heat boiler
ETL	Emissions-to-liquids
MSW	Municipal solid waste
HRSG	Heat recovery steam generator
IGCC	Integrated gasification combined cycle
SOx	Sulphur oxides
NOx	Nitrogen oxides
LHV	Lower heating value
HP	High pressure
LP	Low pressure
BFW	Boiler feed water
HE	Heat exchanger
CWS	Cooling water supply
CWR	Cooling water return
CAPEX	Capital cost

OPEX	Operating cost
LTFT	Low temperature Fischer-Tropsch
CHP	Combined heat and power
t	Metric tonne

Chapter 1

Introduction

1.1 Background

Methanol (CH_3OH) is a clear, volatile and water-miscible liquid alcohol used industrially as a solvent, pesticide and alternative fuel. It is the simplest of the alcohol organic compounds, with a relatively low boiling point of 65 °C at 1 atm. Fuel, polymers and pharmaceutical markets are amongst the largest consumers of methanol. Methanol is an emerging renewable energy resource used in the marine, automotive and electricity sectors and can be produced from renewable feedstocks. Its high octane number makes it a promising substitute for petrol and diesel. Its high energy density and chemical stability makes it well suited for energy storage which can be easily converted to electricity through the direct methanol fuel cell (Balopi et al., 2019; Chou et al., 2013; Dalena et al., 2018). In terms of energy transportation and distribution costs, methanol is a more competitive solution when compared to other energy sources such as synthetic natural gas, hydrogen and ammonia (Babarit et al., 2019).

Methanol is a clean-burning and sustainable fuel which produces less emissions than gasoline. It is used as a lower carbon footprint fuel with lower SOx, NOx, particulate matter and CO_2 than traditional fossil fuel (Day, 2016). It can be produced from different feedstocks such as natural gas, coal, waste and captured CO_2.

Production of methanol is well established worldwide with an overall installed capacity of ~88 million t/year as of 2021 (Methanex Corporation, 2022). A compound annual growth rate of around 5.5% in the global methanol market was observed in the period 2017 – 2021 (EMR, 2022). Projections indicate that the global methanol market may exceed 100 million t/year by 2030 with a forecasted growth rate of nearly 3%. This can be seen in Figure 1 (Methanex Corporation, 2022). The demand is accelerated by clean energy policies, high oil prices and global economic

growth. The largest single methanol plant is in Turkmenistan, Asia, with an installed capacity of 5225 t/day (Brelsford, 2020). Even larger plants of up to 10000 t/day are being considered, taking advantage of the economy of scale (Aasberg-Petersen et al., 2008).

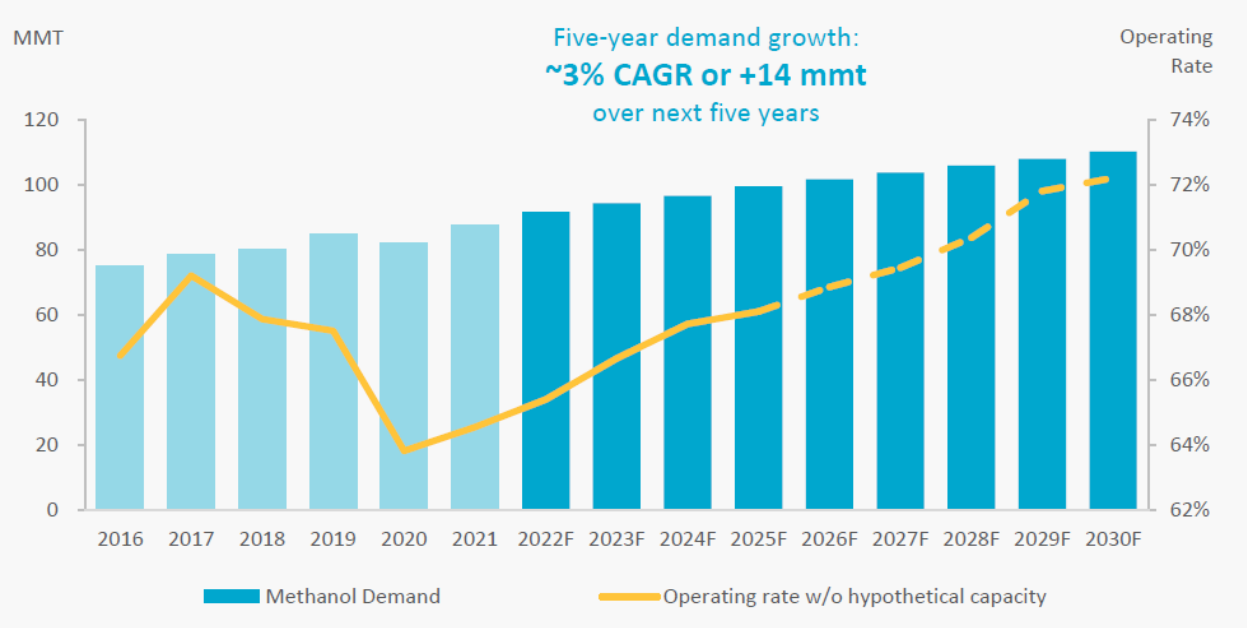

Figure 1 Global methanol demand and forecast (Methanex Corporation, 2022).

The world's largest producer and supplier of methanol is Methanex Corporation (EMR, 2022) with an overall capacity of 9.3 million t/year. Expansion projects are currently being executed by Methanex Corporation with a single methanol production site said to reach a capacity of 4 million t/year. This site is located in Geismar, Louisiana in the USA. Methanex Corporation supplies over 50% of methanol to the global market for traditional chemical applications. Table 1 presents a high-level list of methanol applications and the end products. Nearly 27% is used in the energy market as fuel, that is, dimethyl ether (DME) and direct methanol fuel cell and, nearly 18% is used in the methanol-to-olefins market. The global distribution of methanol usage per market share is presented in Figure 2. Methanol

is currently being used as a lower cost alternative for vehicle fuel in China (EMR, 2022) and by marine vehicles, for example, the Waterfront Shipping Co which runs nearly 50% of its fleet on methanol (Methanex Corporation, 2022).

Table 1 Application of methanol (Methanex Corporation, 2022; Methanol Institute, 2021).

Application of methanol	**Examples**
Chemical derivatives: Methanal, silicone, methyl methacrylate, acetic acid, olefins	Fleece, adhesives, inks, dyes, paints, Liquid crystal display screens, sealants, lubricants, pharmaceutical ingredients (cholesterol, streptomycin, vitamins and hormones), plywood, insulation, plastics, pesticides, antifreeze in windshield washer fluid
Fuel and fuel additives: Petrol and petrol blends, diesel and diesel additive (methyl tertiary butyl ether, tertiary amyl methyl ether and dimethyl ether).	Vehicles, marine vessels, cooking, heating, methanol fuel cell

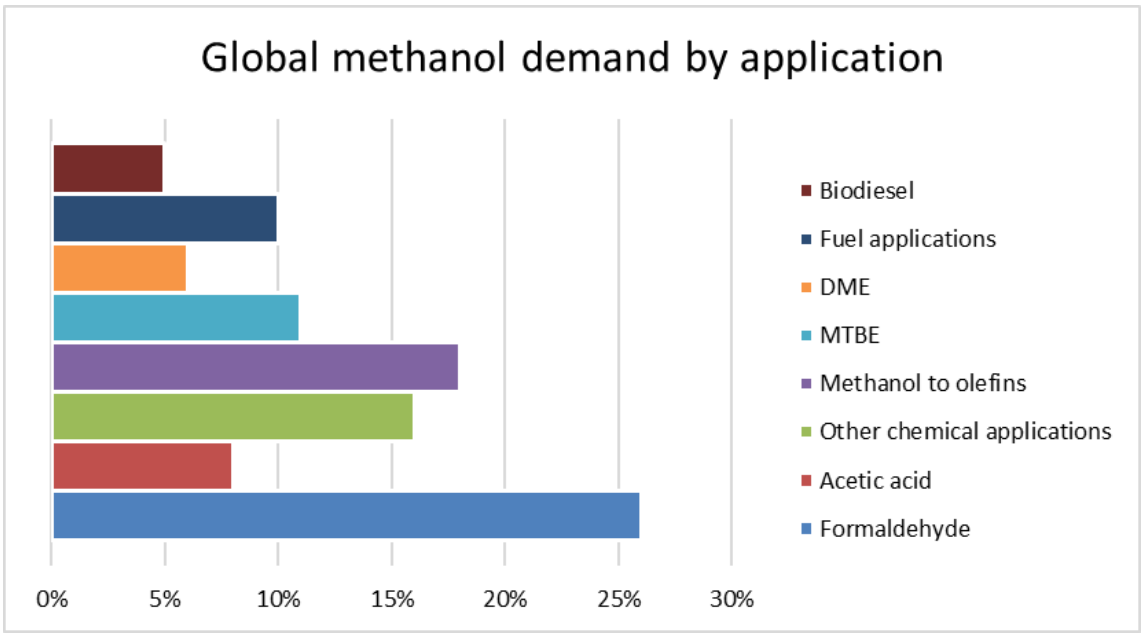

Figure 2 Global methanol demand by application (Methanex Corporation, 2022).

1.2 Problem statement

Methanol is produced mainly from H_2 and CO collectively known as synthesis gas or syngas. Natural gas (containing mainly methane) is the largest consumed feedstock to produce syngas in the methanol industry (Mitsubishi Gas Chemical, 2022) and it is expected that future methanol production expansions will be based on natural gas as a feedstock (Aasberg-Petersen et al., 2008). The choice of technology to use for syngas generation depends on the composition and production capacity requirements of the syngas. The autothermal reformer (ATR) which is an internally fired reactor is a simpler, compact technology with an economy of scale benefit compared to the widely used steam-methane reformer (SMR). This makes the ATR suitable for large-scale application. The required H_2/CO ratio for methanol synthesis can be provided by a single ATR reactor, whereas other technologies are typically paired up in series or parallel to achieve the H_2/CO ratio.

The ATR however requires high purity oxygen. Cryogenic air separation is conventionally applied in industry for the oxygen production. This is because it is a well-developed and reliable technology which can produce high purity oxygen in large volumes. The cryogenic air separation unit (ASU) is energy intensive with large power demands, mainly for the compressors (Den Exter et al., 2009). A portion of the natural gas feedstock is typically used as fuel in a power plant to produce power for oxygen production as shown in Figure 3. This negatively impacts the overall process efficiency and operating costs. Syngas production with ASU-derived oxygen accounts for over 60% of the investment in large-scale methanol production (Aasberg-Petersen et al., 2008). The selection of the syngas and oxygen production technologies, as well as the design of these processes is important. Since the cryogenic ASU is a mature technology, there is little prospect of further drastic improvement and cost reductions (Portillo et al., 2019). Alternative technologies need to be considered. The novel Ion Transport Membrane (ITM) is an alternative technology for oxygen production which promises to compete with the cryogenic ASU. This is because of its high temperature operation which makes it suitable for heat integration with high temperature processes which require oxygen and power (Greeff, 2015). Significant energy can be recovered from the ITM oxygen system in a combined power cycle and by heat integration with process streams. This enables the ITM oxygen technology to show greater advantages in making up for its energy consumption compared to cryogenic ASU (Bai et al., 2021). The feasibility of replacing the cryogenic ASU with the ITM oxygen in natural gas to methanol plants should be explored.

The equilibrium-driven and endothermic steam-methane reforming reactions occur at temperatures in the range of 950 to 1400 °C (Blumberg et al., 2017). Heat input is required to drive the reactions forward. Hot syngas product from the ATR is

conventionally cooled by generating steam in a waste heat boiler (WHB), using a large temperature driving force between the syngas and water. This has been found to contribute 20% to the overall plant exergy losses in a GTL plant based on ATR, cryogenic ASU and FT synthesis. The ATR unit and cryogenic ASU together account for 69% of the plant's total exergy losses (Iandoli et al., 2007). An alternative method to improve the high temperature heat recovery is therefore required.

Methanol synthesis reactions are also restricted by equilibrium, and they are favoured by lower temperatures and higher pressures. Power is therefore required to increase the syngas pressure in a compressor. External power demands to drive this compressor can be supplemented by integrating the process with a turbine expander (Greeff et al., 2002). Efficient and economical recovery of process heat is a challenge in the design of the methanol synthesis unit. This is because the reaction heat needs to be removed at high temperature to maximize the amount of work that can be developed while the synthesis reactions are to be equilibrated at lower temperature to maximize conversion (Aasberg-Petersen et al., 2008).

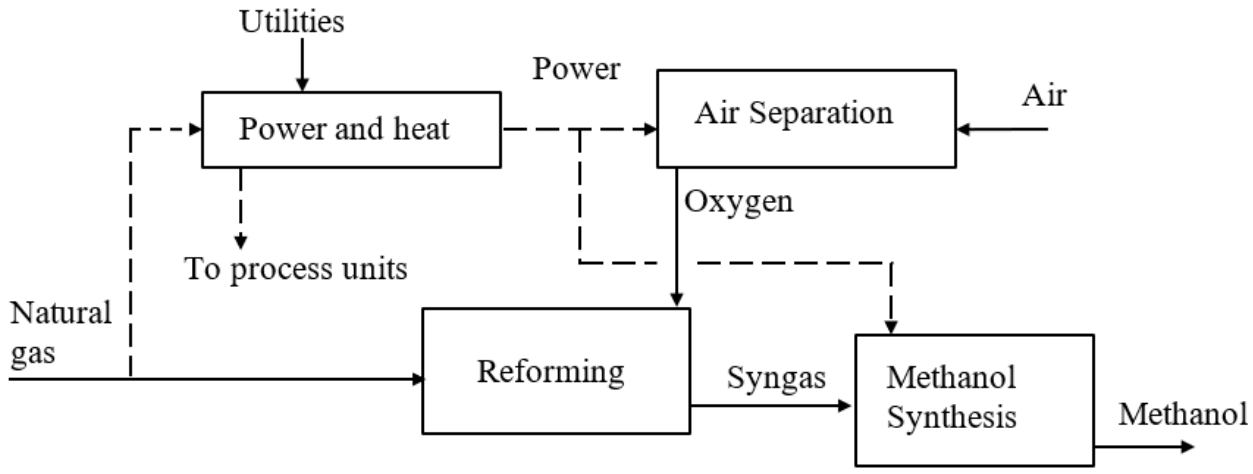

Figure 3 Block flow diagram of a typical natural gas to methanol process.

1.3 Motivation

This work is motivated by the growing drive for solutions to improve energy efficiency in industrial methanol production. Efficiency improvement results in reduction of production costs and carbon emissions. Methanol has, over the conventional fossil fuel, the advantage of being a biodegradable and clean-burning fuel with little to no soot, SOx and NOx compounds and particulate matter. This invites the need to better methanol production processes and advance sustainable methanol production solutions. There is currently no documented record in literature of the assessment of a large-scale natural gas to methanol flow sheet performance by considering the novel ITM oxygen technology and integration of power cycles, to improve the overall energy efficiency. This gap in literature presents an opportunity for this work to perform the assessment and report the results, as even a small efficiency increase is significant in a large-scale process.

1.4 Aim and objectives

The aim of this study is to develop a new and improved chemical process flow sheet for large-scale methanol production from natural gas. The objectives of the research are the following:

- The ITM oxygen technology will be used to replace the conventional cryogenic ASU for oxygen production.
- The pinch analysis method will be applied to assess minimum energy requirements (MER) and integrate energy systems. Practical challenges to achieve the MER in industry will be reviewed.

- Exergy analysis of the overall process as well as the heat engines will be evaluated in each case for comparison and to identify areas of large exergy destruction and opportunities for improvement.
- Power cycles will be integrated to convert process heat to work to reduce net power requirements and increase overall efficiency.

1.5 Scope and outline

This study screened natural gas to methanol technology from literature data to obtain latest developments that contribute to the flow sheet improvement. The study focused on large-scale methanol production and technology to support the growing demand and need for larger single installed plant capacities. Technologies investigated were natural gas reforming for syngas production, air separation for oxygen production and methanol synthesis. The process was modeled on Aspen Plus V10. Three opportunities for efficiency improvement were investigated, namely replacing the cryogenic ASU with the ITM oxygen technology, integrating the ITM oxygen with syngas heat recovery and integration of a turbine expander with methanol synthesis. Flow sheet boundaries were set at the battery limits for natural gas intake and raw methanol liquid product export. Upstream natural gas sourcing, preparation and transportation as well as downstream methanol product distillation and upgrading were not considered. A detailed simulation of the conventional cryogenic ASU was not included as specific power consumption per production capacity data was available to use in the analysis.

The outline of this dissertation is as follows:

Chapter 2 presents a literature survey of the conventional natural gas to methanol flow sheet performance and an overview of research towards flow sheet improvements.

Chapter 3 focuses on the methodology for the development and analysis of an improved natural gas to methanol flow sheet. The pinch and exergy analysis techniques used to assess the flow sheet's energy performance and identify opportunities to improve energy efficiency are discussed. Power cycle integration methods to enable conversion of process heat to power are also discussed. A flow diagram is produced outlining the new flow sheet development method.

Chapter 4 presents the results and discussion of this study. Results of replacing cryogenic ASU with ITM oxygen are discussed. Comparison of efficiencies, exergy losses and power production of the new flow sheet cases relative to the conventional case is conducted with reference to literature data.

Chapter 6 presents the conclusions of this work as well as recommendations for further work.

1.6 References

Babarit A, Body E, Gilloteaux JC, Hetet JF, 2019, “Energy and economic performance of the FARWIND energy system for sustainable fuel production from the far-offshore wind energy resource”, *Fourteenth International Conference on Ecological Vehicles and Renewable Energies (EVER), Monte-Carlo, Monaco*, pp.1-10, chrome-extension://efaidnbmnnnibpcajpcglclefindmkaj/https://hal.archives-ouvertes.fr/hal-02380030/document [Accessed 3 Aug 2022].

Day WH, 2016, “Methanol fuel in commercial operation on land and sea”, *Gas Turbine World*, chrome-extension://efaidnbmnnnibpcajpcglclefindmkaj/https://www.methanol.org/wp-content/uploads/2016/12/Methanol-Nov-Dec-2016-GTW-.pdf [accessed 2 August 2022].

EMR, “Global Methanol Market Outlook”, https://www.expertmarketresearch.com/reports/methanol-market [accessed 20 June 2022].

Den Exter MJ, Haije WG and Vente JF, “ Viability of ITM Technology for Oxygen Production and Oxidation Processes: Material, System, and Process Aspects”, *ResearchGate*, 2009.

Methanex Corporation, The Global Methanol Leader, chrome-extension://efaidnbmnnnibpcajpcglclefindmkaj/https://www.methanex.com/sites/default/files/MEOH%20Investor%20Presentation%20-%20April%202022%20-%20Final.pdf [accessed 15 June 2022].

Mitsubishi Gas Chemical, “Methanol”, https://www.mgc.co.jp/eng/products/nc/methanol.html [accessed 5 May 2022].

Balopi B and Danha PA, “Methanol synthesis chemistry and process engineering aspects - A review with consequences to Botswana chemical industries”, *Procedia Manufacturing*, pp. 367-376, 2019.

Dalena F, Senatore A, Marino A, Gordano A, Basile M, Basile A, "Methanol production and application: An overview” *Science and Engineering*, pp. 3-28, 2018.

Chou H, Hwang B, Sun C, *“New and future developments in catalysis; Chapter 9 - Catalysis in fuel cells and hydrogen production”*, pp. 217-270, Elsevier, 2013.

Greeff IL, “Co-production of syngas and power”, US Patent *US9021814B2*, 2015.

Iandoli CL and Kjelstrup S, “Exergy analysis of a GTL process based on low temperature slurry FT reactor technology with a cobalt catalyst”, *Energy and Fuels*, vol. 21, pp. 2317-2324, 2007.

Aasberg-Petersen K, Stub Nielsen K, Dybkjær I, Perregaard J, 2008, “Large-scale Methanol Production from Natural Gas”, *Research Paper Haldor Topsøe*: *Lyngby,* Denmark, https://www.researchgate.net/profile/Rick_Manner/post/CO2_Hydrogenation_to_produce_methanol_model_simulation/attachment/59d650a279197b80779a963d/AS%3A503928378884096%401497157296471/download/Topsoe_large_scale_methanol_prod_paper.pdf [accessed 10 June 2022].

Portillo E, Alonso-Fariñas B, Vega F, Cano M, Navarrete B, “Alternatives for oxygen-selective membrane systems and their integration into the oxy-fuel

combustion process: A review", *Separation and Purification Technology*, vol. 229, pp. 115708, 2019.

Methanol Institute, "Applications", https://www.methanol.org/applications/. [accessed 30 July 2021].

Blumberg T, Morosuk T, and Tsatsaronis G, "A comparative exergoeconomic evaluation of the synthesis routes for methanol production from natural gas" *Applied Sciences*, pp. 1213, 2017.

Brelsford R, "Turkmenistan commissions new methanol plant", *Oil & Gas Journal*, https://www.ogj.com/refining-processing/article/14074727/turkmenistan-commissions-new-methanol-plant [accessed 17 November 2020].

Bai W, Feng J, Luo C, Zhang P, Wang H, Yang Y, Zhao Y and Fan H, "A comprehensive review on oxygen transport membranes: Development history, current status, and future directions", *International Journal of Hydrogen Energy*, vol. 46, pp. 36257 - 36290 , 2021.

Chapter 2

Literature Review

2.1 Introduction

This dissertation focuses on the development of an improved industrial-scale process flow sheet for methanol production from natural gas. Various techniques have been investigated and applied to improve the conventional flow sheet. However, there still exist large energy inefficiencies, making it costly to operate such processes on a large scale (Zhu et al., 2018). Moreover, to sustain commercial relevance in the rapidly growing global methanol industry and comply with stricter regulations pushing for lower carbon footprint requires reduction in the net energy demand of the existing processes. To identify opportunities to reduce this energy demand, a review of the performance of the conventional flow sheet is conducted.

Various current and developing technologies relevant to methanol production are also reviewed. Focus is on the energy consumption, exergy losses, thermodynamic efficiencies and process heat recovery techniques. A review of historical developments in improving the flow sheet is also included to comprehend the performance status of the conventional flow sheet. The exothermic reactions in this chemical process lead to significant waste heat generation which poses challenges to the flow sheet design and process integration. The conventional flow sheet pinch analysis, utility requirements and practical challenges limiting achievement of theoretical utility targets are reviewed. Opportunities to reduce exergy losses and improve combined heat and power (CHP) production are reviewed and identified.

2.2 Methanol production processes

2.2.1 Syngas production technologies

Methanol is produced from hydrogenation of carbon monoxide at relatively low temperatures and high pressures. The reactants collectively known as syngas are produced from various carbon-bearing resources including coal, natural gas, biomass and waste. Natural gas is the largest consumed feedstock to produce syngas in the methanol industry (Mitsubishi Gas Chemical, 2022) and it is expected that future methanol production expansions will be based on natural gas as a feedstock (Aasberg-Petersen et al., 2008) due to its availability, cost effectiveness and lower carbon footprint than coal. There are multiple technologies which can be applied in the production of syngas from natural gas, namely steam methane reformer (SMR), autothermal reformer (ATR), heat exchange reformer (HER), two-step reforming or partial oxidation (POX) technologies (Greeff, 2020; Aasberg-Petersen et al., 2001). Reforming reactions occur at elevated temperatures, typically above 950 °C (Blumberg et al., 2017). In SMR, air is used to burn a fuel on the outside of a tubular reactor to generate the required heat for the reforming reactions occurring in the catalyst filled tubes. In ATR, high purity oxygen is fed along with the natural gas and steam to the reformer for partial combustion of the natural gas which generates the heat requirements. The ATR combines POX and SMR in a single reactor. In the two-step reforming process, the SMR is configured in series with oxygen-blown secondary reforming. The heat exchange reformer (HER) is typically paired up with an ATR to utilize the high temperature syngas heat as a heat source (Greeff, 2020) or with the SMR to utilize the flue-gas and/or syngas as a heat source. The main problem with the HER is metal dusting corrosion and lower relative heat fluxes (Aasberg-Petersen et al., 2001; Madloch et al., 2018) which may lead to lower

conversion and thus higher methane slip (Ebrahimi et al., 2021). Methane slip is the amount of unconverted methane in the product stream.

The choice of technology to use for syngas generation depends on the composition and production capacity requirements of the syngas. A comparison of these technologies is presented on Table 2. The SMR produces syngas with a H_2/CO ratio of 3.0, whereas a POX reactor produces a lower ratio of 1.7-1.8. The required ratio of 2.0 for a methanol reactor can be achieved by combining SMR with POX into a single reactor which is the ATR technology (Wilhelm, 2001; Aasberg-Petersen et al., 2001). Optimizing the H_2/CO ratio in syngas is important to improve plant production efficiency, reduce recycles and therefore reduce the overall exergy destruction of a GTL plant (Zhu et al., 2018).

Table 2 Natural gas reforming technologies (Aasberg-Petersen et al., 2001; Wilhelm, 2001).

Technology	Advantages	Disadvantages
ATR	• POX and SMR combination enables desired H_2/CO ratio ±2.0 in syngas suitable for methanol production • Higher Operating temperature means lower methane slip • Simpler and compact reactor suitable for large-scale application	• Requires purification of oxygen typically achieved by energy intensive cryogenic air separation

SMR	• Air separation is not required • High H_2/CO ratio ≥3.0 suited for hydrogen production	• Lower operating temperature means higher methane slip • CAPEX increases significantly with capacity due to reactor complexity
POX	• Lower CO_2 formation • Lower methane slip • No catalyst required	• Lower H_2/CO ratio = 1.7-1.8 • Higher soot generation requiring further processing • Higher operating temperature impacting utility requirements and equipment costs
HER	• Efficient high temperature heat recovery	• Metal dusting corrosion • Lower heat fluxes leading to higher methane slip
Two-step SMR and oxygen-blown secondary reforming	• Lower methane slip than SMR	• Requires purification of oxygen typically achieved by energy intensive cryogenic air separation

2.2.2 Natural gas pre-treatment overview

Figure 4 presents a configuration of natural gas pre-treatment in an ATR process. The pre-reformer is placed upstream of the primary reformer to breakdown long-chain heavy hydrocarbons in the natural gas into simple hydrocarbons such as methane. Heavy hydrocarbons are undesired as they result in the formation of coke in the primary reformer and feed preheater. By reducing this problem, the pre-reformer helps to improve process integrity of the plant. This further enables operation at higher temperatures which improves the overall conversion efficiency of the reformer (Greeff, 2020).

Natural gas contains some alkenes which are highly reactive, double-bonded hydrocarbons. Their presence in natural gas to a reformer can lead to formation of hot spots, catalyst sintering and even deactivation. They further result in undesired side reactions involving breaking down of the double bonds. These alkenes are normally pretreated by saturation with hydrogen under controlled conditions prior to feeding the natural gas to a reformer.

The nickel-based catalyst used in ATRs (Boretti et al., 2021) can get severely poisoned by sulfur which may be present in the natural gas. This is because sulfur compounds can be chemisorbed on the catalyst surface, causing deactivation. Sulfur is generally removed from natural gas by absorption over active carbon or zinc oxide. Organic sulfur is hydrogenated over a sulfide Cobalt-Molybdenum catalyst before absorption of hydrogen sulfide.

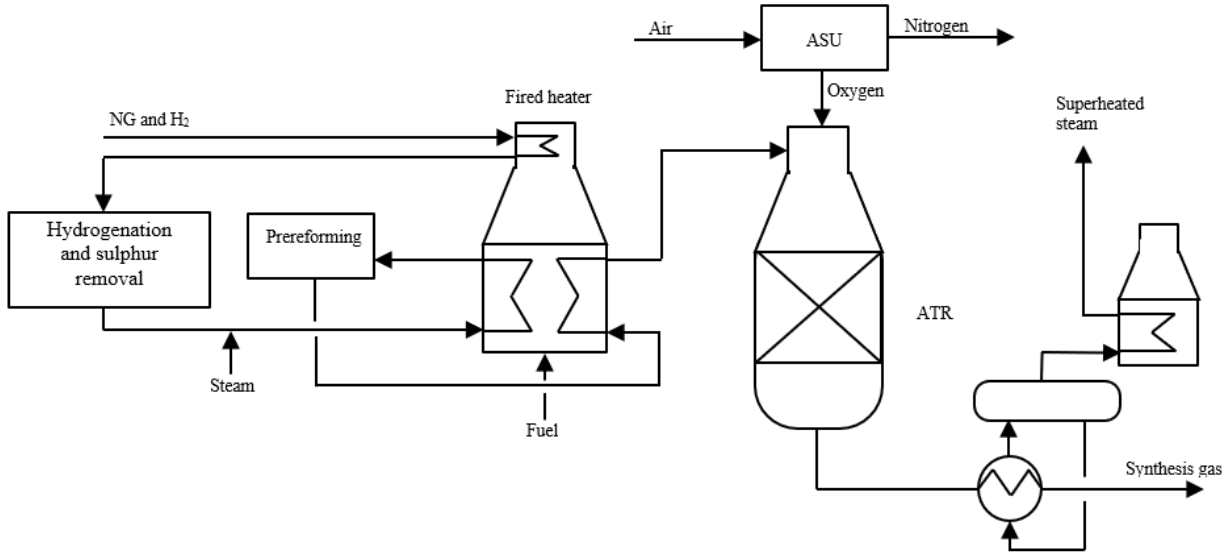

Figure 4 Natural gas pretreatment and ATR process (Haldor Topsoe, 2021).

2.2.3 Chemical reactions

The steam-methane reforming reaction presented by equation 1 is endothermic, equilibrium-driven and occurs at high temperature. In an ATR, the required heat is provided by partial oxidation of methane with oxygen, equation 2. The water-gas shift reaction, equation 3, balances the H_2/CO ratio.

Reforming reaction (Blumberg et al., 2017)

$$CH_4 + H_2O \leftrightarrow 3H_2 + CO \qquad \Delta H_0 = 206 \text{ kJ/mol} \qquad (1)$$

Partial oxidation reaction (Blumberg et al., 2017)

$$CH_4 + 1.5O_2 \rightarrow CO + 2H_2O \qquad \Delta H_0 = -520 \text{ kJ/mol} \qquad (2)$$

Water-gas shift reaction (Lucking, 2017; Blumberg et al., 2017)

$$CO_2 + H_2 \leftrightarrow H_2O + CO \qquad \Delta H_{25\,^{\circ}C,\,5\,MPa} = 41.1\ kJ/mol \qquad (3)$$

Syngas exits the ATR at temperatures in the range of 950 to 1400 °C (Blumberg et al., 2017). Cooling and condensate removal are required before the syngas is sent to the liquid synthesis process. A waste heat boiler (WHB) is used in a conventional ATR process to cool the syngas as shown in Figure 4. This is because no heat integration is done on the process streams in the conventional industrial plants, mainly to limit the effect of metal dusting corrosion which occurs at high temperatures and pressures in the presence of carbon compounds (Madloch et al., 2018). Shell however recently filed a patent application attempting to claim feed/effluent heat exchange over an ATR combined with sulphur dosing upstream of the cooling step, to limit metal dusting corrosion (Smit et al., 2016).

Methanol is produced over a copper-based catalyst, that is, copper-zinc oxide with aluminum oxide or chromium (III) oxide Cu-ZnO-Al_2O_3/Cu-ZnO-Cr_2O_3. The selectivity of methanol is over 99%, thus, side reactions and by-products can be considered negligible (Balopi et al., 2019; Greeff et al., 2002; Lucking, 2017). The main reactions taking place in this process are the hydrogenation of carbon monoxide and carbon dioxide to methanol presented by equation 4 and 5 as well as the water-gas shift, equation 3. The single-pass conversion of methanol is typically low at about 25% per pass. This necessitates recycling unconverted feed gas. With the use of an active catalyst, an overall conversion of up to 80% can be achieved (Lucking, 2017). The conversion of methanol has a direct dependence on pressure

and inverse dependence on temperature (Balopi et al., 2019). Operating pressure ranges between 40 to 110 bar and temperature between 250 to 300 °C (Greeff et al., 2002).

Since methanol synthesis is favoured by relatively higher pressures compared to the syngas generation process, syngas is compressed prior to entering the methanol reactor. Preheating is also required to increase the syngas temperature to the required inlet temperature. The reactor inlet temperature is maintained above 210 °C for catalyst activity. However, it is not to exceed 300 °C to prevent the catalyst from sintering and de-activating (Greeff et al., 2002). The methanol synthesis reactions are exothermic and therefore, require temperature control to maintain the reactor temperature within limits. A schematic of the conventional methanol synthesis process using an isothermal reactor is presented in Figure 14.

Hydrogenation of CO and CO_2 (Greeff et al., 2002; Lucking, 2017)

$$CO + 2H_2 \leftrightarrow CH_3OH \qquad \Delta H_{25\,°C,\,5\,MPa} = -90.7\ kJ/mol \qquad (4)$$

$$CO_2 + 3H_2 \leftrightarrow CH_3OH + H_2O \qquad \Delta H_{25\,°C,\,5\,MPa} = -49.5\ kJ/mol \qquad (5)$$

2.2.4 Methanol synthesis technologies

Two main types of reactors are used for the synthesis, namely an isothermal reactor and an adiabatic reactor as depicted in Figure 5 and Figure 6, respectively. The main differences between these reactor types are temperature control and introduction of fresh feed gas.

The isothermal methanol reactor is based on Lurgi's design technology. It is a heat exchange design with a cooling medium such as boiler feed water (BFW) circulated to recover the heat of reaction to produce steam. This reactor design is considered more efficient due to the energy recovery, longer catalyst life and higher conversion (Greeff et al., 2002; Lucking, 2017). Its relatively higher conversion means a lower volume of catalyst bed is required. However, the reactor's slightly complex design has higher associated installation costs (Balopi et al., 2019).

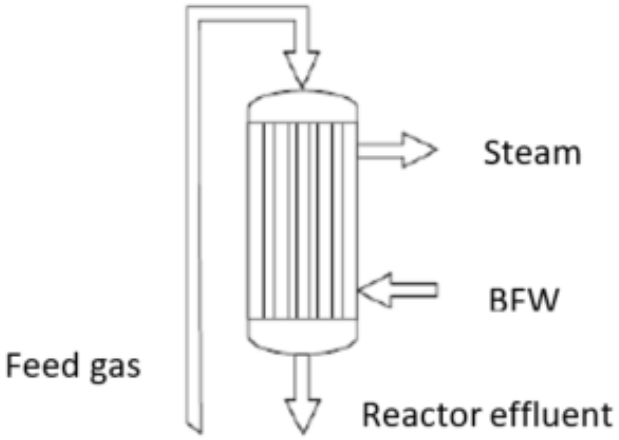

Figure 5 Schematic of an isothermal methanol reactor (Lucking, 2017).

The adiabatic methanol reactor is a multi-stage fixed catalyst bed reactor based on the Imperial Chemical Industries' design. The feed gas to the reactor is split up to enter at various stages between the catalyst beds as a quench to control reactor temperature. The adiabatic reactor has a lower conversion due to the higher equilibrium temperature compared to the isothermal reactor. This leads to a higher recycle ratio necessitating a larger reactor with a high catalyst volume. High temperature is also a problem to the catalyst because it can lead to sintering and deactivation, shortening its life (Balopi et al., 2019; Lucking, 2017).

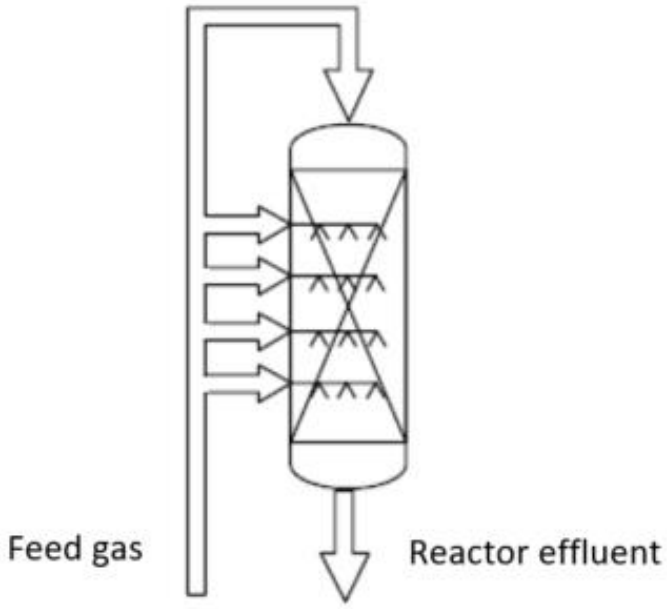

Figure 6 Schematic of an adiabatic methanol reactor (Lucking, 2017).

2.3 Conventional process energy efficiency performance

Typical specific energy consumption to produce methanol from natural gas, coal and CO_2 capture are 8.0, 23.7 and 35.5 GJ/t methanol, respectively (Matzen et al., 2015). Methanol derived from natural gas remains the most economical in energy costs. Specific natural gas efficiencies of 37 to 39 GJ/t methanol can be achieved (Stanbridge, 2016). Although green technologies such as CO_2 capture and biomass gasification have significantly low carbon footprint, energy requirements and therefore production costs in these processes remain a challenge (Clausen et al., 2010; Machado et al., 2014).

In conventional GTL and CTL processes, high temperature heat from the syngas is recovered by raising steam in a WHB. The steam is used in Rankine steam power

cycles to develop work over steam turbines. The net work produced from the cycles is used to produce some of the plant's power requirements. The temperature at which steam can be generated is limited by its critical temperature of 374 °C which limits the work developed by the steam turbine. As a result, the steam is generally superheated to a higher temperature prior to entering the turbine. However, for material of construction considerations, it is not superheated to significantly high temperatures. The large temperature differences between syngas and steam in the WHB lead to degradation of the quality of the syngas heat or exergy loss. Iandoli et al. (2007) reported that conventional methods of syngas cooling by generating steam contributes 20% to the overall plant exergy losses. This is based on a GTL plant with the low temperature Fischer-Tropsch (LTFT) synthesis and the cryogenic ASU. The combined ATR and ASU units were found to contribute 69% to the total plant's exergy loss.

Production of syngas via SMR is associated with high exergy losses. This is attributed to the combustion of large amounts of fuel in the SMR furnace. Hinderink et al. (1996) found that nearly 50% of the exergy losses in an SMR unit is associated with the fuel combustion. A methanol plant with syngas production via SMR has an estimated exergy loss of 8.5 GJ/t methanol. In alternative syngas production technologies such as the ATR paired with a convective reformer to utilize the process heat to produce syngas, the net heat production is reduced. As a result, a lower exergy destruction of 4.9 GJ/methanol can be achieved which is significantly lower than the SMR-based plant. A recent study by Blumberg et al. (2017) showed that SMR-based methanol production plants have the lowest exergetic efficiency when compared to alternative technologies such as the ATR. This is mainly due to the SMR furnace which significantly hampers the plant costs. Alternative technologies

with less fuel combustion are therefore more favourable over the SMR from an energy perspective.

2.4 Developments in methanol process flow sheet improvement

2.4.1 Production capacity

The SMR technology is typically applied in small to medium capacity plants of up to 2500 t/day. This is because while the SMR does not require an ASU, its complex tubular reactor design requires a larger capital investment into the reformer unit and the economy of scale differs significantly with production capacity. Oxygen-based technologies are recommended for capacities above 2500 t/day. A two-step SMR followed by oxygen-blown secondary reforming technology is recommended for capacities of 2500 to 5000 t/day while the ATR is recommended for capacities greater than 5000 t/day due to its simpler design (Blumberg et al., 2017).

In line with increasing global market demands, production capacity of methanol plants has been increasing over the years, taking advantage of the economy of scale. The largest single methanol plant has a capacity of 5225 t/day (217.7 t/h) and employs the ATR technology for its syngas generation. This ATR-based methanol plant is in Turkmenistan, Asia, and is licensed by Haldor Topsoe (Brelsford, 2020). A larger natural gas to methanol plant located in Odioma, Nigeria, with the capacity of up to 10 000 t/day is planned to be in operation in 2024 (Air Liquide, 2021). This plant will also use the ATR technology for conversion of natural gas to syngas. The ATR is therefore the preferred technology for large-scale methanol production (Aasberg-Petersen et al., 2008).

2.4.2 Carbon emissions reduction

One of the main issues with fossil fuel-based GTL and CTL plants is the production of significant amounts of CO_2, a greenhouse gas which affects climate change. This is produced mainly in the syngas generation step and in combustion of fuel for power generation and heating. In natural gas reforming, the more CO_2 generated, the less CO, which is the preferred component in the syngas. This leads to production inefficiencies where a significant portion of feedstock is used to produce waste. The excess CO_2 is conventionally sent to the atmosphere with an associated carbon tax.

The methanol production process presents opportunities for CO_2 recovery because CO_2 can be chemically hydrogenated to produce methanol. There are several developments presented in literature which focus on recovering waste CO_2 to use as feedstock for methanol production in so-called emissions-to-liquid (ETL) plants. QAFAC currently captures nearly 500 t/day of CO_2 from flue gas for methanol production, which has led to an increase in the capacity of its methanol plant by 300 t/day. The Carbon Recycling International also produces methanol directly from captured CO_2 with a first commercial scale ETL methanol reactor installed in Anyang, China, with a capacity of 330 t/day (Carbon Recycling International, 2022).

Electrified reverse water-gas-shift is a technology of industrial interest for the conversion of CO_2 to syngas in power to liquids plants (Haldor Topsoe, 2022). Other methanol projects based on captured CO_2 are expected to start operations over the next few years for example in China and Norway (Carbon Recycling International, 2022). Sustainable methanol production can also be based on municipal solid waste (MSW), waste wood or biomass and black liquor as feedstock. Enerkem Alberta Biofuels is the world's first commercial biofuel company to produce methanol from MSW with the capacity of 38 million L/year. Chemrec produces 4 t/day of methanol-

based bio-DME from black liquor (Methanol Institute, 2016). Varlandsmetanol is progressing a world's first commercial scale project to produce 130 000 m^3/year methanol from wood in Sweden via gasification (VarmlandsMetanol, 2021). Compared to fossil fuel-based methanol, the cost of producing sustainable methanol is still significantly higher. This is mainly due to the production cost of hydrogen as required to achieve the desired syngas composition, that is, H_2/CO ratio (Nyari, 2018). Development of innovative solutions to reduce the cost of green hydrogen production and improve profitability of sustainable methanol synthesis is required.

2.4.3 Methanol process flow sheet performance developments

2.4.3.1 Process conversion efficiency

Production of syngas from natural gas via steam-methane reforming is a well-known, cost-effective and mature technique. The conversion efficiency is favoured by low steam-to-carbon (S/C) ratio, medium pressures and high reactor operating temperatures (Haldor Topsoe, 2021). Enhancements to improve the catalyst continue to be investigated, namely better promoters, surface area and structural support (Boretti et al., 2021). Lower S/C ratios and higher temperatures result in higher CO yield and reduced methane slip in the syngas. The typical S/C ratio in ATRs is 0.6, however, lower S/C ratios are being investigated.

Methanol synthesis is favoured by lower temperatures and higher pressures. The selectivity is typically high at >99%. With a feed gas recycle and the use of an active catalyst, an overall conversion of up to 80% can be achieved (Balopi et al., 2019; Lucking, 2017). Various studies have been performed, listing recommendations to improve the conversion efficiency of CO and CO_2 to methanol (Redondo et al., 2019;

Mbatha et al., 2021; Izabassarov et al., 2021). These recommendations include improving the catalyst and reactor temperature control.

2.4.3.2 Oxygen production challenges in syngas generation processes

High purity oxygen is used in large-scale industrial chemical and power generating processes such as syngas production, combustion chambers, iron and steel manufacture. The oxygen is typically produced via cryogenic air separation. The cryogenic air separation process separates gases from air via cooling, liquefaction and distillation. Energy for refrigeration is provided by the compression of air at the inlet. The technology is mature and used in large-scale plants (Den Exter et al., 2009). There is no scope for heat integration between these units and other blocks in the natural gas to methanol flow sheet as cryogenic ASUs operate at very low temperatures. The units are integrated indirectly with the process via the power obtained from power cycles driven by process heat.

The cryogenic ASU technology consumes large amounts of energy, mainly for the compressors, contributing significantly to the overall production costs of syngas. 40% of the operating costs in natural gas-based syngas manufacture are attributed to oxygen production (Aasberg-Peterson et al., 2001; Den Exter et al., 2009). Specific power consumption of 0.38 kWh/Nm^3 (Tesch, 2019) is reported for a large-scale cryogenic ASU in China. Advanced Linde cryogenic ASUs have reported lower specific power consumptions of 0.237 kWh/Nm^3 for oxygen purity of $\geq$ 95% and 0.33 kWh/Nm^3 for purity of $\geq$ 99.5% (Beysel, 2009). Portillo et al. (2019) recently reviewed literature on oxygen production technologies for oxy-fuel combustion power plants, where high purity oxygen is used in the combustion chamber to enable

ease of CO_2 capture from the flue gas. In integrated gasification combined cycle (IGCC) where oxygen is required for gasification, the cryogenic ASU contribute 15% to the cost of an IGCC power plant (Portillo et al. 2019).

The cryogenic ASU further suffers significant exergy destruction. A cryogenic ASU with the capacity of 10 kNm^3/h was found to have an exergy destruction of 2240 kW (Taniguchi et al., 2015). The air compressors being the largest energy consumers were found to also contribute the largest exergy destruction of 38.4% of total cryogenic ASU exergy losses (Fu and Gundersen 2012). Syngas production with ASU-derived oxygen accounts for over 60% of the investment in large-scale natural gas to methanol production (Aasberg-Petersen et al., 2008). The selection of the syngas and oxygen production technologies as well as the design of the flow sheet are therefore very important. Since cryogenic air separation is a mature technology, there is little prospect of further drastic improvement and cost reductions (Portillo et al., 2019; Fu and Gundersen, 2012). Alternative technologies for oxygen production therefore need to be considered.

2.4.3.3 ITM oxygen technology

Technologies for oxygen production such as pressure swing adsorption (PSA), chemical looping combustion, electrolysis and polymeric membranes presently cannot compete for the capacity of the cryogenic ASU (Rao et al., 2007; Greeff, 2004). The ITM oxygen is a novel technology which promises to compete with the cryogenic ASU (Anderson et al., 2011). The technology has been under development since the mid 1990's by Air Products and Ceramatec. It uses mixed-metal oxide ceramic materials which are oxygen-ion-conducting and can separate oxygen from an oxygen-containing gas, such as air. The membranes are operated at high

temperatures ranging from 800 to 900 °C (Miller et al., 2014; Anderson et al., 2016). Figure 7 presents a simplified schematic of the membrane separator. At high temperature, the oxygen adsorbed on the membrane dissociates into anions and electrons. The selectively permeable and non-porous membrane allows only the oxygen ions to permeate through. The driving force for the ion transfer is the difference in oxygen partial pressures between the feed side and permeate side. The driving force can be achieved by pressuring the feed side, operating the permeate side at vacuum pressure or using a sweeping medium to remove the permeate. The oxygen-depleted stream is removed from the membrane separator as a reject stream.

Effective energy recovery is important when designing the ITM oxygen system to ensure its competitiveness. Its high temperature operation presents attractive opportunities to recover the energy by integrating with power cycles. This can potentially reduce exergy losses when compared to the cryogenic ASU (Anderson et al., 2011; National Energy Technology Laboratory, 2022).

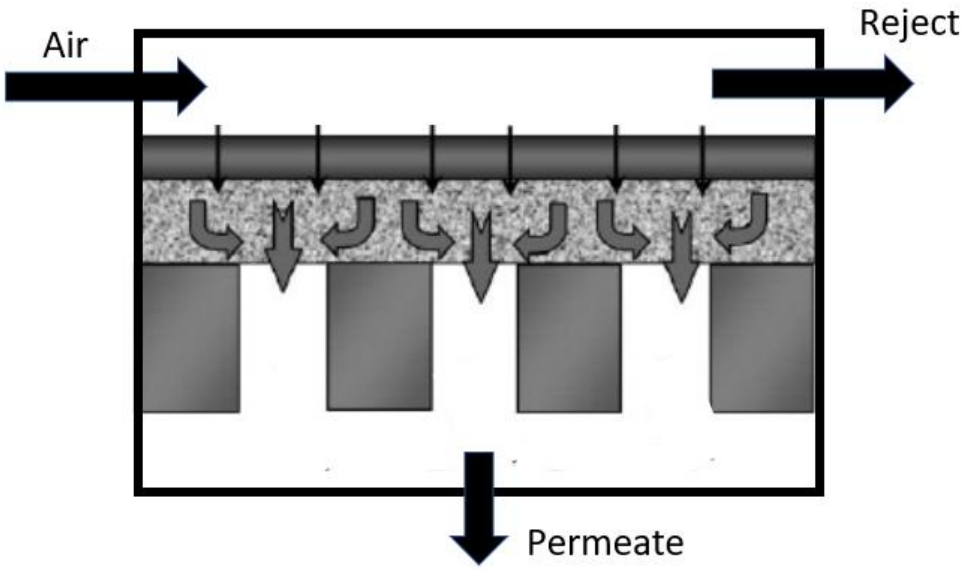

Figure 7 Schematic of an ITM oxygen separator (Rao at al., 2007).

Long-term chemical stability and reliability of the membrane is an important factor in ensuring industrial suitability. A common limiting factor for the oxygen flux through the membrane is the surface resistance caused by surface reactions on either side of the membrane. These reactions are, namely oxygen dissociation on the air side and hydration on the permeate side. Addition of porous layers on both sides of the membrane surface increases the surface area available for the surface reactions, to improve the oxygen flux (Miller et al., 2014; Anderson et al. (2016). An experimental study conducted by Anderson et al. (2016) showed that the membrane is reliable and can achieve high purity 99.9% oxygen, suitable for industry.

2.4.3.4 Costs of oxygen production

Seltzer and Robertson (2006) compared oxygen production by cryogenic ASU and ITM oxygen in a power plant. They found that the ITM oxygen-based power plant had a higher electrical output and therefore lower operating costs. This finding supports the goal to reduce energy costs in syngas manufacture. There is however a trade off on the capital cost as it was also found that the ITM oxygen-based plant had a 32% higher capital cost than the cryogenic ASU-based plant. The capital cost of an ASU for a capacity of 181 t/h oxygen was estimated at $115 million for the cryogenic ASU and $188 million for the ITM oxygen unit (Seltzer and Robertson 2006). A cost breakdown of the ITM oxygen configured as a power producing cycle presented by Den Exter et al. (2009) shows that 96% of the capital cost for process equipment is attributed to the cost of the reject gas turbine expander (66%) and the membrane separator (30%). This is based on an oxygen production rate of 30 kNm^3/h (375 t/h). Further economic evaluation indicates that with revenue from the

oxygen and electrical power, the ITM oxygen unit can pay out its total capital costs over 16.8 years.

2.5 Minimum energy requirements

The pinch analysis is a technique used to assess and integrate heating and cooling systems to reduce external heating and cooling utility requirements. Minimum energy requirements (MER) and the heat exchange network design depend on the chosen minimum pinch point approach temperature (ΔT_{min}). A high ΔT_{min} means high energy requirements and therefore higher operating costs and a low ΔT_{min} means high capital investment costs. The balance between the capital and energy costs when designing the flow sheet should be determined. For chemical processes, a typical ΔT_{min} of 10-20 °C is used. For a methanol synthesis plant based on methane feedstock, the optimum ΔT_{min} was found to be 10 °C (Philia et al., 2020).

In the conventional ATR process, to limit the effect of metal dusting corrosion, no heat integration is done between the ATR product syngas and feed gas process streams (Madloch et al., 2018). This results in high utility and energy consumptions as well as large temperature driving forces in heat exchangers. The claim by Shell to enable feed/effluent heat exchange over an ATR by sulfur dosing upstream of the heat exchanger may be the solution to improve process heat integration in this process (Smit et al., 2016).

Philia et al. (2020) performed a pinch analysis study to improve the process heat integration of a methanol plant. The HINT heat exchanger network design software was used to design an improved configuration of the heat exchanger network. A sensitivity analysis of the energy requirements was conducted at various ΔT_{min} of

10, 15 and 20 °C. From the study it was found that a ΔT_{min} of 10 °C yielded the lowest energy costs. The integration also resulted in lower heat exchanger capital cost compared to the conventional flow sheet. Nayana et al. (2021) also performed a similar heat integration study using pinch technology for a natural gas-based methanol plant also on a HINT software. In this study a new heat exchanger network was developed which resulted in an improved utilization of process heat and reduced utility requirements. This led to significant savings in plant capital and operating costs (Nayana et al., 2021).

2.6 Power production

2.6.1 Power cycles

2.6.1.1 Integrating power cycles with chemical processes

Power cycles are important components in heat recovery and conversion to work. The Rankine and Brayton power cycles are the common power cycles used in power generation. The main difference is the type of working fluid used, that is, liquid/vapour in a Rankine cycle and gas in a Brayton cycle. Figure 8 presents a typical Rankine power cycle. This is a vapour-liquid cycle where the liquid is pumped, vaporized and heated through the boiler and then expanded through the turbine. The turbine exhaust steam is condensed and circulated through the cycle. Closed and open Brayton power cycles are shown in Figure 9 and Figure 10. The combustion gas turbine is an example of an open cycle where fuel is fed along with compressed air to the combustion chamber. The combustion products are expanded before they are removed from the cycle. A closed cycle is typically where combustion does not occur, but heat is transferred from an external source also

known as externally fired. In such a cycle, the composition of the working fluid typically remains unchanged.

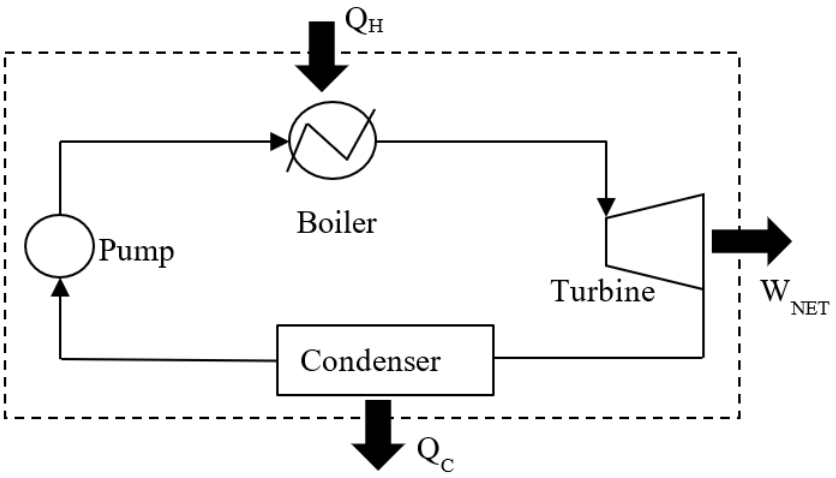

Figure 8 Schematic of a simple Rankine power cycle.

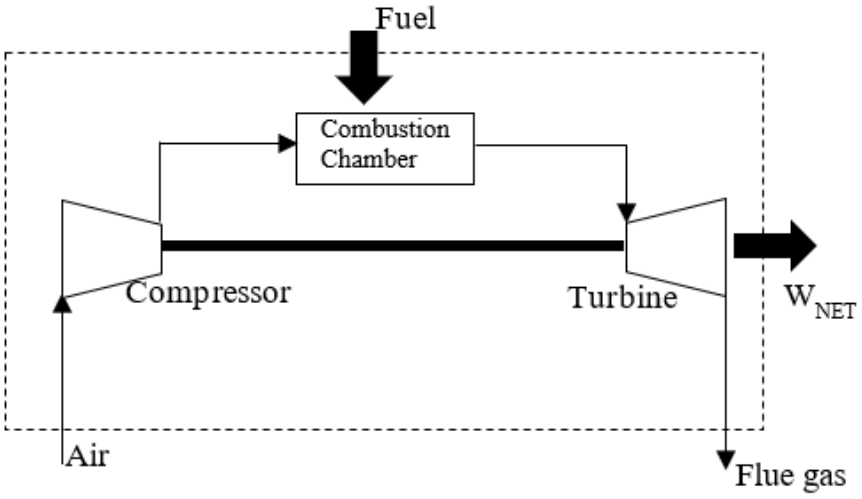

Figure 9 Schematic of a simple open Brayton power cycle.

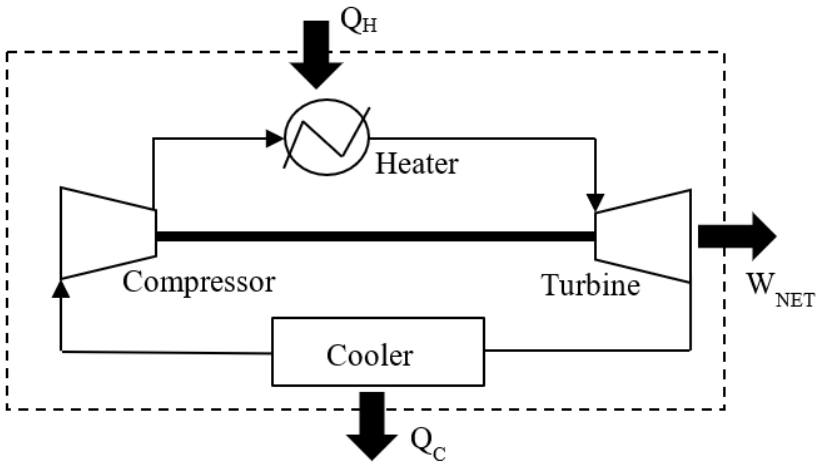

Figure 10 Schematic of a simple closed Brayton power cycle.

2.6.1.2 Combined power cycle

Figure 11 shows a combined power cycle which involves two power cycles coupled by heat transfer from one cycle to the other. Heat of the turbine exhaust stream from the one cycle which is still at a high temperature is transferred to the adjacent cycle, to reduce the temperature at which heat, Q_C, is discharged from the system boundary. The combined cycle typically involves a gas power cycle as the topping cycle and a vapor power cycle as the bottoming cycle. The combined power cycle is commonly used in industry as it can generate more power and achieve a higher thermal efficiency for the same fuel source when compared to a conventional simple power cycle.

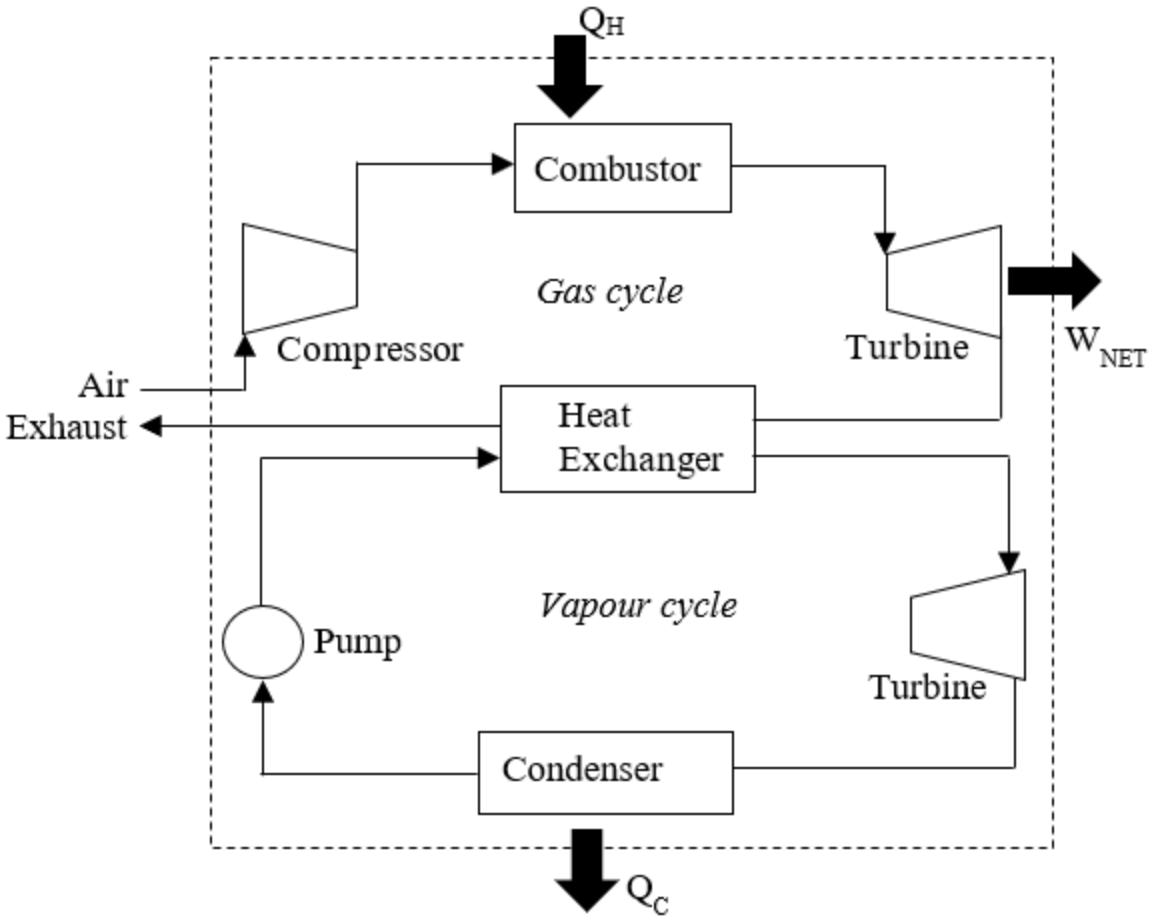

Figure 11 Schematic of a gas turbine combined cycle (Moran et al., 2006).

2.6.2 Industrial power generation

Sub-critical steam power plants typically operate at thermal efficiencies of 33% (Ramireddy, 2012), that is, the power output from the cycle is a third of the heat input into the cycle. For an ideal Rankine cycle, the thermal efficiency is limited to about 42% as a result of low critical temperature of water. This is explained by the Carnot cycle efficiency which is the maximum thermal efficiency a heat engine operating between two temperatures (T_C and T_H) can achieve. The Carnot cycle efficiency is expressed as follows:

$$\eta_{carnot} = 1 - \frac{T_C}{T_H} \quad (6)$$

In industrial power plants, a gas turbine power cycle is coupled to a steam cycle through a heat recovery steam generator (HRSG) and the combined cycle can generate over 50% more power from the same fuel source compared to a conventional simple power cycle (Mitsubishi Power Ltd, 2022). In 2018, Siemens, Orascom Construction and Elsewedy Electric commissioned the world's largest gas-fired combined cycle power plants in Egypt with the total capacity of 14.4 GW. Each of the 12 single combined cycle power plant blocks have a capacity of 1.2 GW with an overall thermal efficiency of over 60% (Encz, 2018).

Since 60% of the world's electricity is produced from fossil fuel, there is an associated carbon footprint from power plants contributing to greenhouse gas production and global warming (Han et al., 2018). Ghasemzadeh et al. (2018) showed that process power demands can be satisfied in a methanol plant with the Integrated Gasification Combined Cycle (IGCC), where a combined gas and steam power cycle is integrated into the coal gasification unit. This can significantly reduce the CO_2 produced from burning a fossil fuel, in this case coal, to produce power.

2.6.3 Integrating power production systems into chemical processes

Combined heat and power (CHP) systems are important in chemical processes where thermal energy and power are required because they can be cogenerated from the same energy source. This presents opportunities to improve the thermodynamic efficiency, reduce energy costs and carbon footprint. CHP is achieved by configuring typical chemical processes to satisfy heating requirements to achieve the process intent while waste heat is efficiently converted to electrical power.

Syngas is an important intermediate in many chemical synthesis processes, such as, in the production of methanol. Typically, in an ATR process where syngas is produced from natural gas, a steam generating WHB is used to cool syngas. The WHB is integrated into a Rankine steam cycle where the generated steam is expanded in a turbine generator. The hot syngas can also be directly expanded in a gas turbine cycle as an alternative method to convert the process heat to work (Greeff et al., 2004). There are many patents in literature presenting invented ideas of combined production of syngas, liquids and power. Some of these patents include configuration ideas to enhance the thermodynamic performance of these systems.

Where the ITM oxygen technology is applied for oxygen production, the overall heating requirements can be reduced if the system is carefully integrated into the high temperature chemical processes (Anderson et al., 2011). Integrating power generating devices into the ITM oxygen unit to recover the waste heat from the product streams can result in co-production of oxygen and power, to reduce the net compressor duty requirements for the unit (Ziqubu and Greeff, 2021). Figure 12 presents a simplified schematic of the ITM oxygen unit configured into a Brayton power cycle. In this figure, fuel is used to heat the air before it is sent to the membrane separator where the air is separated into the reject and permeate streams. The reject stream is subjected to further heating to higher temperatures before being expanded. The temperature is increased to increase the work developed by the turbine. The air-standard model equation for a Brayton power cycle using an ideal gas as the working fluid shows the parameters which affect the work output of a turbine or power input to a compressor as follows (Moran et al., 2006):

$$W = \frac{nkRT_{in}}{k-1}\left[\left(\frac{P_{out}}{P_{in}}\right)^{\frac{k-1}{k}} - 1\right] \quad (7)$$

where n is the mole flowrate of the working fluid in mol, k is the ratio of the heat capacities at contact pressure and at constant volume, R is the universal gas constant = 8.3145 $J.mol^{-1}.K^{-1}$, T_{in} is the turbine or compressor inlet temperature in K and, P_{out} and P_{in} are the outlet and inlet pressures, respectively.

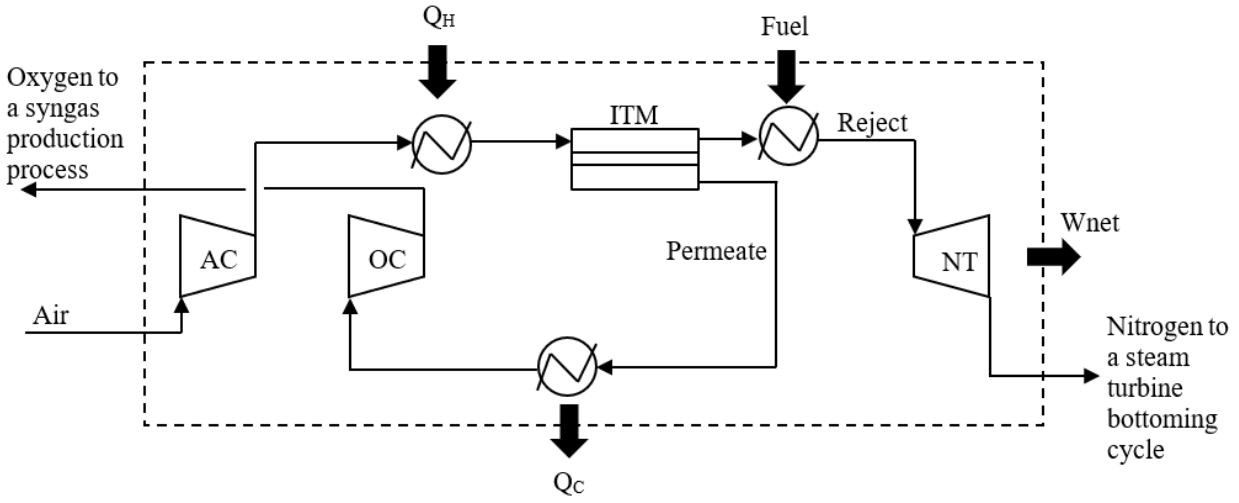

Figure 12 Integrated ITM oxygen with a power cycle (Anderson et al., 2011).

2.7 Review of research on methanol flow sheet improvements

2.7.1 Co-production of methanol and power

Blumberg et al. (2016) performed an exergy analysis for the natural gas to methanol flow sheet. The authors found that exergetic efficiency of the flow sheet is low at 29.4%, with the ATR and HRSG being amongst the main contributors to exergy losses. Exergy destruction was identified to occur mostly in the reforming, methanol and steam cycle subsystems. These subsystems should be further investigated for

improvement. It is suggested that this can be done by improving heat integration and performing an in-depth exergy analysis. Zhang et al. (2014) showed that energy savings can be realized if the process is configured to co-produce methanol and electricity. This was based on the use of coal and natural gas as feedstock or energy source. With CHP integration, process heat is integrated to reduce utility and net power requirements. The reduction in power requirement has the potential to increase the plant's annual profit (Kralj et al., 2007). Otaraku et al. (2014) studied process optimization of a natural gas to hydrocarbon liquids flow sheet and found that significant amounts of heat can be recovered for power production as a result of process integration and using exergy analysis as a guide. This was based on the ATR and FT synthesis process. Li et al. (2020) showed that in a methanol production flow sheet, increasing the operating temperature and pressure in the partial oxidation reformer can reduce both production costs and emissions (SOx, NOx, CO_2 and soot). A higher temperature, however, has an associated higher capital cost and therefore a trade-off between capital and operating costs should be determined.

2.7.2 Co-production of oxygen and power

Inventions by Air Products and Chemicals Inc. present integration opportunities to co-produce oxygen and power where a fuel source is used to heat the air feed to the ITM oxygen process (Kang et al., 2006; Kang et al., 1998) and power production is enabled by applying principles of a combined cycle. This novel ITM oxygen technology shows greater advantages in making up for its energy consumption compared to cryogenic ASU (Bai et al., 2021).

Kang et al. (1998) presented an invention of an ITM oxygen unit to co-produce oxygen, steam and power with lower energy costs compared to a typical cryogenic

ASU. The authors found that the specific energy cost of $10/t oxygen in a cryogenic ASU can be reduced to $7.30/t oxygen and less in various ITM oxygen unit configurations. This was made possible through process heat integration and the integration of turbine expanders to develop work from the reject and steam streams (Kang et al., 1998). The developed work is used to drive compressors and electrical power generators.

An invention by Greeff (2015) presents a process heat integration of the syngas generation and the ITM oxygen units. Syngas heat is used to further heat the reject stream from the ITM oxygen process to increase the work output from the turbine expander. This is an effective method to recover process heat and was found to improve the thermal efficiency of the power cycle. In the ITM oxygen power cycle configured in Figure 12, the thermal efficiency can be improved by sending the exhaust reject stream to a HRSG to produce more power in a steam bottoming cycle. Anderson et al. (2011) similarly, suggests heating the reject stream to a higher temperature to improve the power cycle thermal efficiency.

2.7.3 Syngas cooling

Various alternative methods to recover or utilize syngas heat have been investigated, including raising the steam pressure in the WHB, direct expansion of the syngas in a turbine expander, feed/effluent heat exchange over the ATR, and gas heated reforming where the syngas heat is used as a heat source for further steam reforming.

The direct expansion of syngas in a turbine is shown in Figure 13 where the hot product stream from the reactor is expanded in a product expander, developing work. Greeff (2020) showed that an increase in net power generation of up to 37% can be

achieved in an ATR process integrated with a turbine expander where the hot syngas from the ATR is directly expanded. This is relative to a conventional process, where the heat is used to generate steam. Greeff (2013) presents an invention where syngas and power can be co-produced by transferring the syngas heat to a power cycle working fluid which is already at a fairly high temperature before it is expanded to increase power production and thermal efficiency. Greeff (2022) found that in a helium-steam combined power cycle, the integration of hot syngas gas to provide additional heat to the cycle increases the work output by 19% when compared to a standalone power cycle, resulting in reduced net power demand for the integrated process.

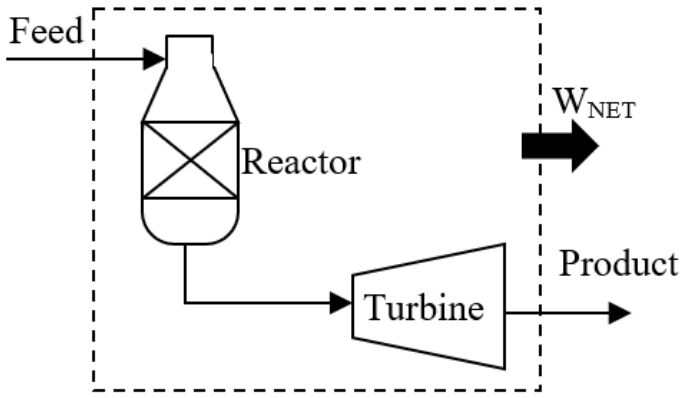

Figure 13 Integrated product turbine expander (Greeff, 2004)

2.7.4 Direct process gas expansion in the methanol synthesis loop

The methanol synthesis loop is energy intensive because significant compression of the syngas is required prior to feeding the methanol reactor. Efficient and economical recovery of the exothermic heat of reaction is a challenge in the design of the methanol synthesis unit. This is because the reaction heat needs to be removed

at high temperature to maximize the amount of work that can be developed while the synthesis reactions are to be equilibrated at low temperature to maximize conversion (Aasberg-Petersen et al., 2008). Figure 14 shows a simplified schematic of a conventional methanol synthesis loop using an isothermal reactor. The isothermal reactor temperature is controlled by generating steam. This steam can be used in a Rankine power cycle to generate work to supplement the power requirements of the syngas feed compressor.

If the steam generated from the reactor temperature control system is expanded in a steam turbine cycle, the net compressor power requirement can be reduced by 43% (Greeff et al., 2002). The product stream from the reactor needs to be cooled to separate the unreacted gases from the raw methanol product. This is typically achieved by indirect heat exchange with the feed gas to the reactor. Greeff et al. (2002) however also found that it is possible to incorporate the direct turbine expansion concept into the process to generate more power for the feed gas compressor. In this type of integration, a process gas power cycle with a chemical reactor on the high pressure side, and separation on the low pressure side is created. The high gas recycle rate and high operating pressure of the methanol reactor are exploited to run the gas power cycle using the methanol synthesis loop process gas directly as a working fluid. The integrated system in the study by Greeff et al. (2002) consumes 24% less power compared to the conventional case. Azadi et al. (2016) elaborated on the concept proposed by Greeff et al. (2002) by applying combined pinch and exergy analysis to such a system. Kotowicz et al. (2022) did a further study on the effect of variation of pressure and temperature on the power production and chemical conversion in a methanol process gas power cycle.

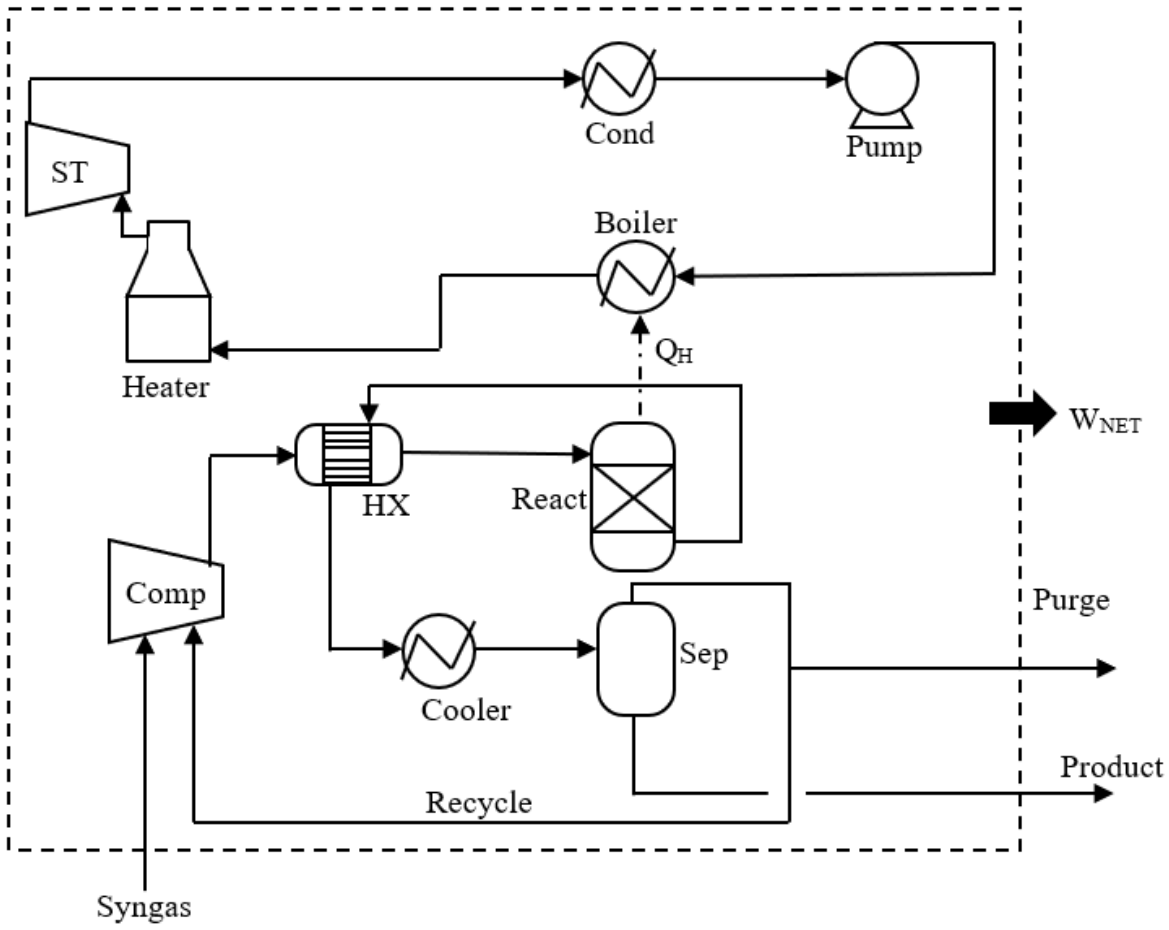

Figure 14 Conventional methanol synthesis process using an isothermal reactor.

2.8 Opportunities for further research

The ATR is the technology of choice for large-scale syngas manufacture in natural gas to methanol plants because of its simple, compact and low-cost design. Oxygen production costs contribute significantly to the capital and operating cost of an ATR-based syngas unit. Investigating low-cost oxygen production is an attractive opportunity to improve the cost of syngas manufacture. Further process heat integration and alternative methods to improve heat recovery are required to reduce the typical flow sheet's energy efficiency performance. Focus should be placed on

the syngas plant and ASU because they are the major contributors to the plant's overall exergy destruction (Iandoli et al., 2007; Blumberg et al., 2016).

Replacing cryogenic ASU with the novel ITM oxygen in the natural gas to methanol flow sheet presents opportunities to improve the energy efficiency. Integration of this ITM oxygen and evaluation of the new flow sheet efficiency performance relative to the conventional flow sheet requires an investigation. Process heat recovery and conversion to work in the methanol synthesis loop is one promising method to reduce the unit's high compressor power requirements. This can be achieved by integrating power cycles to configure the process as a heat engine. Potential benefits of co-producing methanol and power in a natural gas to methanol flow sheet with the oxygen production based on the ITM oxygen technology have not been found in literature and will be investigated in this study.

2.9 Summary

Current industrial GTL processes suffer large energy inefficiencies, making it costly to operate such processes on a large scale. With the increasing demand for methanol and stricter regulations requiring reduced carbon intensity, there is a need to improve sustainability of existing processes. Large exergy losses exist due to poor process heat integration and recovery, mainly in the ATR and ASU processes of conventional large-scale natural gas to methanol plants. Energy improvement can be realized by alternative technologies which integrate heat with the high temperature syngas generation. The ITM oxygen technology has the potential to replace the conventional cryogenic air separation and reduce the large power demands associated with oxygen production. Since the ITM oxygen operates at high temperatures, it requires a source of heat, but also provides the opportunity for

energy recovery from the hot permeate and reject streams. There is an opportunity not found in literature to further improve the natural gas to methanol flow sheet by considering the ITM oxygen technology for oxygen production and process heat recovery to improve exergy destruction, reduce energy costs and emissions.

2.10 References

Azadi M, Tahouni N, Panjeshahi MH, “Energy conservation in methanol plant using CHP system”, *Applied Thermal Engineering*, vol. 107, pp. 1324-1333, 2016.

Ghasemzadeh K, Tilebon , SMS, Basile A, *“Chapter 15 - Coproduction of Electrical Energy and Methanol in IGCC Plants”,* Methanol, Elsevier, pp. 399-428, 2018.

Den Exter MJ, Haije WG and Vente JF, *“Chapter 2 - Viability of ITM Technology for Oxygen Production and Oxidation Processes: Material, System, and Process Aspects”,* Inorganic Membranes for Energy and Environmental Applications, 2009.

Fu C and Gundersen T, “Using exergy analysis to reduce power consumption in air separation units for oxy-combustion processes”, *Energy*, vol. 44, pp. 60-68, 2012.

Seltzer A and Robertson A, “Economic Analysis for Conceptual Design of Supercritical O_2-Based PC Boiler”, *Foster Wheeler Power Group*, Inc, 2006.

Mitsubishi Gas Chemical, “Methanol”, https://www.mgc.co.jp/eng/products/nc/methanol.html [accessed 5 May 2022].

Rao, P & Muller, M, “Industrial Oxygen: Its Generation and Use”, *ACEEE Summer study on Energy Efficiency in Industry*, The State University of New Jersey, 2007.

Aasberg-Petersen K, Bak Hansen J-H, Christensen TS, Dybkjaer I, Seier Christensen P, Stub Nielsen C, Winter Madsen SEL, Rostrup-Nielsen JR, “Technologies for large-scale gas conversion”, *Applied Catalysis*: General 221, 379-387, 2001.

Balopi B and Danha PA, “Methanol synthesis chemistry and process engineering aspects - A review with consequences to Botswana chemical industries”, *Procedia Manufacturing*, pp. 367-376, 2019.

Kang DM, Srinivasan RSA, Thorogood RMC and Foster EPW, “*Integrated high temperature method for oxygen production”,* EU Patent EP0658367B1, 1998.

Beysel G, 2009, “Enhanced cryogenic air separation. A proven process applied to oxyfuel-Future Prospects, 1st Oxyfuel Combustion Conference”, *The Linde Group,* https://ieaghg.org/docs/oxyfuel/OCC1/Plenary%201/Beysel_ASU_1stOxyfuel%20Cottbus.pdf [accessed 5 July 2021].

Greeff IL, “Integration of a turbine expander with syngas process – using process gas as a working fluid”, *Applied Thermal Engineering*, pp. 165, 2020.

Greeff IL, “Process for co-producing syngas and power”, US Patent *US9021814B2*, 2015.

Greeff IL, “Recovery of work from exothermic chemical reaction systems by means of turbine expansion”, *Eindhoven: Technische Universiteit Eindhoven*, 2004.

Ebrahimi H, Benhroozsaranda A, Zamaniyana, A, “Arrangement of primary and secondary reformers for syngas production” *Chemical Engineering Research and Design*, pp. 1342-1350, 2010.

Haldor Topsoe, “SynCOR™ - Autothermal Reformer (ATR)”, https://www.topsoe.com/products/equipment/syncortm-autothermal-reformer-atr [accessed 10 May 2021].

Greeff IL, Visser JA, Ptasinski KJ, Janssen FJJG, “Using turbine expanders to recover exothermic reaction heat - flowsheet development for typical chemical processes”, *Energy*, pp. 2045-2060, 2004.

Greeff IL, Visser JA, Ptasinski KJ, Janssen FJJG, "Utilization of reactor heat in methanol synthesis to reduce compressor duty - application of power cycle principles and simulation tools", *Applied Thermal Engineering*, pp. 1549-1558, 2002.

Greeff IL, “Co-production of syngas and power”, US Patent *US8424308B2*, 2013.

Iandoli CL, Kjelstrup S, “Exergy analysis of a GTL process based on low temperature slurry FT reactor technology with a cobalt catalyst”, *Energy and Fuels*, vol. 21, pp. 2317-2324, 2007.

Aasberg-Petersen K, Stub Nielsen K, Dybkjær I, Perregaard J, 2008, “Large-scale Methanol Production from Natural Gas”, *Research Paper, Haldor Topsøe: Lyngby*, Denmark, https://www.researchgate.net/profile/Rick_Manner/post/CO2_Hydrogenation_to_produce_methanol_model_simulation/attachment/59d650a279197b80779a963d/AS%3A503928378884096%401497157296471/download/Topsoe_large_scale_methanol_prod_paper.pdf [accessed 10 June 2022].

Portillo E, Alonso-Fariñas B, Vega F, Cano M, Navarrete B, “Alternatives for oxygen-selective membrane systems and their integration into the oxy-fuel combustion process: A review”, *Separation and Purification Technology*, vol. 229, pp. 115708, 2019.

Anderson LL, Armstrong PA, Repasky JM and Stein VE, “Enabling clean coal power generation: ITM oxygen technology”, *International Pittsburgh Coal Conference*, Pittsburgh: Air Products and Chemicals, Inc, 2011.

Anderson LL, Armstrong PA, Broekhuis RR, Carolan MF, Chen J, Hutcheon MD, Lewinsohn CA, Miller CF, Repasky JM, Taylor DM, Woods CM, “Advances in ion transport membrane technology for oxygen and syngas production” *Solid state Ionics,* vol. 288, pp. 331-337, 2016.

Lucking LE, “Methanol production from syngas, process modelling and design utilization biomass gasification and integration hydrogen supply”, PhD Thesis, Delft university of technology, 2017.

Moran MJ, Shapiro HN, *“Chapter 7 - Exergy analysis in Fundamentals of engineering thermodynamics”,* pp. 272-324. John Wiley & Sons Inc, 2006.

Miller CF, Chen J, Carolan MF, and Foster EP, “Advances in ion transport membrane technology for syngas production”, *Catalysis Today*, pp. 228, 2014.

Mitsubishi Power Ltd, “Gas turbine combined cycle (GTCC) power plants”, https://power.mhi.com/products/gtcc [accessed 22 July 2021].

Encz P, 2018, “Completion of world's largest combined cycle power plants in record time”, https://press.siemens.com/global/en/feature/completion-worlds-largest-combined-cycle-power-plants-record-time [accessed 10 September 2021].

Tesch S, Morosuk T, Tsatsaronis G, 2019, “Comparative evaluation of cryogenic air separation units from the exergetic and economic points of view”, https://www.intechopen.com/books/low-temperature-technologies/comparative-

evaluation-of-cryogenic-air-separation-units-from-the-exergetic-and-economic-points-of-v [accessed 6 August 2021].

Blumberg T, Morosuk T, and Tsatsaronis G, “A comparative exergoeconomic evaluation of the synthesis routes for methanol production from natural gas”, *Applied Sciences*, pp. 1213, 2017.

Wilhelm, D., Simbeck DR, and Dickenson AD, Karp RL, "Syngas production for gas-to-liquids applications: technologies, issues and outlook”, *Fuel Processing Technology,* pp. 139-148, 2001.

Brelsford R, “Turkmenistan commissions new methanol plant”, Oil & Gas Journal, https://www.ogj.com/refining-processing/article/14074727/turkmenistan-commissions-new-methanol-plant [accessed 17 November 2020].

Air Liquide, 2021, “Air Liquide supports the development of the largest Methanol plant in Africa”, https://www.engineering-airliquide.com/air-liquide-supports-development-largest-methanol-plant-africa#:~:text=This%20Methanol%20plant%2C%20to%20be,methanol%2C%20Lurgi%20MegaMethanol%E2%84%A2%2C%20which [accessed 2 April 2022].

Kang DM, Russek SL, Agrawal RE, Brengel DDS, and Foster EPW, “Production of oxygen by ion transport membranes with steam utilization”, EU Patent *EP132126B1*, 2006.

Kang DM, Thorogood RMC, Allam RJC, James AK, “Production of oxygen by ion transport membranes with steam utilization”, EU Patent *EP0658366B1*, 1998.

Han L, Deng G, Li Z, Fan Y, Zhang H, Wang Q and Ileleji KE, " Simulation and optimization of ion transfer membrane air separation unit in an IGCC power plant", *Applied Thermal Engineering,* vol. 129, pp. 1478–1487, 2018.

Kotowicz J, Brzeczek M, Walewska A and Szykowska K, "Methanol Production in the Brayton Cycle", *Energies*, vol. 15, pp. 1480, 2022.

Bai W, Feng J, Luo C, Zhang P, Wang H, Yang Y, Zhao Y and Fan H, "A comprehensive review on oxygen transport membranes: Development history, current status, and future directions", *International Journal of Hydrogen Energy,* vol. 46, pp. 36257 - 36290 , 2021.

Zhang X, Li S and Jin H, "A polygeneration system based on multi-input chemical looping combustion", *Energies*, pp. 7, 2014.

Kralj AK and Glavic P, "Optimization of gas turbine using NLP model", *Applied Thermal Energy*, pp. 454-548, 2007.

Methanol Institute, 2016, "MI-Combined-Slide-Deck-MDC-slides-Revised", chrome-extension://efaidnbmnnnibpcajpcglclefindmkaj/https://www.methanol.org/wp-content/uploads/2016/06/MI-Combined-Slide-Deck-MDC-slides-Revised.pdf [accessed 30 July 2022].

VarmlandsMetanol, 2021, "Methanol from wood residues – an excellent multipurpose fossil free chemical!", chrome-extension://efaidnbmnnnibpcajpcglclefindmkaj/http://www.varmlandsmetanol.se/dokument/Folder%20VM%202021%20eng.pdf [accessed 7 July 2022].

Carbon Recycling International, 2022, “CRI’s Largest CO_2-to-Methanol reactor installed in Anyang”, https://www.carbonrecycling.is/news-media/co2-to-methanol-reactor-installed-in-anyang [accessed 7 August 2022].

National Energy Technology Laboratory, “Air Separation Technology”, https://netl.doe.gov/carbon-management/gasification/air_separation [accessed 16 August 2022]

Carbon Recycling International, “Projects”, https://www.carbonrecycling.is/projects [accessed 6 August 2022].

Nyari J, “Techno-economic feasibility study of a methanol plant using carbon dioxide and hydrogen”, MSc thesis, KTH School of Industrial Engineering and Management, 2018.

Clausen LR, Houbak N and Elmegaard B, “Technoeconomic analysis of a methanol plant based on gasification of biomass and electrolysis of water”, *Energy*, vol. 35, pp. 2338-2346, 2010.

Machado CFR, de Medeiros JL, Araujo OFQ and Alves RMB, 2014, “A comparative analysis of methanol production routes: synthesis gas versus CO_2 hydrogenation”, *Proceedings of the 2014 International Conference on Industrial Engineering and Operations Management Bali,* Indonesia, chrome-extension://efaidnbmnnnibpcajpcglclefindmkaj/http://ieomsociety.org/ieom2014/pdfs/294.pdf [accessed 5 July 2022].

Matzen M, Alhajji M, Demirel Y, “Technoeconomics and Sustainability of Renewable Methanol and Ammonia Productions Using Wind Power-based Hydrogen”, *Journal of Advanced Chemical Engineering*, vol. 5, pp. 128, 2015.

Haldor Topsoe, “G2L™ eFuels Technology”, https://www.topsoe.com/our-resources/knowledge/our-products/process-licensing/g2ltm-efuels-technology [accessed 5 March 2022].

Otaraku IJ and Dada MA, “Energy Analysis of the Natural Gas to Hydrocarbon Liquids (GTL) Process Units”, *International Journal of Science and Technology*, vol. 4, 2014.

Zhu L, Zhou M, Shao C and He J, “Comparative exergy analysis between liquid fuels production through carbon dioxide reforming and conventional steam reforming”, *Journal of Cleaner Production*, pp. 88-98, 2018.

Li W, Zhuang Y, Liu L, Zhang L and Du J, “Process evaluation and optimization of methanol production from shale gas based on kinetics modeling”, *Journal of Cleaner Production*, pp.274, 2020.

Blumberg T, Morosuk T, and Tsatsaronis G, 2016, “Exergy-based evaluation of methanol production from natural gas”, *Research Gate*, conference paper, https://www.researchgate.net/publication/320271856_Exergy-based_evaluation_of_methanol_production_from_natural_gas [accessed 7 Aug 2022].

Philia J, Prameswari J and Widayat, “Pinch analysis of methane derived methanol plant using HINT software”, *E3S Web of conferences*, pp. 202, 2020.

Greeff IL, “Using synthesis gas heat to produce work via an externally fired gas power cycle”, *Energy*, vol 239, pp. 15, 2022.

Nayana VT and Gigi S, 2021, “Methanol synthesis – Dynamic simulation and heat integration”, *SSRN*, https://papers.ssrn.com/sol3/papers.cfm?abstract_id=3992757 [accessed 5 Aug 2022].

Boretti A and Banik BK, “Advances in hydrogen production from natural gas reforming”, *Advanced energy and sustainability research*, vol. 2, 2021.

Redondo B, Shah MT, Pareek V, Utikar RP, Webley PA, Patel J, Lee WJ and Bhatelia T, “Intensified isothermal reactor for methanol synthesis”, *Chemical Engineering and Processing*, pp 143, 2019.

Mbatha S, Everson RC, Musyoka NM, Langmi HW, Lanzini A and Brilman W, “Power-to-methanol process: A review of electrolysis, methanol catalysts, kinetics, reactor designs and modelling, process integration, optimisation, and techno-economics”, *Sustainable Energy and Fuels*, vol. 5, pp. 11, 2021.

Izabassarov D, Nyari J, Tekgul B, Laurila E, Kallio T, Santasalo-Aarnio A, Kaario Ossi and Vuorinen V, “A numerical performance study of a fixed-bed reactor for methanol synthesis by CO_2 hydrogenation” *International Journal of Hydrogen Energy*, vol. 46, 2021.

Madloch S, Dorcheh AS and Galetz MC, “Effect of Pressure on Metal Dusting Initiation on Alloy 800H and Alloy 600 in CO-rich Syngas”, *Oxidation of Metals*, vol.89, pp.483–498, 2018.

Smit R, Sprachman G, “Process for the preparation of syngas”, WO2016/074976A1, applicant Shell Internationale Research Maatschappij B.V, *The Hague*, 19 May 2016.

Ramireddy V, 2012, “An overview of combined cycle power plant”, *Electrical Engineering Portal,* https://electrical-engineering-portal.com/an-overview-of-combined-cycle-power-plant [accessed 21 September 2022].

Greeff IL and Ziqubu PP, “Flow sheet synthesis with heat engines for ITM air separation-based GTL processes”, *South African Chemical Engineering Congress*, pp. 210-220, 2021.

Taniguchi M, Asaoka H and Ayuhara T, “Energy saving air-separation plant based on exergy analysis”, KEBELCO Technology Review No. 33, *Shinko Air Water Cryoplant, Ltd.*, 2015.

Stanbridge S, (2016), “Teaching an old plant new tricks: The rise of the methanol plant revamp”, *Hydrocarbon Processing*, https://www.hydrocarbonprocessing.com/magazine/2016/july-2016/special-report-refinery-of-the-future/teaching-an-old-plant-new-tricks-the-rise-of-the-methanol-plant-revamp [accessed 1 September 2022].

Chapter 3

Methodology

3.1 Process flow sheet development

Development of a process flow sheet involves integration of multiple unit operations that characterize the process. The fundamental requirement is the identification of chemical reaction systems that convert and process the feedstock material into the desired product. Once the main chemical processing systems are set, utility systems can be defined and integrated. This involves rigorous process heat integration, determining heating and cooling requirements and developing a heat exchanger network. In high temperature processes such as the natural gas to methanol production process, efficient heat recovery is of prime concern. Converting the process heat to power is an important consideration as it can reduce the plant's net power requirements, and thus reduce the operating costs. This chapter outlines the methods applied in modeling and analyzing the conventional natural gas to methanol flow sheet and the development of a new, improved flow sheet.

3.1.1 Conventional case flow sheet process description

Figure 15 and Figure 16 present the conventional syngas and methanol production processes used to represent case A, the conventional case. The ATR technology was used for the conversion of natural gas to syngas. Methanol synthesis was achieved by employing an isothermal reactor technology. Cooling of syngas from the ATR is achieved by using a WHB, generating high pressure (HP) steam. Heating of the ATR feed is achieved by using a fired heater, with natural gas used as the fuel.

Syngas from the liquid knockout drum in the ATR process first enters the syngas compressor in the methanol synthesis process as can be seen in Figure 16. This is to increase the syngas pressure as methanol reactions occur at higher pressures than the

reforming reactions. From the compressor, the syngas is then preheated to the required inlet temperature of the methanol reactor. Due to the relatively lower methanol reactor temperature, medium pressure (MP) BFW is used as the cooling medium to control the reactor temperature, generating MP steam. The reactor product stream is conventionally cooled down by heat exchange with the reactor feed. The condensate from the product separator exits as crude methanol. The overheads from the separator is returned to the reactor as a recycle stream. A portion of the recycle is purged to remove inerts (nitrogen and argon) from the process. Further processing of the crude methanol product is not included in the scope of this work as it does not affect the objectives of the study. HP and MP steam generated in the ATR and methanol synthesis processes, respectively, are used to develop work in utility turbines. HP steam is superheated using natural gas as fuel in a fired heater before it is sent to the steam turbine, whereas purge gas is used as the fuel source for MP steam superheating.

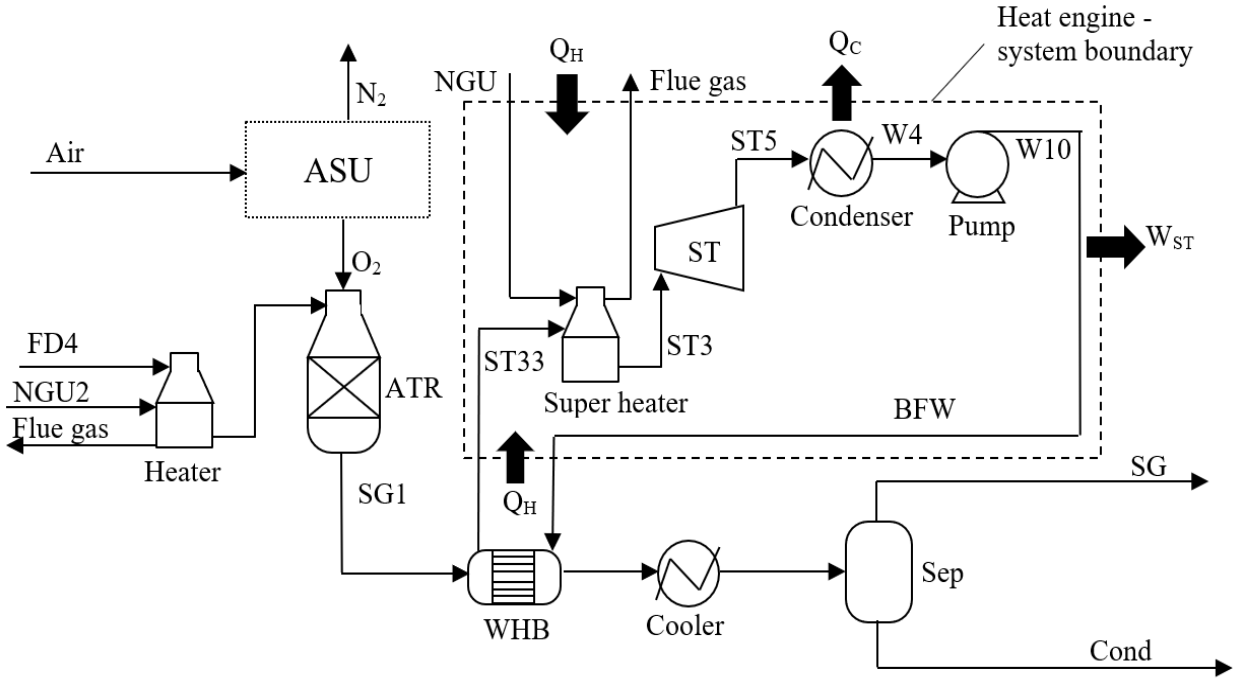

Figure 15 Conventional ATR process flow diagram, case A.

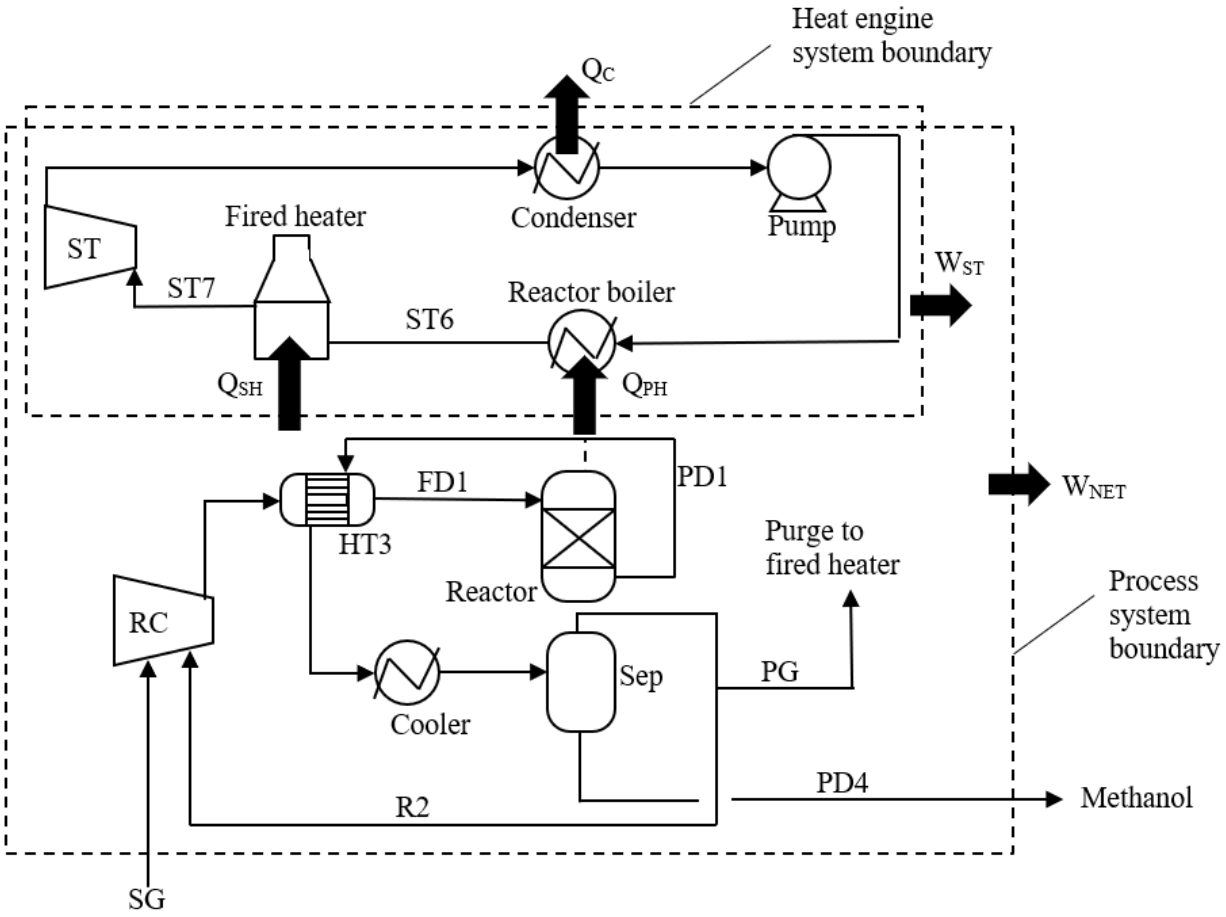

Figure 16 Conventional methanol synthesis process flow diagram, case A.

3.1.2 New flow sheet development

Figure 17 presents a summary of the steps taken in developing the new flow sheet. Starting with case A, presented in Figure 15 (ATR process) and Figure 16 (methanol synthesis), three opportunities for flow sheet improvement are explored.

The first opportunity is the replacement of the cryogenic ASU with an alternative technology, namely the novel ITM oxygen technology to produce a new flow sheet case, case B. Since the ITM oxygen technology operates at high temperatures similar

to the ATR technology (Blumberg et al., 2017), the integration of these technologies presents opportunities for alternative ways to cool the syngas, convert process heat to power, and possibly improve the overall plant efficiency by reducing energy costs for oxygen production.

The second opportunity is the heat recovery from the hot syngas leaving the ATR. Heat recovery from hot syngas in conventional processes is achieved by generating steam in a WHB. This steam is used to generate power, mostly consumed by the cryogenic ASU. The large temperature difference between the steam and syngas leads to a large exergy loss or energy penalties due to degradation of the quality of the available process heat. The amount of power that can subsequently be generated using the process heat, is also reduced, which translates to reduced overall plant thermal efficiency. Iandoli et al. (2007) reports that conventional methods of syngas cooling by generating steam contribute 20% to overall plant exergy losses for a gas-to-liquids plant comprising ATR technology, LTFT synthesis and a cryogenic ASU.

The third opportunity is the incorporation of the direct turbine expansion concept in the methanol synthesis loop. The conventional methanol synthesis process is typically well heat integrated by heat exchange between the reactor feed and product streams, with an acceptable temperature driving force of ±30 ºC. However, it was shown in previous research work that the net power requirement for syngas compression can be reduced if methanol reaction heat is converted to work by integrating a turbine expander on the outlet of the methanol reactor.

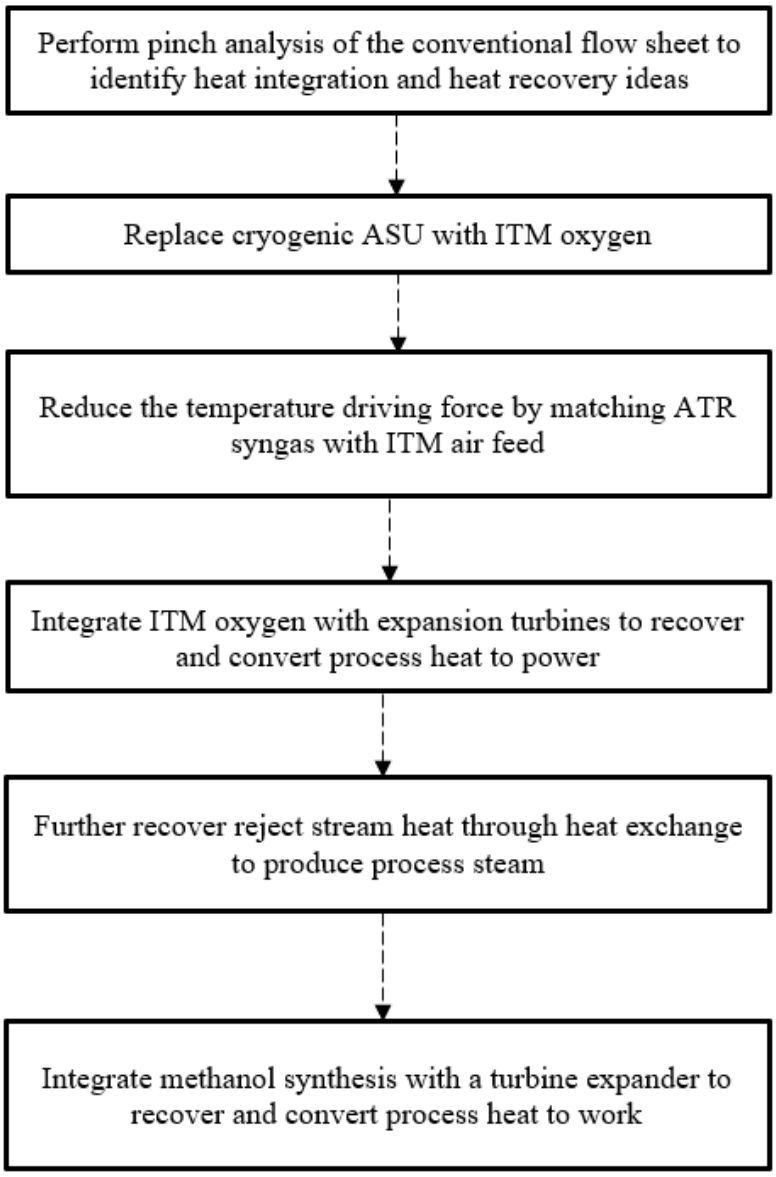

Figure 17 Flow sheet improvement flow diagram.

3.1.3 Process heat recovery

Power cycles are integrated into the ITM oxygen unit to configure the unit as a heat engine. This means that the system can be conceptually designed to co-produce oxygen and power as shown in Figure 18. Although there is no chemical reaction in

the membrane separator, the working fluid composition is changing from air which is compressed, to permeate and reject streams which are expanded in separate turbines. The reject stream exits the system boundary still at high temperature. Further heat recovery of the expanded reject stream is typically achieved by the use of a heat recovery steam generator (HRSG) (Anderson et al., 2011). In this flow sheet, the generated steam is used as process feed to the ATR.

Heat integration between the ATR and methanol synthesis units was considered impractical. This is based on the authors' work experiences in GTL and CTL processes in South Africa, where the ATR and methanol synthesis units are generally in separate geographical locations on a large petrochemical facility, making distance a limiting factor. Further, the different technologies may be provided by different licensors, making it a challenge to integrate a process stream of one technology unit with another stream from another technology unit. This limits integrating the existing MP steam cycle in the methanol synthesis unit with the reject stream from the ITM oxygen unit or the ATR syngas as a combined cycle to improve power production and thermal efficiency.

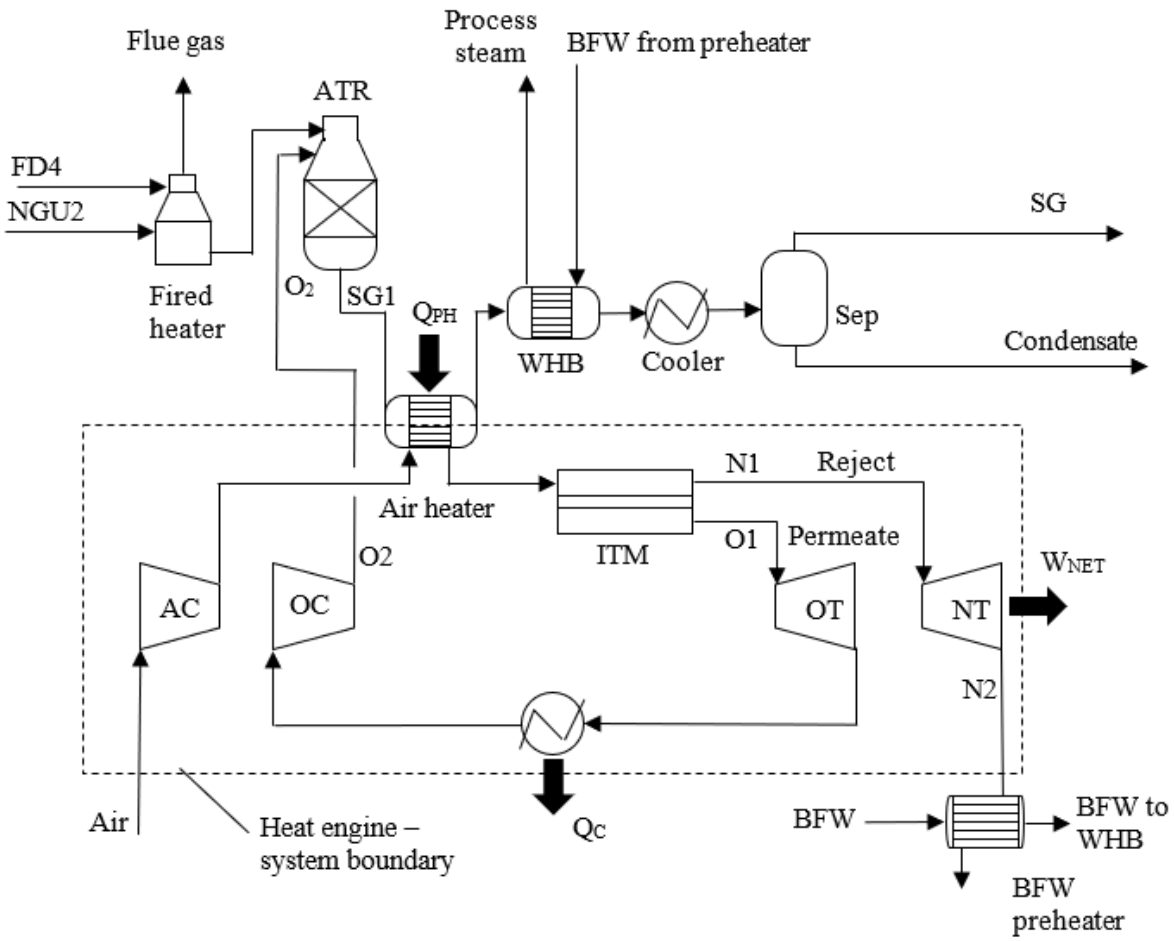

Figure 18 Integrated ITM oxygen power cycle, case B.

Since the methanol synthesis loop is typically well heat integrated, literature research for this unit is mostly focused on improving power production to supplement the syngas compressor power requirements. In this work, configuring the methanol synthesis process as a power production cycle by integrating a turbine expander on the outlet of the reactor was explored, as shown in Figure 19. Care should be taken however to maintain the process requirement to preheat the reactor feed to the required inlet temperature. This can be affected by the integrated turbine expander which reduces the temperature of the turbine exhaust stream.

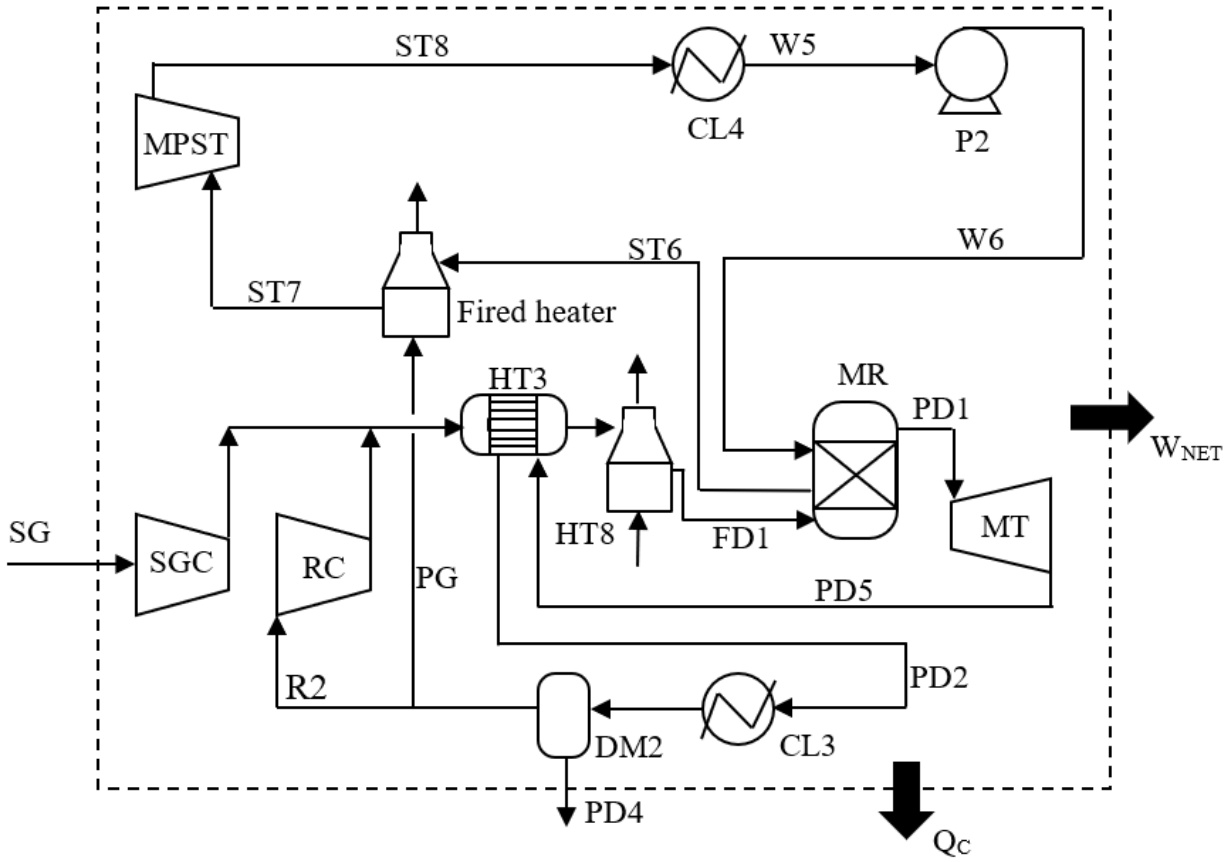

Figure 19 Integrated methanol synthesis process heat engine, case C

3.2 Flow sheet modeling

3.2.1 Simulation model construction

Aspen Plus V10 was chosen as the software for the simulation of the flow sheets in this work. The Soave-Redlich-Kwong (SRK) property method was selected in Aspen Plus to model the flow sheet cases (Greeff, 2004; Blumberg et al., 2016). The SRK equation of state is an empirical correlation that relates temperature, pressure and molar volume of gases to a compressibility factor. It is simple, reasonably accurate and commonly used in simulations where vapor-liquid equilibrium properties are required. Steam tables were used to determine properties of water and

steam. The ATR and methanol reactors were modeled as Gibbs equilibrium reactor models which determine the product composition at equilibrium by calculating the Gibbs free energy of the reaction systems. The reactions presented in equations 1-3 were specified for the ATR reactor and in equations 3-5 were specified for the methanol reactor. Construction of the model in Aspen Plus required specification of chemical components which were selected from a list of existing components within the software's databank. Process model palettes exist in Aspen Plus to choose from to model process equipment with associated libraries for calculation of process conditions such as temperature, pressure, composition, flowrates, duty and power.

Table 3 presents the composition of the main components in natural gas which was used as feed to the ATR reactor for syngas generation. This composition is similar to the composition used by Venter (2002) and Iandoli et al. (2007) to model an ATR. The composition of air feed to the cryogenic ASU that was specified in the model is presented on Table 4.

Table 3 Natural gas composition (Venter, 2002)

Component	**Composition (mol. %)**
CH_4	94.8
C_2H_6	2.6
N_2	1.60
CO_2	0.81

Table 4 Composition of dry air major components (Linde, 2019)

Component	**Composition (vol. %)**
N_2	78.08
O_2	20.95
Ar	0.93

3.2.2 Simulation model validation

The flow sheet model is validated using literature data for ATR and methanol synthesis model results. The ATR process model is validated using the work of Venter (2002) where an ATR operated at 24 bar and 975 °C generated syngas composition as presented on Table 5.

Table 5 ATR syngas composition (Venter, 2002)

Component	**Composition (mol/mol)**
CO	0.18
H_2	0.39
CO_2	0.08
H_2O	0.30
N_2	0.05

Figure 20 presents the product composition of the methanol reactor of Lucking (2017) used to validate the methanol reactor in this work.

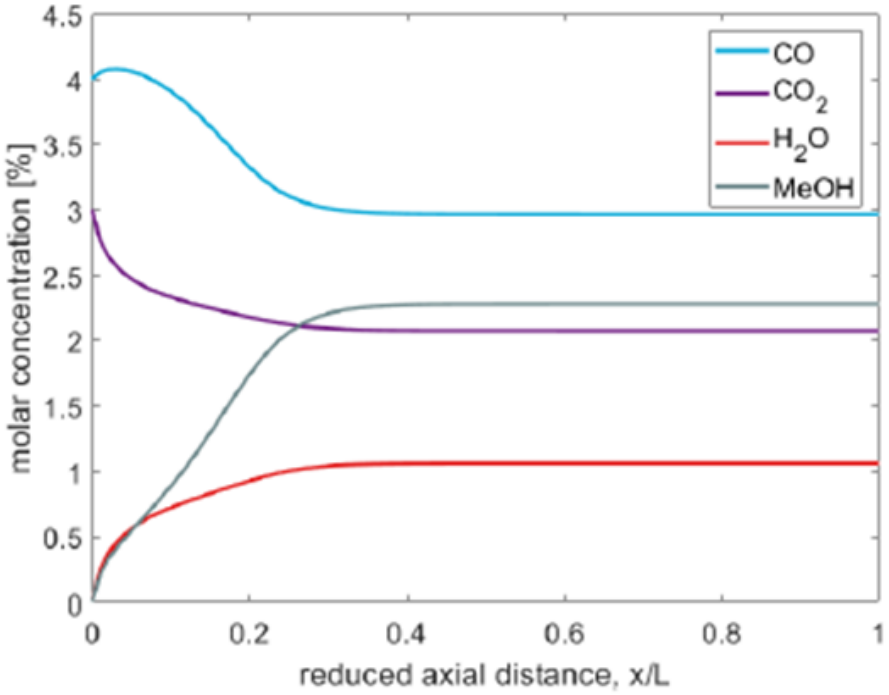

Figure 20 Methanol reactor product concentration profile (Lucking, 2017)

3.2.3 Aspen Plus process flow sheet model

Flow sheet models of the natural gas to methanol process were constructed in Aspen Plus V10. Figure 21 and Figure 22 present the conventional ATR and methanol synthesis flow sheet models, namely case A. It was not necessary to model the ASU in detail as the power requirement is known and the ASU cannot be directly integrated with the rest of the process as it operates at very low temperatures.

Figure 23 presents a new ATR flow sheet model, case B, with the integrated ITM oxygen as constructed in Aspen Plus. Figure 24 presents a model of the methanol synthesis process flow sheet, case C, configured as a power production cycle. Mass balance convergence within the typical tolerance of 0.0001 could be achieved in the flow sheets within the typical 30 number of iterations. Stream FD2 in Figure 22 and

Figure 24 is specified as a tier stream with a tolerance of 0.0001 for convergence of the circular iteration of the methanol recycle loop. 3.5% of the separator drum DM2 overheads is removed from the system as a purge. This is used as fuel gas in the MP steam superheater HT4. These Aspen Plus models were used to determine the stream and equipment material, heat and power results. The results of the Aspen Plus models were analyzed as discussed in section 3.3 below to investigate the objectives of this work.

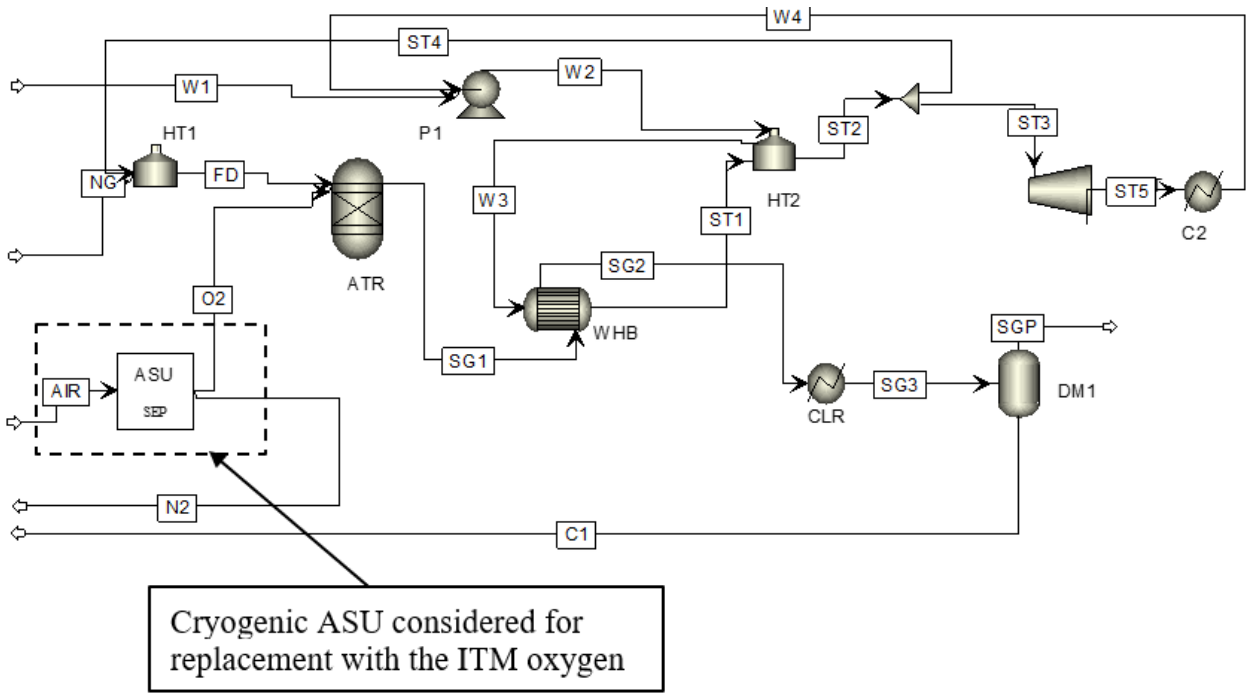

Figure 21 Conventional ATR process model in Aspen Plus, case A.

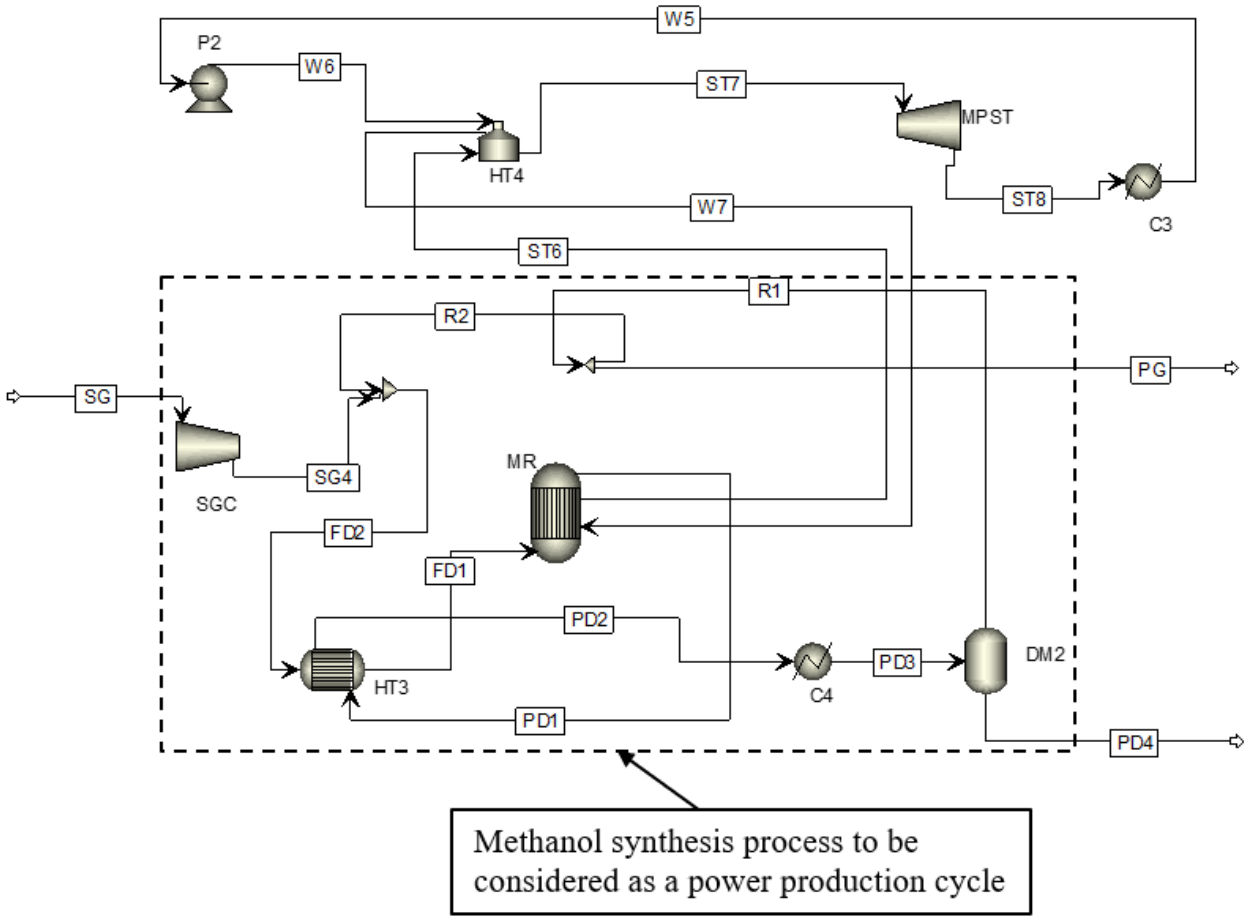

Figure 22 Conventional methanol synthesis model in Aspen Plus, case A.

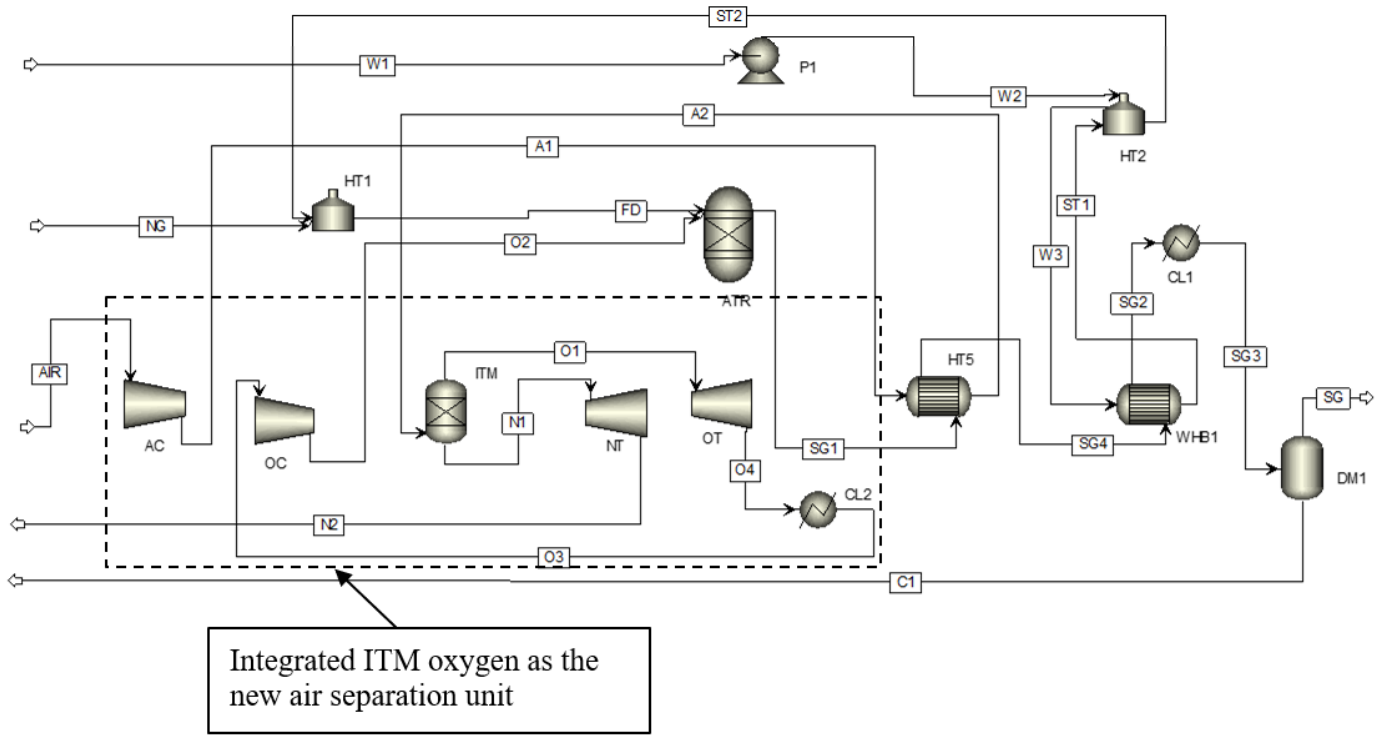

Figure 23 ATR process with integrated ITM oxygen in Aspen Plus, case B.

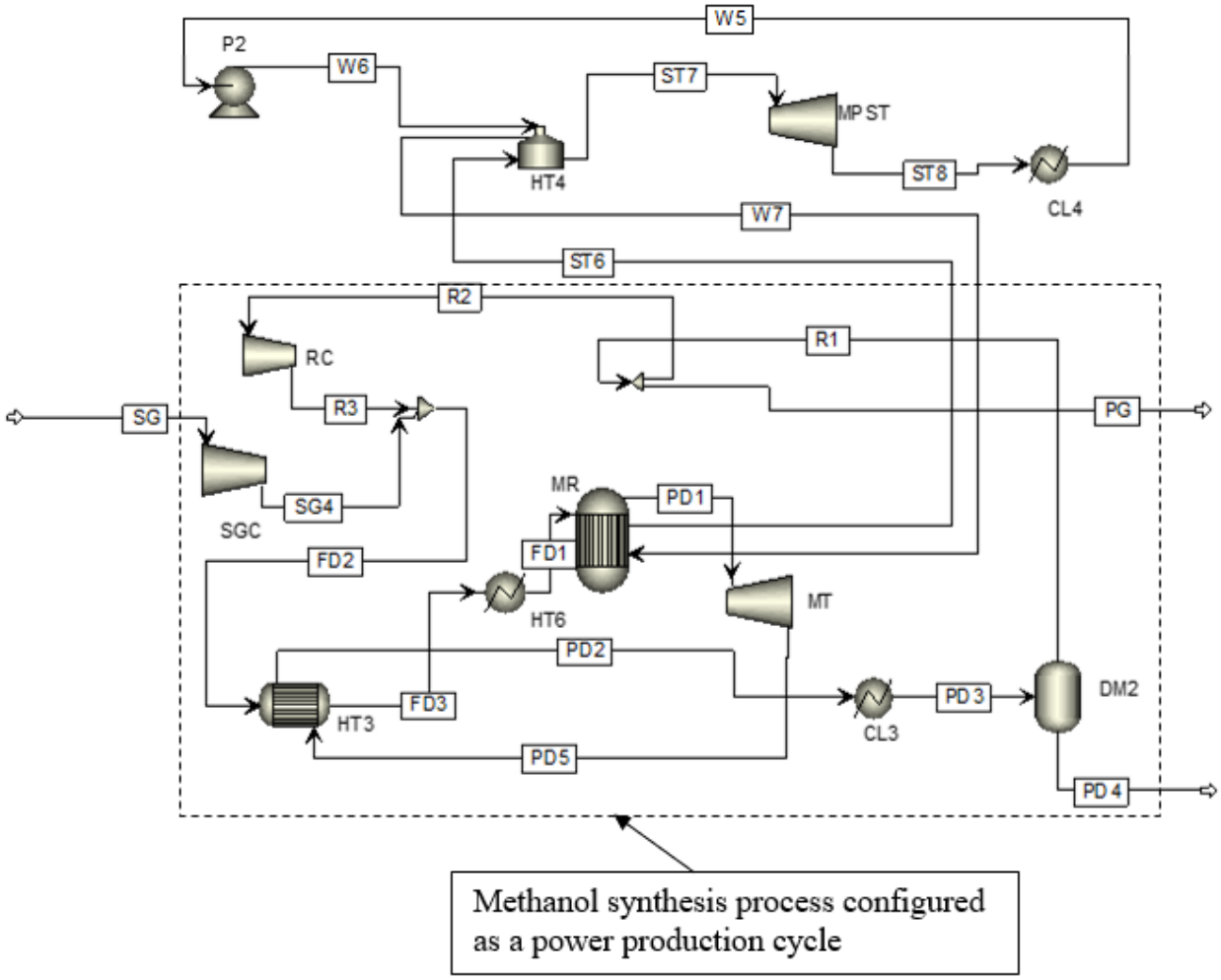

Figure 24 Methanol synthesis power cycle configured in Aspen Plus, case C.

3.2.4 Modeling of fired heaters

The natural gas and steam feed to the ATR as well as HP and MP steam are heated in fired heaters. The fired heaters were modeled as heat exchangers consisting of 2 sections, namely the radiation and convection sections as shown in Figure 25 and Figure 26. The convention section is used for preheating while the higher temperature radiation section is used for superheating. Natural gas is used as fuel for the ATR feed and steam, while the purge gas from the methanol synthesis loop is

used in the MP steam fired heater as fuel. Air is used as the source of oxygen for the combustion of the fuel. In Aspen Plus, the amount of heat transferred in the radiation section was determined by modeling the combustion reaction in a Gibbs reactor. The convection section is modeled as a heat exchanger with flue gas as the heating medium.

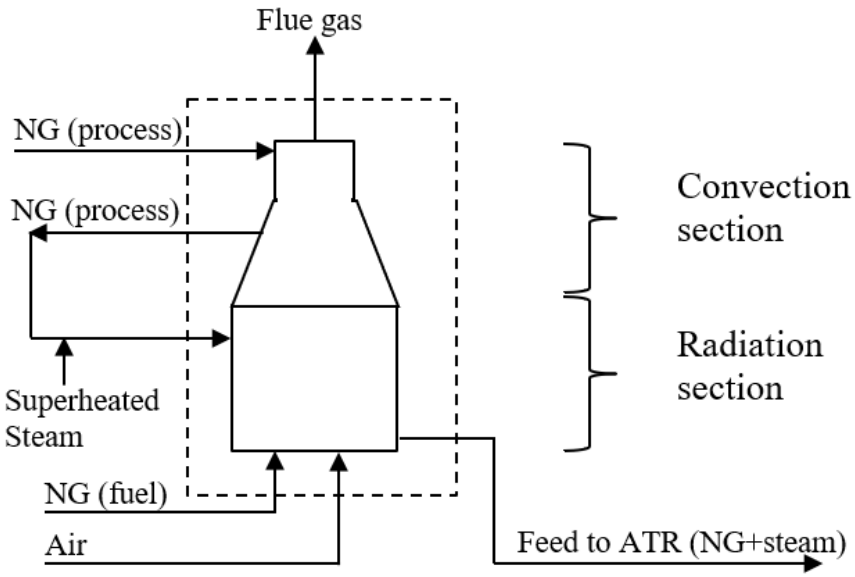

Figure 25 Fired heater used for ATR feed (NG and steam) preheating.

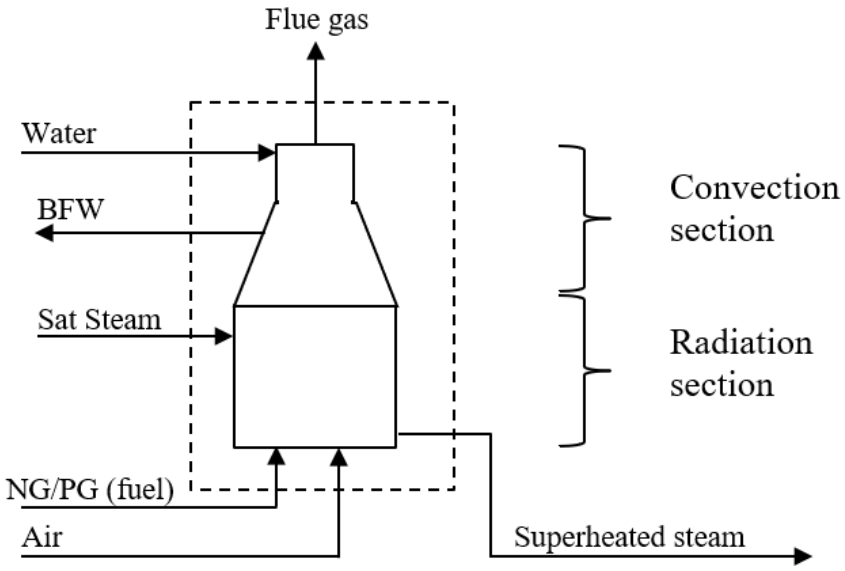

Figure 26 Fired heater used for water preheat and steam superheat.

3.2.5 Flow sheet basis and assumptions

The flowrate specification in the model was based on the largest single installed methanol plant in Turkmenistan, having the capacity of 5225 t/day methanol. A specific power consumption of 0.33 kWh/Nm^3 oxygen (Beysel, 2009) was used to determine the unit power consumption for the required oxygen production capacity in the cryogenic ASU in case A.

The main assumptions made in the simulation of the natural gas to methanol flow sheet cases are as follows;

- The ATR reactor is well insulated and therefore adiabatic. Equipment are also adequately insulated and heat loss to the environment is negligible.
- There are no long-chain heavy hydrocarbons in the natural gas requiring a pre-reformer simulation.
- There is no sulfur in natural gas requiring sulfur removal simulation.

- There are no alkene and alkyne hydrocarbons in natural gas requiring saturation.
- The ATR and methanol reactors are equilibrium reactors.
- Line frictional losses are relatively small compared to the flow sheet pressure profile and therefore negligible. Pressure losses through the equipment was also assumed to be negligible.
- An isentropic efficiency of 85% was specified for all compressors and turbines.
- The process is modeled at steady state conditions.
- Natural gas enters the flow sheet boundary at ambient temperature of 30 °C and at the required ATR pressure of 24 bar.
- Air enters the flow sheet boundary at standard temperature and pressure of 25 °C and 1 atm.
- Selectivity of methanol is over 99%, thus, side reactions and by-products are considered negligible.

3.3 Flow sheet analysis

3.3.1 Introduction

This section presents the methods applied in the analysis of the process flow sheet models. The pinch analysis method, used to evaluate the minimum energy requirements and identify opportunities for process heat integration, is discussed. Methods applied in the analysis of the exergy performance of the flow sheet cases is also discussed. For the power cycles, thermal efficiency calculation methods are discussed, and the applicable equations are presented. The overall plant and process efficiency as well as the specific gas efficiency calculation methods are also

discussed. These were used to assess and compare efficiency and energy performance in each process flow sheet case.

3.3.2 Pinch analysis

Pinch analysis of the flow sheet cases was conducted in Aspen Energy Analyzer. The steps followed in the pinch analysis method are summarized in Figure 27. The analysis begins by labelling each process stream in the flow sheet with temperature, pressure, flow and composition. This data was then used to generate the composite curves (temperature-enthalpy curves) of the cooling and heating streams, plotted on one graph. The pinch point was determined as the point of minimum temperature deference between the cold and hot composite curves. The minimum heating and cooling requirements were determined from the curves as the targets. The cooling and heating process streams were then matched starting from the pinch point and moving up or downwards to avoid cross pinch (Kemp, 2007).

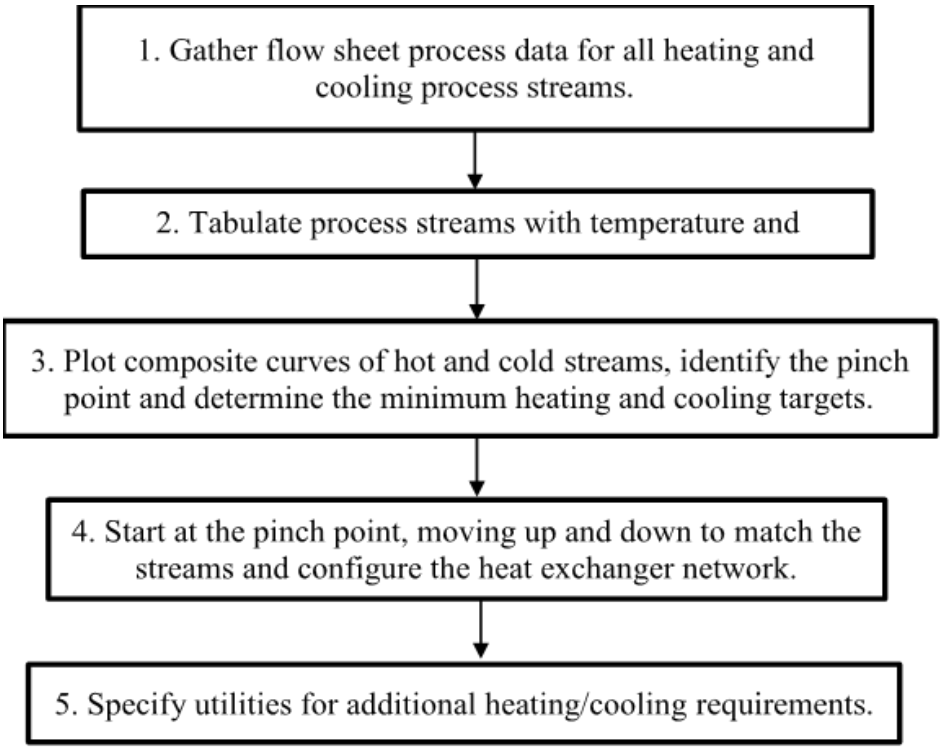

Figure 27 Heat transfer pinch analysis methodology (Kemp, 2007).

3.3.3 Exergy analysis techniques

Exergy is the maximum work which can be theoretically recovered from a system that is in equilibrium with its environment within a system boundary. It is based on the second law of thermodynamics which describes the amount of useful work which can be developed from a system as it transfers heat or does work.

The exergy rate balance which is made up of exergy transfer accompanying heat transfer (E_q) and work (E_w) and, exergy destruction (E_d), was used to calculate the plant equipment's exergy destruction in each flow sheet case (Moran et al., 2006).

$$0 = \sum_j \left(1 - \frac{T_0}{T_j}\right) Q_j - W_{cv} + \sum_i m_i e_{fi} - \sum_e m_e e_{fe} - E_d \quad (8)$$

where e_f is the exergy of the stream components entering the system at inlet i and exiting at exit e, Q_j is the heat transfer at temperature T_j, T_0 is the reference temperature and W_{cv} is the work done by the controlled volume.

This exergy rate balance can also be expresses as follows:

$$0 = \sum_j E_{Qj} - W_{cv} + \sum_i E_i - \sum_e E_e - E_d \quad (9)$$

With the assumption that equipment is adequately insulated and heat loss to the environment is negligible, the exergy transfer accompanying heat transfer is considered negligible. The exergy destruction can then be evaluated as follows:

$$E_d = -W_{cv} + \sum_i E_i - \sum_e E_e \quad (10)$$

The exergy destruction of the methanol reactor where heat is transferred to a steam system was evaluated as follows:

$$E_d = \sum_j E_{Qj} + \sum_i E_i - \sum_e E_e \quad (11)$$

For equipment with no work done such as heat exchangers, reactors and separators, the exergy destruction was evaluated as follows:

$$E_d = \sum_i E_i - \sum_e E_e \quad (12)$$

The stream exergy for the ITM oxygen, flash separators as well as the ATR and methanol reactors with composition changes was evaluated using the following equation which is a combination of thermomechanical and chemical exergy (Moran et al., 2006);

$$e_f = h - h_0 - T_0(s - s_0) + \frac{V^2}{2} + gz + e^{ch} \quad (13)$$

where the mixture chemical exergy e^{ch} of a stream is defined as follows (Moran et al., 2006);

$$e^{ch} = \sum_{i=1}^{j} y_i' e_i^{ch} + RT_0 \sum_{i=1}^{j} y_i' \ln y_i^i \quad (14)$$

where y'_i is the mole fraction of component i and e_i^{ch} is the standard molar chemical exergy of component i. The standard molar chemical exergy values for the stream components, presented on Table 21, Appendix D, were obtained from Moran et al. (2006).

Thermomechanical exergy of streams and components were determined using the Aspen Plus software. The software however does not calculate chemical exergy. Several authors have generated tools to calculate chemical exergy of chemical processes (Gray, 2019). In this work, an excel tool was developed by the authors for the chemical exergy calculations using standard molar chemical exergy values.

3.3.4 Thermal efficiency

The performance of a heat engine can be measured by its thermal efficiency. The thermal efficiency is generally defined as the ratio of the work done over the heat input. There can be many definitions depending on the application and the configuration of the heat engine. The thermal efficiency is affected by that not all the heat input is converted to work, some of it is lost because of the real system's irreversibilities caused by mechanical friction, heat losses and design inefficiencies. As a result of irreversibilities, isentropic efficiencies for compressors and turbines typically range from 70 to 90% (Connor, 2019).

The thermal efficiency of the ITM oxygen cycle in case B in Figure 18 is defined as follows:

$$\eta_{ITM} = \frac{W_{NT}+W_{OT}-W_{AC}-W_{OC}}{Q_{AH}} = \frac{W_{NET}}{Q_{AH}} \quad (15)$$

where W_{NT}, W_{OT}, W_{AC} and W_{OC} are the work of the nitrogen turbine, oxygen turbine, air compressor and oxygen compressor and Q_{AH} is the duty of the air heater.

Thermal efficiency of the MP and HP steam Rankine cycles in case A are defined as follows:

$$\eta_{MP\ steam} = \frac{W_{MPST}}{Q_{MR}+Q_{HT4}+Q_{HT7}} \quad (16)$$

$$\eta_{HP\ steam} = \frac{W_{HPST}}{Q_{WHB}+Q_{HT9}+Q_{HT10}} \quad (17)$$

where W_{MPST}, W_{HPST} are the work of the MP and HP steam turbines, Q_{MR} is heat removed from the methanol reactor, Q_{WHB} is the WHB duty, Q_{HT7} and Q_{HT9} are the MP and HP steam preheaters, Q_{HT4} and Q_{HT10} are the MP and HP steam superheaters, respectively.

The ITM oxygen power cycle was configured to also provide process heat via BFW preheat and saturated steam superheat. The saturated steam is produced in a WHB downstream of the air heater and is used as feed to the ATR. For this unique combined steam, oxygen and power production system, the following energy-based efficiency definition is proposed:

$$\eta = \frac{W_{NET}+P_{ST}}{Q_{SG}} = \frac{W_{NET}+P_{ST}}{Q_{AH}+Q_{WHB}} \quad (18)$$

where P_{ST} is the load of steam in MW which is determined using the steam flow rate and the specific enthalpy of evaporation. Q_{SG} is the total syngas process heat used, which comprises Q_{AH} and Q_{WHB}. Figure 28 shows a schematic with the system boundary for this system.

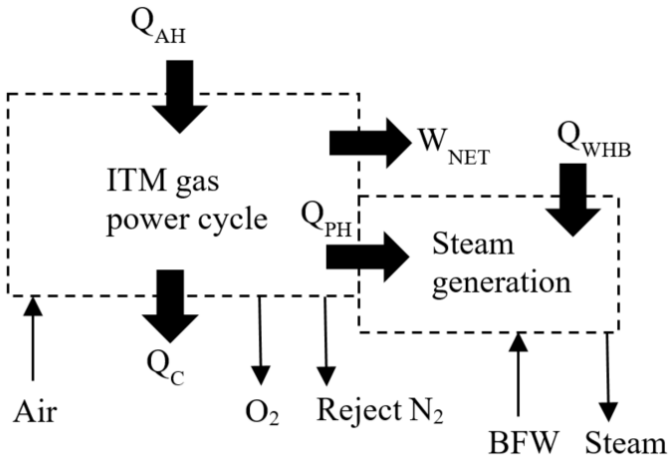

Figure 28 ITM oxygen combined steam, oxygen and power production system.

The methanol power production cycle however, resembles the combustion gas turbine cycle because the source of heat is the exothermic chemical reactions occurring in the methanol reactor as shown in Figure 19. Some of the heat from the reactor is used in the MP steam cycle where steam generated from the reactor temperature control system is used as the working fluid. The combined gas and steam power cycle net work and the lower heating value (LHV) energy input are used to determine the thermal efficiency as follows:

$$\eta_{\text{meth cycle}} = \frac{W_{NET}}{LHV_{feed} - LHV\ prod} \qquad (19)$$

3.3.5 Overall process and plant efficiency

The two main parameters often used to express the efficiency of a process are the process efficiency and the carbon efficiency. Process efficiency is a measure of the utilization of the energy of the natural gas feedstock to make the product (in this case methanol), whereas carbon efficiency is a measure of the conversion of the carbon atoms in the feedstock to make the product. The process efficiency of a natural gas to methanol plant is about 75% (Matzen et al., 2015). GTL plants typically have carbon efficiencies of about 77%, with the balance being due to the production of CO_2 (Dong et al., 2008).

The carbon efficiency was determined as follows:

$$\eta_{\text{carbon}} = \frac{\text{Carbon molecules in product}}{\text{Carbon molecules in natural gas}} \quad (20)$$

To determine the process efficiency of the overall flow sheet the following equation is proposed:

$$\eta_{\text{process}} = \frac{\text{LHV}_{\text{crude methanol}} + W_{\text{NET}}}{\text{LHV}_{\text{NG to process}}} \quad (21)$$

where $\text{LHV}_{\text{crude methanol}}$ is the lower heating value of the crude methanol product and $\text{LHV}_{\text{NG to process}}$ is the lower heating value of the natural gas feed to the ATR in MW.

For the overall plant efficiency, the following equation is proposed:

$$\eta_{plant} = \frac{LHV_{crude\ methanol} + W_{NET}}{LHV_{NG\ to\ process\ and\ utility}} \quad (22)$$

where $LHV_{crude\ methanol}$ is the lower heating value of the crude methanol product and $LHV_{NG\ to\ process\ and\ utility}$ is the lower heating value of the natural gas feed to the ATR and to the utility system in MW.

3.3.6 Specific gas efficiency

Specific gas efficiency is a measure of the utilization of the natural gas feedstock to produce methanol. The specific gas efficiency was evaluated as follows:

$$\text{Specific gas efficiency} = \frac{LHV_{NG} - W_{NET}}{m_{meth}} \quad (23)$$

where LHV_{NG} is the LHV of natural gas, W_{NET} is the net work output and m_{meth} is the mass flowrate of methanol product.

3.4 References

Gray TD, "An introduction to exergy and its evaluation using Aspen Plus", MSc thesis, Kansas State University Center for Advanced Energy Systems, 2019.

Dong L, Wei S, Tan S, & Zhang H, "GTL or LNG: Which is the best way to monetize "stranded" natural gas?", *Petroleum Science*, pp. 388-394, 2008.

Greeff IL, "Using synthesis gas heat to produce work via an externally fired gas power cycle", *Energy*, vol 239, pp. 15, 2022.

Moran MJ, Shapiro HN, "Chapter 7 - Exergy analysis in Fundamentals of engineering thermodynamics", pp. 272-324. *John Wiley & Sons Inc*, 2006.

Kemp IC, "Pinch analysis and process integration", *Elsevier*, 2nd Ed, 2007.

Connor N, 2019, "*What is Thermal Efficiency of Steam Turbine – Definition",* https://www.thermal-engineering.org/what-is-thermal-efficiency-of-steam-turbine-definition/ [accessed 20 May 2022].

Philia J, Prameswari J and Widayat, "Pinch analysis of methane derived methanol plant using HINT software", *E3S Web of conferences*, pp. 202, 2020.

Venter JA, "Modelling and exergy analysis of the natural gas to hydrocarbon liquid (GTL) process", MSc thesis, University of Pretoria, 2002.

Linde, 2019, "History and Technological Progress. Cryogenic Air Separation", *Linde Engineering: Air Separation*, chrome-extension://efaidnbmnnnibpcajpcglclefindmkaj/https://www.linde-engineering.com/en/images/Air-separation-plants-history-and-technological-progress-2019_tcm19-457349.pdf [accessed 13 April 2021].

Chapter 4

Results and Discussion

4.1 Introduction

This chapter presents the results of this study to develop an improved natural gas to methanol flow sheet. The conventional flow sheet efficiency performance is analyzed, and the results are used for comparison with the new flow sheet. Results of these flow sheets are presented in graphical and tabular format to clearly outline their differences. Available literature references of plant performance are quoted for comparison. Combined heat and power results are discussed to highlight improvement in power production which results in reduced overall energy requirements. Pinch analysis results are discussed, highlighting cost implications to achieve minimum energy requirements. Exergy analysis results of the entire flow sheets are then analyzed to identify sections of the flow sheets with high exergy losses. Improvement in exergy losses of the new flow sheet is discussed and compared to the conventional case.

4.2 Model validation

Validation of a model is important to ensure that the model reflects and represents a real process. The Aspen Plus models used to simulate the flow sheet were validated using literature data gathered for the ATR and Methanol synthesis processes. For the ATR process, the validation was carried out by using the work of Venter (2002). The syngas composition results from this model were compared to that of Venter (2002) as presented on Table 6. Some slight deviations, within 10%, in the results were noted mainly due to the assumptions made in the models of this work. The ATR temperature of this work was increased to a temperature of 1033 °C to adjust the H_2/CO ratio in the syngas as required for a methanol synthesis. This is because the work of Venter (2002) generated syngas for a Fischer-Tropsch process which is

different to methanol synthesis. This temperature is still within typical ATR operating temperatures (Blumberg et al., 2017). The syngas composition is presented on Table 7. For the methanol synthesis process, the validation was carried out by using the reactor conversion results of Lucking (2017) as presented on Table 8. The methanol conversion was found to be 0.30 mol/mol in this work, while the work of Lucking (2017) achieved a conversion of 0.33 mol/mol per reactor pass, reflects a 9% deviation. The assumptions made in the models can be found in section 3.2.5. These validated models were used to perform the study of this work as per the study objectives.

Table 6 ATR syngas composition (975 °C, 24 bar)

Component	Unit	Syngas composition (Venter, 2002)	Syngas composition in this work	% deviation(1)
CO	mol/mol	0.18	0.17	6%
H_2	mol/mol	0.39	0.43	10%
CO_2	mol/mol	0.08	0.08	0%
H_2O	mol/mol	0.30	0.31	5%

(1) $\%\ deviation\ = \frac{Literature\ data - Data\ in\ this\ work}{Literature\ data}$

Table 7 ATR syngas composition (1033 °C, 24 bar)

Component	Syngas composition in this work
CO	0.23
H_2	0.53
CO_2	0.04
H_2O	0.19

Table 8 Methanol reaction conversion

	Conversion of Lucking (2017)	Conversion in this work	% deviation(1)
Methanol single pass conversion	0.33	0.30	9%

(1) $\% \, deviation = \frac{Literature\ data - Data\ in\ this\ work}{Literature\ data}$

4.3 Aspen simulation results

4.3.1 Summary of main process stream results

The main process and utility stream conditions for the three cases; A, B and C are shown on Table 9. Detailed material and heat balance tables can be found in Appendix A. Case A shows the results of the base case flow sheet. Case B shows the results of the flow sheet where the main change was the replacement of the cryogenic air separation unit with the ion transport membrane oxygen unit for oxygen production. Case C presents a case where case B is further modified by configuring the methanol synthesis loop as a power production cycle. Comparison of the results show that there are no significant differences in the process material and heat results of these cases. This is because the flowrate basis and the main processing steps were maintained in all cases to achieve a fair comparison and enable quantifying of the results of the modification in each flow sheet case. Stream entropy and exergy destruction results are also presented to reflect the amount of irreversibilities in the streams. Similarly, there were no major differences in the stream entropy and exergy destruction in each case as a result of the processing steps being maintained. The ATR process in the new flow sheet contains no steam power cycle. This is because the syngas was found to only have enough heat to produce process steam for the ATR feed after the ITM oxygen was integrated.

Table 9 Conventional and integrated flow sheet mass balance

Case A							
Stream	Fluid	*m*	*P*	*T*	*H*	*S*	E_d
		ton/h	bar	°C	MW	MW/°C	MW
FD4	Natural gas and steam	225	24	274	-472	-0.20	1802
NGU2	Natural gas	7.0	24	30	-8.9	-0.012	93
O2	Oxygen	136	24	150	4.3	-0.019	15
NGU	Natural gas	10	24	30	-12.6	-0.017	139
SG1	Syngas	360	24	1033	-423	0.33	1702
SG	Syngas	267	24	30	-333	0.034	1534
FD1	Syngas	663	90	250	-758	0.058	3412
PD1	Methanol product	663	90	280	-921	-0.22	3334
R2	Syngas	396	90	30	-529	-0.17	1831
PG	Syngas	14	90	30	-19	-0.0062	66
ST33	Steam	265	40	250	-964	-0.24	116
ST3	Steam	265	40	448	-930	-0.18	134
ST5	Steam	265	1	102	-981	-0.16	75
W4	Condensate	265	1	102	-1150	-0.61	6
W10	Condensate	265	1	102	-1150	-0.61	7
ST6	Steam	305	10	180	-1136	-0.28	105
ST7	Steam	305	10	229	-1106	-0.22	121
PD4	Methanol product	252	90	30	-555	-0.50	1389
Case B							
Stream	Fluid	*m*	*P*	*T*	*H*	*S*	E_d
		ton/h	bar	°C	MW	MW/°C	MW
FD4	Natural gas and steam	225	24	274	-472	-0.20	1801
NGU2	Natural gas	7.0	24	30	-8.9	-0.012	93
O2	Oxygen	136	24	153	4.4	-0.019	15
SG1	Syngas	360	24	1034	-423	0.33	1702
Air	Air	585	1.0	25	-0.046	0.026	1

O1	Oxygen	136	24	900	34	0.021	32
N1	Nitrogen	449	24	900	120	0.071	103
N2	Nitrogen	449	24	337	41	0.096	16
SG	Syngas	267	24	30	-333	0.033	1534
FD1	Syngas	674	90	250	-762	0.058	3413
PD1	Methanol product	674	90	280	-925	-0.22	3334
R2	Syngas	407	90	30	-534	-0.17	1832
PG	Syngas	15	90	30	-19	-0.0063	66
ST6	Steam	305	10	180	-1136	-0.28	105
ST7	Steam	305	10	230	-1106	-0.22	121
PD4	Methanol product	252	90	30	-555	-0.50	1388

Case C

Stream	Fluid	*m*	*P*	*T*	*H*	*S*	E_d
		ton/h	bar	°C	MW	MW/°C	MW
FD4	Natural gas and steam	225	24	274	-487	-0.22	1802
O2	Oxygen	136	24	153	4.4	-0.019	15
SG1	Syngas	361	24	1034	-423	0.33	1703
Air	Air	585	1.0	25	-0.046	0.026	1
O1	Oxygen	136	24	900	34	0.021	32
N1	Nitrogen	449	24	900	120	0.071	103
N2	Nitrogen	449	24	337	41	0.096	16
NGU2	Natural gas	7.0	24.0	30	-8.9	-0.012	93
SG	Syngas	267	24	30	-333	0.034	1534
FD1	Syngas	711	90	250	-837	0.069	3398
PD1	Methanol product	711	90	280	-1000	-0.21	3320
PD5	Methanol product	711	70	253	-1011	-0.21	3307
PD2	Methanol product	711	70	131	-1077	-0.36	3285
R2	Syngas	445	70	30	-611	-0.15	1813
PG	Syngas	16	70	30	-22	-0.0053	66
ST6	Steam	305	10	180	-1137	-0.28	105
ST7	Steam	305	10	226	-1107	-0.22	120

ST8	Steam	305	1	102	-1137	-0.20	84
W5	Condensate	305	1	102	-1324	-0.70	7
W6	Condensate	305	1	102	-1324	-0.70	8
PD4	Methanol product	250	70	30	-551	-0.50	1386

4.3.2 Natural gas consumption

Figure 29 presents the overall natural gas consumption for case A, B and C, including utility natural gas. 128 t/h natural gas (94.8 wt.% methane) is used as process feed to produce 252 t/h crude methanol containing 88 wt.% methanol in case A and B. Case C consumes the same 128 t/h natural gas to produce 250 t/h crude methanol, also containing 88 wt.% methanol purity. The production rate of pure methanol is 5322 t/day for case A/B and 5280 t/day for case C. This is in line with the target capacity of 5225 t/day. The methanol synthesis process configured as power production cycle in case C as shown in Figure 24 results in a 2 t/h (0.8%) decrease in the production rate of crude methanol. This is due to the flash pressure of 70 bar which is lower than case A pressure of 90 bar in the liquid knockout drum DM2, as can be seen in Figure 24. The lower pressure is caused by turbine expansion of the reactor product stream in case C. This 2 t/h product is circulated in the process together with the feed gas recycle. The circulated product negatively impacts the energy efficiency as it needs to be re-heated and re-compressed to the reactor inlet conditions. To mitigate this effect, a lower flash temperature in DM2 is required which can be achieved at a cost.

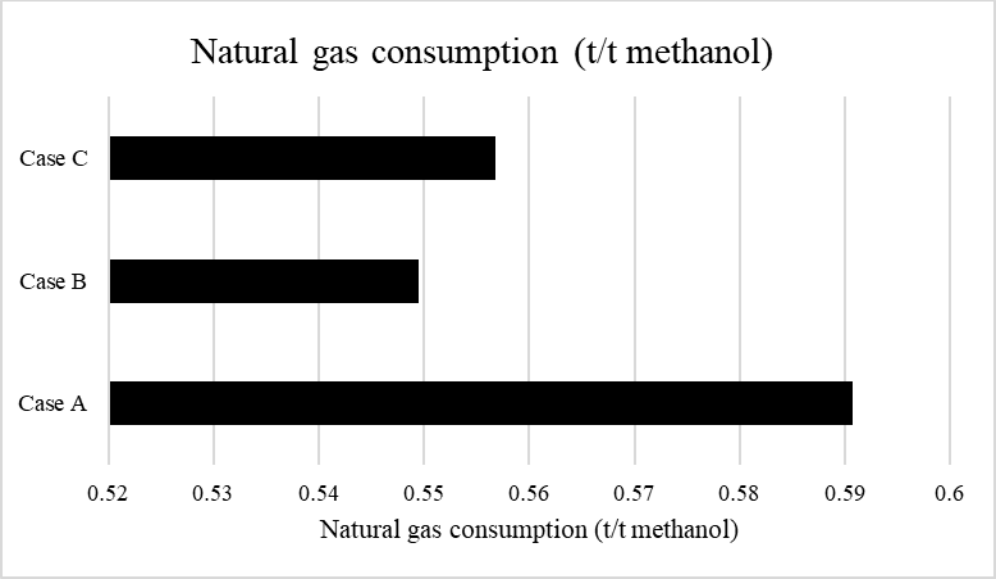

Figure 29 Overall specific natural consumption including utility fuel

Case A further consumes 17 t/h of natural gas as fuel gas. This is used in fired heaters for feed gas and steam heating. The feed gas preheater consumes 7 t/h to heat up a mixture of steam and natural gas before it is fed to the ATR in cases A, B and C. Saturated HP steam from the WHB is superheated in a fired heater consuming 10 t/h of natural gas in case A. The specific methane consumption for methanol production in case A, B and C, which was found to be 0.52, 0.52 and 0.53 t/t methanol, is similar to typical specific methane consumptions found in literature (Blumberg et al., 2016).

4.4 Flow sheet block flow diagrams

Figure 30, Figure 31 and Figure 32 show the block flow diagrams for case A, B and C, respectively. These figures are useful to demonstrate the changes in the new flow sheet synthesis compared to the conventional case. The block flow diagrams are made up of the main process units, namely, the ATR process, ASU and methanol

synthesis as well as the utility unit, product distillation and storage and, offsite facilities. There was no need to include the product upgrading units and offsite facilities in this study as it did not have a significant impact on the study objectives and results. A condensate stream from the ATR syngas product is removed as reaction water. This can be sent for further processing in an offsite facility and potentially reused as cooling water. Flue gas, containing mainly CO_2 and steam, is removed from fired heaters and sent to the atmosphere. In each unit block, net utility and/or power requirements are shown.

Analysis of these figures shows that is it possible to integrate the ITM oxygen into the natural gas to methanol process. Case A in Figure 30 presents the conventional flow sheet block flow diagram. In case B, the cryogenic ASU of case A is replaced by the ITM oxygen unit. The air heating and power requirements of the ITM oxygen unit are provided from internal process heat recovery. From case A to case B, the amount of natural gas used as utility fuel decreased from 17 t/h to 7 t/h. Similarly, the amount of flue gas generated, which is a waste stream composed mostly of nitrogen and CO_2, decreased significantly from 466 t/h to 247 t/h. This is due to the significantly reduced steam system and use of fired heaters. Further, the 32 MW of power requirement by the cryogenic air separation unit in case A is eliminated by the integration of the ITM oxygen unit in case B. Replacing the cryogenic ASU with the ITM oxygen therefore facilitated the improvement in power production from case A to case B. Case B is further modified to develop case C. In case C, the methanol unit is configured to co-produce methanol and power by direct gas turbine expansion. As a result, the net cooling utility requirements for the crude methanol product decreased from 295 MW to 108 MW. The amount of crude methanol product slightly decreased due to flash separation at a lower pressure caused by the direct turbine expansion. In all the flow sheet cases it was found that enough power

is generated to drive all the power-driven machines, with an excess of 19 MW case A, 28 MW case B and 32 MW case C.

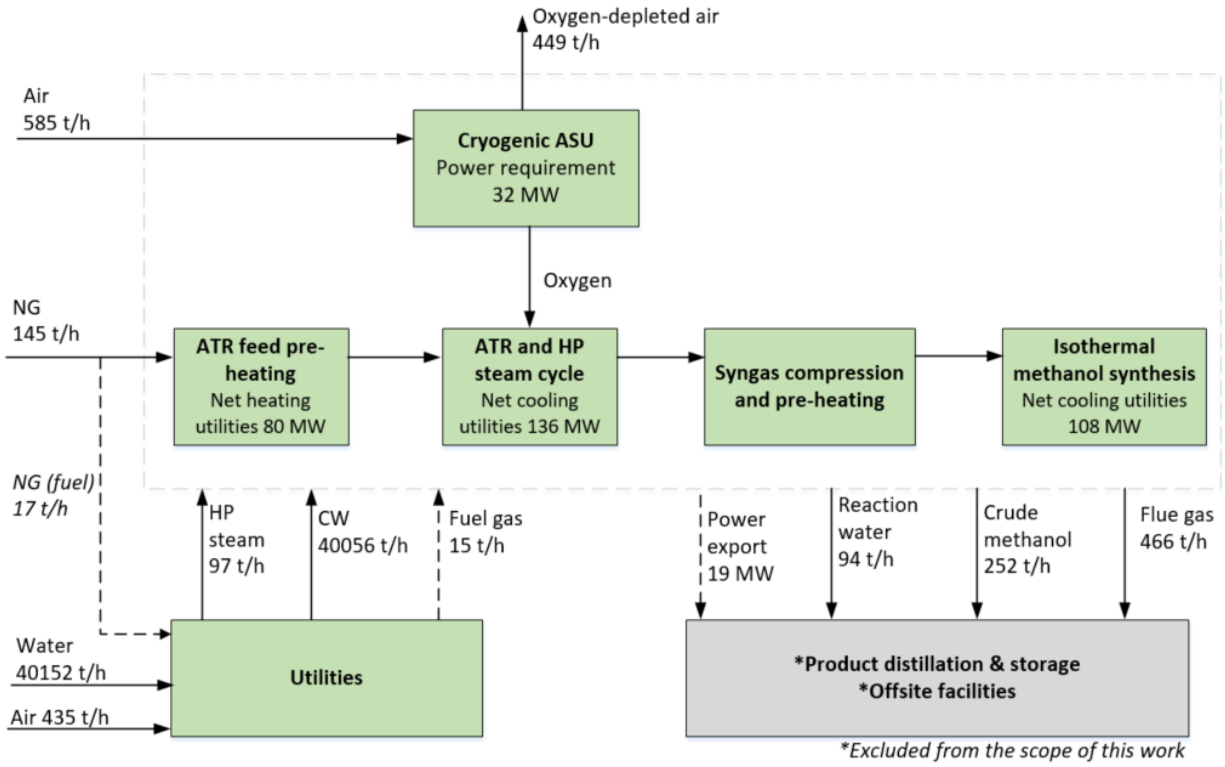

Figure 30 Block flow diagram of the conventional process flow sheet, case A.

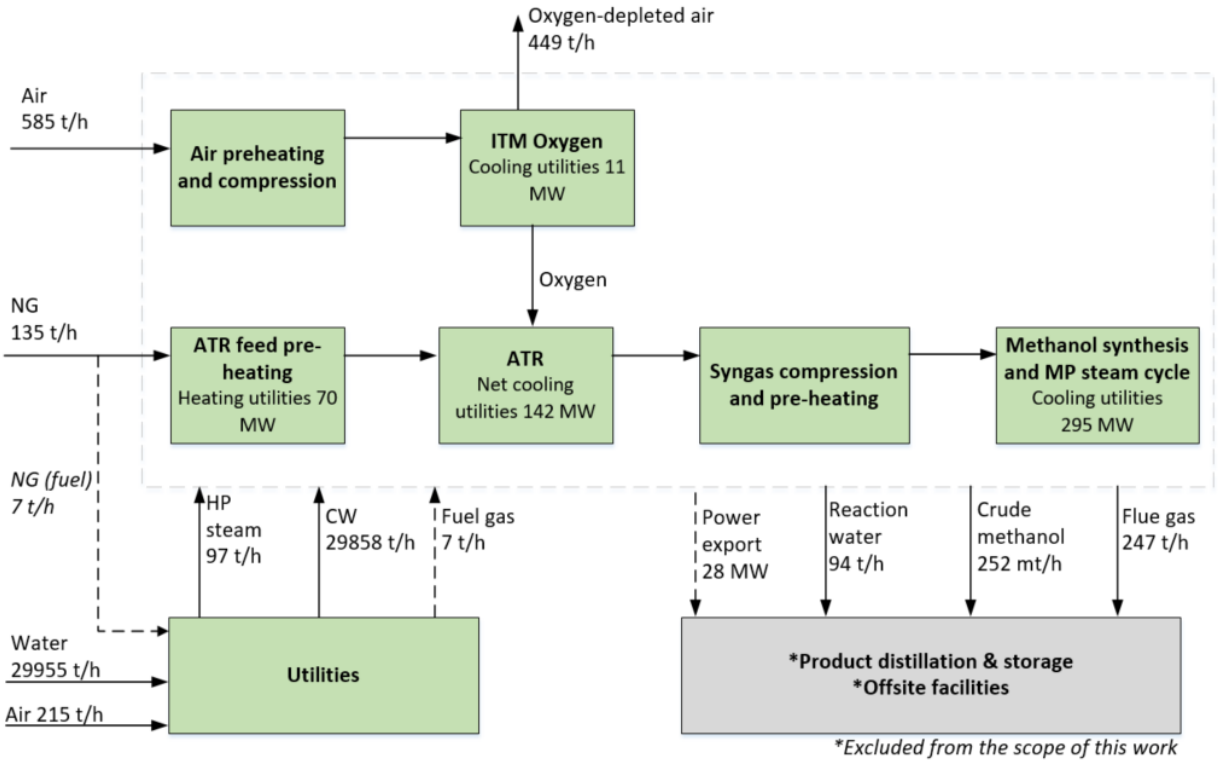

Figure 31 Block flow diagram of the developed process flow sheet, case B.

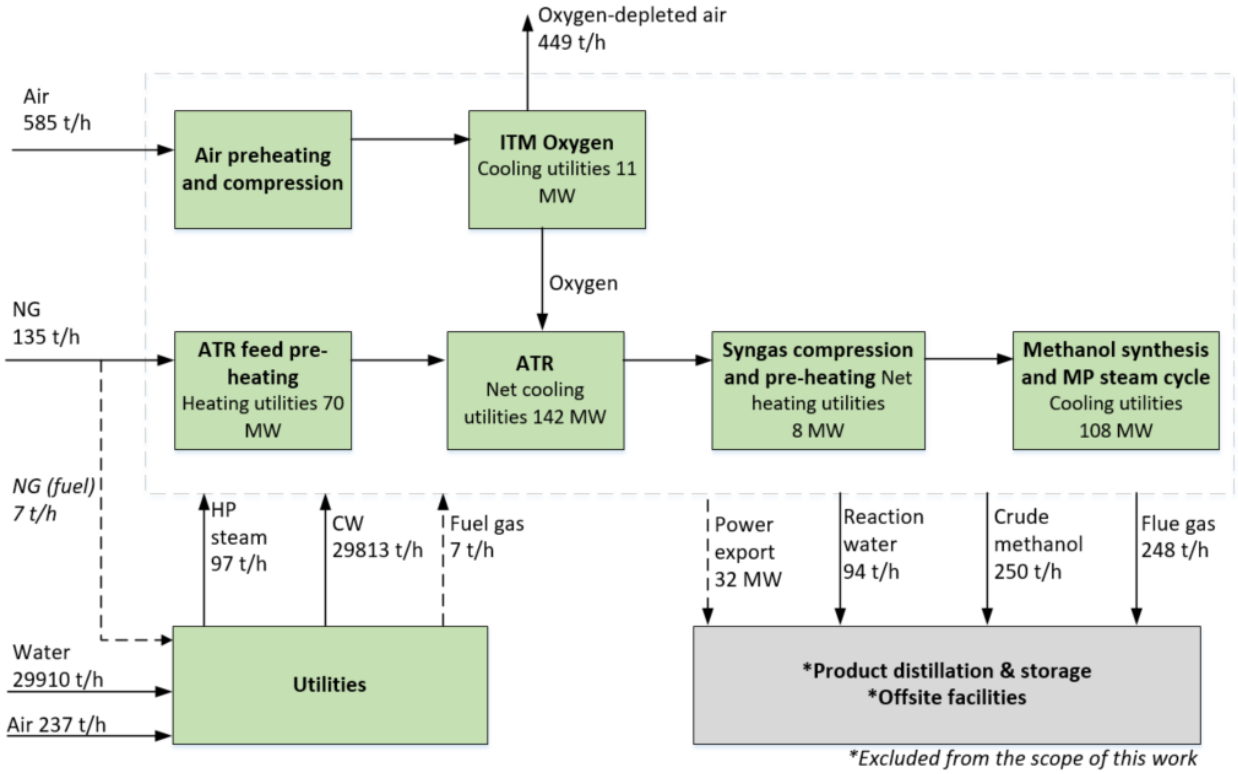

Figure 32 Block flow diagram of the developed process flow sheet, case C.

4.5 Pinch analysis

4.5.1 Process heat integration

Hot and cold composite curves were generated in Aspen Energy Analyzer software and presented in Figure 33 and Figure 34. The curves were generated for the ATR processes for case A and B to study integration of the ITM oxygen unit compared to the conventional case. A pinch analysis for case C was excluded as the methanol synthesis unit is already subjected to adequate process integration via the feed/effluent heat exchange. The conventional cryogenic ASU was not included in the pinch analysis either. This is due to the cryogenic nature of the process limiting process heat integration. Stream enthalpies and temperatures are plotted on the x- and y-axis, respectively, of the composite curves. It can be seen from the figures that there is enough process heat to achieve the process heating requirements and therefore an external heating source is not required.

Figure 33 shows that the ΔT_{min} of the conventional ATR is high at 200 °C if the ATR feed and product are heat integrated as a result of the large temperature driving forces between the heating and cooling streams. This ΔT_{min} is significantly higher than the typically recommended 10 to 20 °C. The ΔT_{min} would be even higher for the conventional case where water limited by the critical temperature of 374°C is used to cool syngas in a waste heat boiler instead of integrating the feed stream which operates at 600 °C. This heat integration between the ATR product syngas and feed gas process streams is typically not done in industry to limit the effect of metal dusting corrosion on heat exchangers (Madloch et al., 2018). The larger ΔT_{min} leads to higher utility and energy requirements. The integration of the ITM oxygen presents attractive opportunities to improve this large temperature driving force. This is because heating of air to temperatures of 900 °C is required. Further, the risk

of metal dusting corrosion is reduced in the case of air because of the absence of carbon compounds.

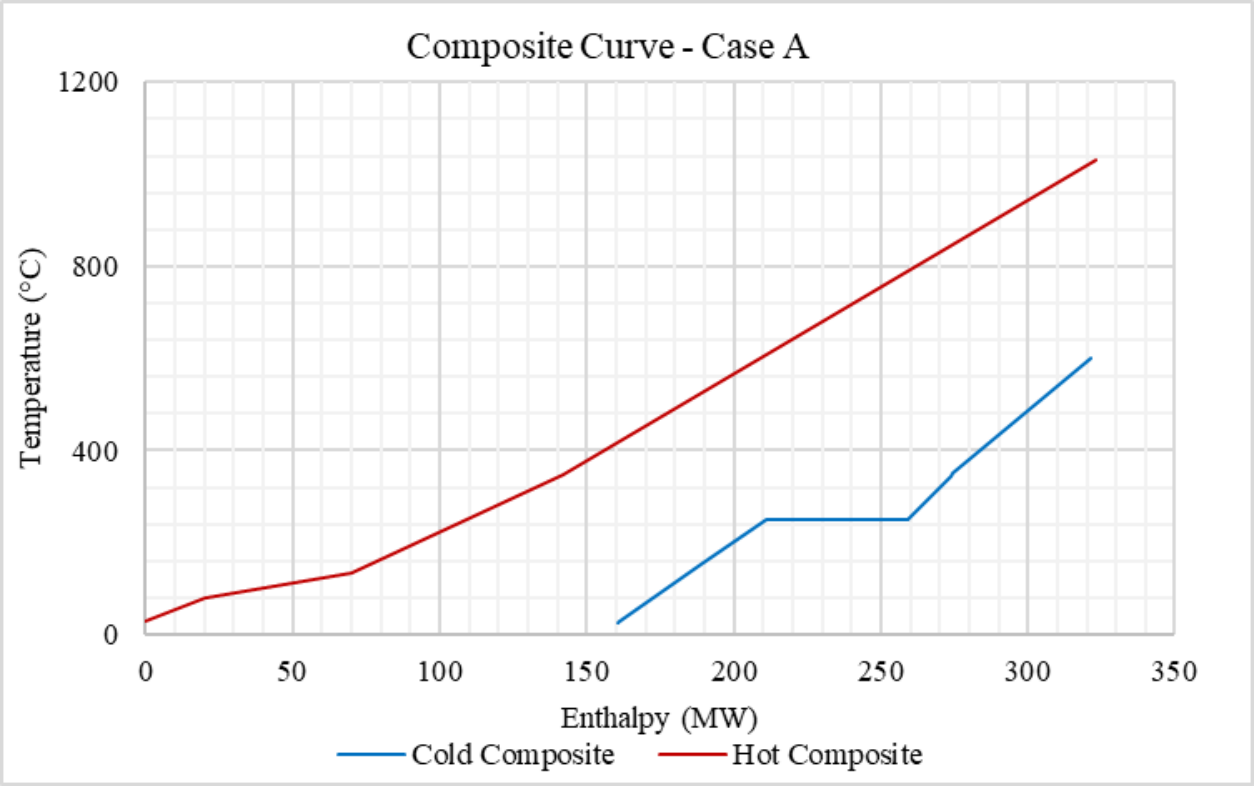

Figure 33 Composite curves of the conventional ATR process.

Figure 34 presents the composite curves for the new flow sheet where the cryogenic ASU was replaced with the ITM oxygen unit. The streams of the ITM oxygen unit requiring heating and cooling are included in the composite curve analysis. A pinch point ΔT_{min} of 15 °C was obtained from the composite curves. This shows that integrating the ITM oxygen has potential to reduce the temperature driving force, compared to the conventional case. The minimum energy requirements for this new case are also reduced as a result. It is evident from the composite curves that the

syngas stream cooling from 1033 °C and the air stream heating up to 900 °C can be matched in a process heat exchanger reducing the need for an external heating source.

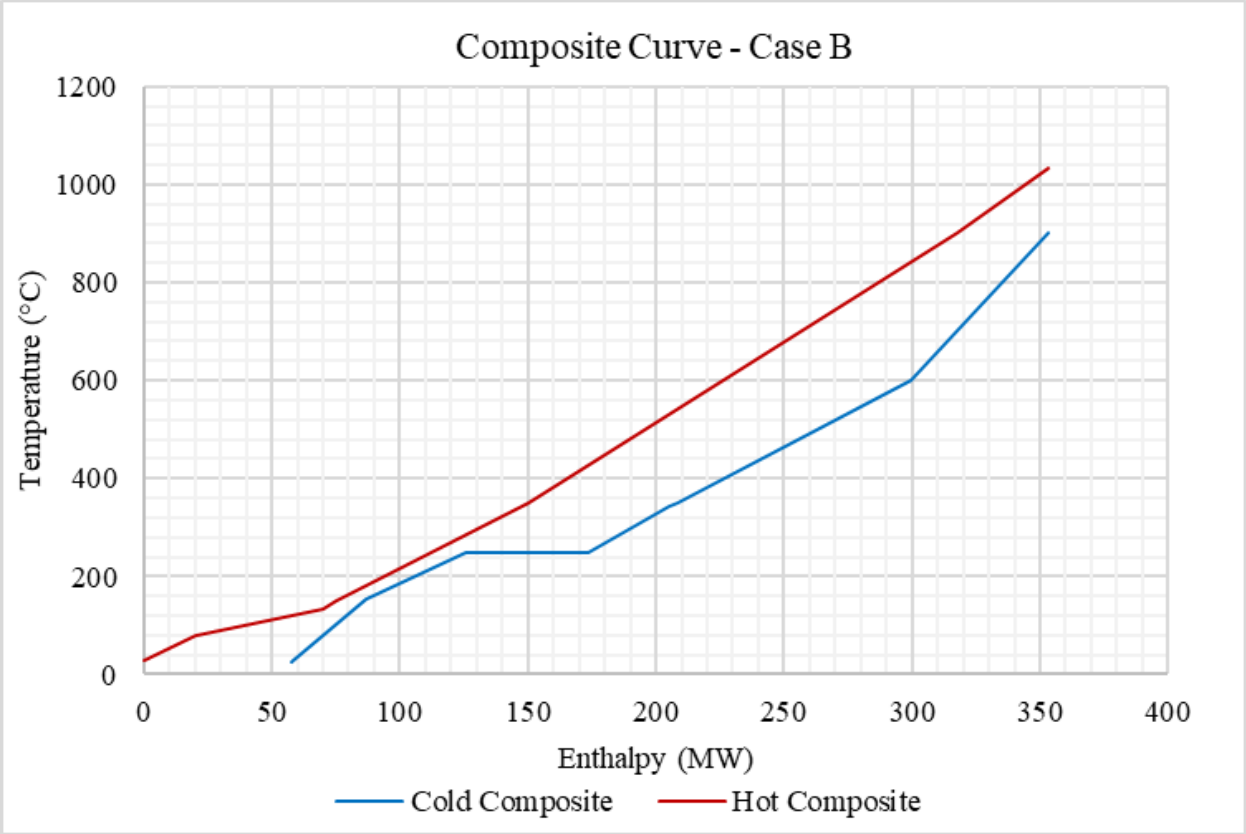

Figure 34 Composite curves of the ATR process and integrated ITM oxygen.

Table 10 presents the results from the pinch study of case A and B. For case A, the heating and cooling targets were found to be 0 and 161 MW. The actual heating and cooling duties of case A as presented in Figure 15 are significantly higher than the targets, at 115 and 275 MW, respectively. This indicates that the process operates far from the theoretical targets as a result of practical heat integration challenges such as metal dusting corrosion

Figure 34 shows that the pinch point approach temperature decreased significantly from case A to case B. This reduces energy penalties or exergy losses as a results of lower temperature driving forces. The cooling target for case C with the integrated ITM oxygen unit was found to be 58 MW while the heating target remained at 0. This shows a 61% decrease in the target utility requirement compared to case A. With some of the high temperature syngas heat utilized to heat up the air feed to the ITM oxygen, the actual heating and cooling requirements were found to be 82 and 152 MW, respectively. The higher actual heating requirement is mainly due to the conventional use of fired heaters to preheat the feed to the ATR. The feed preheating is not process heat integrated for material of construction considerations. A pinch analysis for case C was excluded as the methanol synthesis unit is already subjected to process integration via the feed/effluent heat exchange.

Table 10 ATR process actual and target utility requirements.

	Actual	**Target**
	Case A	
Heating (MW)	115	0
Cooling (MW)	275	161
	Case B	
Heating (MW)	82	0
Cooling (MW)	154	58

4.6 Energy analysis

4.6.1 Heat and power

Table 11 to Table 13 present the energy analysis results for case A, B and C. Duties of heat exchangers are presented on Table 11. In case B and C, syngas is cooled in the air heater AH, whereas a WHB is used in case A, both with a duty of 133 MW. Process steam is generated in WHB1 with a duty of 48 MW on all three cases and used as feed to the ATR. 21 MW is consumed to preheat the natural gas feed. The natural gas and process steam are mixed together to form the ATR feed stream. Significant heat is required to preheat the ATR feed. The conventional concept of preheating the ATR feed via a fired heater was maintained through all the cases where 60 MW of duty was required. In the methanol synthesis loop, the syngas is preheated via a feed/effluent heat exchanger HT3 as it is typically done in literature as shown in Figure 16 and Figure 19. The duty of HT3 in case C is slightly lower due to insufficient process heat, as a result of the gas turbine integration. The additional heater HT8 supplements this shortage. The results of Table 11 indicate that the elimination of the HP steam cycle has resulted in the elimination of the HP steam preheater and superheaters with duties of 52 MW and 33 MW, respectively. This can be considered a benefit in terms of capital investment and utility requirements.

Table 11 Heat exchanger duties.

Case		A	B	C
Heat (MW)				
$Q_{WHB/AH}$	Syngas waste heat boiler	133	133	133
Q_{WHB1}	Syngas waste heat boiler 1	48	48	48
Q_{HT1}	ATR feed preheat	60	60	60
Q_{HT2}	Process steam preheat	29	29	29
Q_{HT3}	Syngas preheat	74	75	66
Q_{HT4}	Fired MP steam superheat	30	30	30
Q_{HT5}	Natural gas preheat	21	21	21
Q_{HT6}	Process steam superheat	4	4	4
Q_{HT7}	MP steam preheat	24	24	24
Q_{HT8}	Additional syngas preheat	-	-	8
Q_{HT9}	HP steam cycle preheat	52	-	-
Q_{HT10}	HP steam cycle superheat	33	-	-

Table 12 presents a summary of the compressors and turbines work as well as the excess power in each case. All cases can produce enough power to drive its compressors and pumps, with some excess power. Excess power is produced in case A from the MP and HP steam Rankine cycles. The excess power can be supplied to other units on the plant such as the product upgrading units. The main power consuming systems in case A are the cryogenic ASU and the syngas compressor. The cryogenic ASU power consumption is based on specific power consumptions from literature. The integrated system was found to produce enough power to supply these system in excess of 19 MW.

In case B, the air, oxygen and syngas compressors are the main power consuming equipment. The integrated ITM oxygen power cycle in case B resulted in excess

power production of 28 MW, indicating an overall power production improvement of 47% compared to case A.

Case C focused on configuring the methanol process into a power production cycle as presented by Figure 18. A recycle compressor added to the recycle loop further contributed to the power demand compared to case B. However, the power production produced enough power to drive this compressor and with an excess. This resulted in the overall excess power production of 32 MW in case C. This is an overall 68% power production improvement compared to case A. A relatively low pressure ratio of 1.3 was chosen for this cycle. This was done to limit the effect of a lower pressure on the crude methanol flow rate from the separator drum DM2 as can be seen in Figure 24, which can be mitigated at a cost.

Table 12 Compressors and turbines work results.

Case		**A**	**B**	**C**
Compressors				
W_{ASU}	Cryogenic ASU	32 (1)	-	-
W_{AC}	ITM air comp	-	61	61
W_{OC}	ITM oxygen comp	-	13	13
W_{SGC}	Syngas comp	30	30	30
W_{MRC}	Recycle comp	-	-	6
Expanders				
W_{NT}	Reject expander	-	-80	-80
W_{OT}	Oxygen expander	-	-22	-22
W_{HPST}	HP steam	-51	-	-
W_{MPST}	MP steam	-30	-30	-30
W_{MT}	Methanol gas expander	-	-	-10
Total				

W_{REF}	Total reformer block	-19	-28	-28
W_{MET}	Total Methanol block	-	-	-4
W_{NET}	Plant net work	-19	-28	-32

(1) Beysel, 2009

4.6.2 Thermal and LHV efficiencies

Table 13 presents the thermal and LHV efficiencies used to evaluate performance of the various flow sheet cases. HP steam from the WHB in case A is used in a Rankine cycle to produce power. Similarly, MP steam generated from the methanol isothermal reactor is used in a separate Rankine cycle to produce power. The thermal efficiencies were found to be 23% and 14% for the HP and MP steam cycles, respectively. Typical Rankine cycle thermal efficiencies of 33% are reported in literature (Ramireddy, 2012). The deviation from literature may be attributed to lower pressure ratios and superheat temperatures in this work.

The ITM oxygen cycle as shown in Figure 18 is an open Brayton power cycle with a thermal efficiency of 21%. The oxygen compressor which increases the oxygen pressure to 24 bar as a process requirement contributes to this low efficiency. This thermal efficiency is lower than typical gas turbine cycle efficiencies of 44.7% (Langston, 2020). These however operate at significantly higher turbine inlet temperatures and pressure ratios. The ITM oxygen cycle is configured to also provide process heat via BFW preheat and superheat using the reject stream heat. The thermal efficiency of this unique combined steam, oxygen and power production system was found to be 40%.

Case C presented in Figure 19 shows the methanol synthesis process configured as a heat engine. This is a combined gas and steam turbine cycle, where heat from the

gas turbine cycle is transferred to the steam cycle through the methanol reactor instead of a HRSG as in a typical combined power cycle. The thermal efficiency of this cycle was found to be very low at 2%. This can be mainly attributed to the large pressure ratio across the syngas compressor SGC of 3.75 which is a process requirement and the low gas turbine pressure ratio of 1.3. The low turbine pressure ratio was specified to limit the effect of flash pressure on the amount of condensate product, that is, crude methanol from the separator drum DM2, as can be seen in Figure 24. Integration of a gas turbine expander on the outlet of the methanol reactor is found to cause insufficient heat available for feed heating requirements. As a result, an additional 8 MW source of heat is required. If natural gas is used to provide this heat, 0.7 t/h is consumed.

The carbon efficiency for case A was found to be comparable to typical GTL carbon efficiencies reported in literature. An improvement in the carbon efficiency was observed in case B and C, mainly due to the reduction in usage of natural gas as utility fuel gas.

A specific natural gas efficiency of 31 GJ/t methanol was obtained for case A. This is comparable to literature specific gas efficiencies of 37-39 GJ/t methanol (Stanbridge, 2016). Case C specific gas efficiency improved by 6% compared to case A. Waste CO_2 is produced from combustion reactions in fired heaters and from the ATR. The CO_2 emission in case B and C decreased by 40% from case A as the amount of gas combusted for heating is reduced. Specific gas efficiency, CO_2 emissions and utility fuel split are lower than typical values reported in literature. This is attributed to lower fuel gas requirement for utilities as power requirements are supplemented by power production in power cycles. Heat and power requirements for other systems such as product upgrading were not included in this work. This has also contributed to the differences in the reported values.

Table 13 Power cycle thermal and plant LHV efficiencies.

Case	A	B	C	Literature
Cycle thermal efficiency (%)				
MP Rankine steam cycle	14	14	14	33 (1)
HP Rankine steam cycle	23	-	-	33 (1)
ITM oxygen Brayton cycle	-	21	21	44.7 (7)
ITM cycle combined power and steam	-	40	40	
Methanol combined gas and steam cycle	-	-	2	
LHV efficiency (%)				
Reforming block	92	92	92	70 (2)
Methanol block	87	87	88	
Total process	79	79	79	
Total plant	69	75	75	75 (3)
Carbon efficiency (%)				
Reforming block	98	98	98	
Methanol block	93	93	93	89-95 (4)
Total process	91	91	91	
Total plant	81	87	86	77 (6)
Specific gas efficiency (GJ/t methanol)				
Total plant	31	29	29	37-39 (4)
CO_2 emissions (t/t methanol)				
Total plant	0.25	0.14	0.15	0.462-0.881 (5)
Fuel gas split (%)				
Natural gas to process	88	5	95	80 (4)
Natural gas to utilities	12	4.8	4.8	20 (4)

(1) Ramireddy, 2012

(2) Khan et al., 2020

(3) Matzen et al., 2015

(4) Stanbridge, 2016

(5) Kajaste et al., 2018

(6) Dong et al., 2008

(7) Langston, 2020

4.7 Exergy analysis

The exergy analysis for case A, B and C was conducted and the results are shown on

Table ***14***. The results are presented as absolute exergy loss in MW and percent of total exergy losses over the equipment and unit blocks. This was done to identify areas of large exergy destruction and opportunities to reduce exergy destruction and improve the process thermal efficiencies. The exergy results were also presented for selected sections of the flow sheet for comparison with literature findings. The reforming block with ASU in case A was found to have exergy loss of 81% of the flow sheet total exergy loss. This is similar to the finding of Iandoli et al. (2007) where it was found to be 69% for an ATR, cryogenic ASU and FT synthesis-based plant. The different liquid synthesis processes, that is, FT synthesis vs methanol synthesis, is expected to have contributed to the difference in these figures. Exergy destruction for the cryogenic ASU in case A was obtained from literature as 2240 kW for a 10 kNm^3/h oxygen capacity unit (Taniguchi et al., 2015). This value was scaled up using a typical factor of 0.6 that accounts for economy of scale (Ring, 2020) to obtain an estimate at the capacity (95 kNm^3/h) in this work. The ATR was found to have the highest exergy destruction at 133 MW, which amounts to a 32% of the total exergy losses, comparable to the finding of Iandoli et al (2007). This can be attributed to entropy production due to chemical reactions and large temperature changes. Exergy destruction in the methanol reactor is significantly lower than that of the ATR. This can be attributed to the absence of large entropy producing

chemical reactions such as the combustion reaction and lower temperature changes. This finding is similar to that of Blumberg et al. (2016).

Fired heaters were found to also contribute significantly to exergy destruction. This is expected as these are combustion reactors. The exergy destruction can be reduced if alternative heating methods are identified and the process heat integration in the flow sheet is improved to avoid or reduce the use of fired heaters. The WHB is another significant contributor to exergy destruction, contributing 9% to the total exergy losses in case A. This is attributed to the large temperature driving forces between the syngas at 1033 °C and water at 250 °C.

In case B, replacing the cryogenic ASU with the ITM oxygen resulted in a decrease in the overall plant exergy destruction by 21%. In this case, the WHB is replaced by the air heater and the exergy destruction is seen to decrease from 38 MW in the WHB of case A to 15 MW in the air heater of case B. Like the cryogenic ASU (Fu and Gundersen, 2012), the largest contributor to exergy losses in the ITM oxygen unit is the air compressor. Although case C produces higher net power than case B, this is done at some energy penalty. The slight increase in the total exergy destruction is attributed to the additional equipment namely methanol turbine MT, recycle compressor RC and the additional syngas feed preheater HT8 as can be seen in Figure 19, required to configure the process as a power production cycle.

Table 14 Exergy destruction over equipment

Case		A		Iandoli, 2007	B		C	
Exergy		**MW**	**%**	**%**	**MW**	**%**	**MW**	**%**
HT1	Feed fired heater	49	12%	7%	58	18%	58	17%
ATR	Autothermal reformer	134	32%	33%	133	41%	133	40%
WHB	Waste heat boiler	38	9%		-		-	
AH	Air heater	-			15	5%	15	5%
WHB1	Waste heat boiler	7.2	2%		7	2%	7.2	2%
DM1	Syngas liquid knockout drum	3.6	1%		4	1%	3.6	1%
	HP steam fired heater	87	21%		-		-	
HPST	HP steam turbine	6.6	2%		-		-	
	Cryogenic ASU [(1)]	8.6	2%	9%	-		-	
	ITM oxygen ASU	-			28	9%	28	9%
SGC	Syngas compressor	2.6	1%		3	1%	2.6	1%
HT3	Syngas preheater	2.9	1%		3	1%	2.0	1%
HT8	Syngas additional preheater	-			-		5.7	2%
MR	Methanol reactor	22	5%		22	7%	22	7%
MT	Methanol turbine	-			-		2.4	1%
DM2	Methanol product separator	1.0	0%		1.0	0%	1.0	0%
RC	Recycle compressor	-			-		2.4	1%
	MP steam fired heater	44.2	11%		44		44	13%
MPST	MP steam turbine	4.6	1%		4.5	1%	4.5	1%
	Total							
	Reformer + ASU block	334	81%	69%	246	67%	246	65%
	Methanol block	78	19%		78	24%	87	26%
	Overall plant	411	100%		323	100%	333	100%

Specific overall (MJ/kg_{CH3OH})	6.7	5.2	5.4

(1) Taniguchi et al., 2015

Table 15 presents a breakdown of the exergy analysis results of the cryogenic ASU and Rankine steam cycle in case A for comparison with ITM oxygen Brayton power cycle in case B. The exergy losses associated with oxygen and power production decreased from 141 MW in case A to 40 MW in case B. This shows a 72% improvement in exergy losses for combined power and oxygen production as a result of the replacement of the cryogenic ASU and steam cycle with the ITM oxygen unit configured as a Brayton power cycle. The fired heater in case A, with exergy destruction of 87 MW, was eliminated in case B due to the absence of the HP steam cycle. The elimination of the HP steam cycle and improvement of the temperature driving forces in the syngas cooler (WHB vs air heater), are the main reasons for the improvement in the exergy destruction in case B. This confirms that replacing the cryogenic ASU with ITM oxygen and integrating ITM oxygen into the ATR process is a more efficient method to recovery process heat.

Table 16 presents exergy destruction results for the equipment in the methanol synthesis process. Configuring the methanol synthesis loop as a power production cycle in case C has resulted in the addition of the methanol turbine MT, recycle compressor RC and additional syngas preheater HT8. This led to an increase in the total exergy destruction from 29 to 38 MW. Integrating the methanol turbine on the outlet of the reactor led to reduced process heat for feed/effluent heat exchange in HT3. As a result, the duty in HT3 is lower and insufficient to achieve the reactor inlet temperature. This necessitated adding another preheater HT8. The exergy destruction in HT8 is higher than that in HT3 because it is modeled as a fired heater.

Table 15 Exergy destruction of the HP steam and ITM oxygen power cycles.

	Unit	Case A	Case B
ITM oxygen ASU and power cycle			
Air compressor (AC)	MW	-	13
Permeate compressor (OC)	MW	-	3
Reject turbine (NT)	MW	-	7
Permeate turbine (OT)	MW	-	2
Air heater (HT5)	MW	-	15
Cryogenic ASU and HP steam cycle			
Cryogenic ASU [(1)]	MW	8.6	-
HP steam turbine (HPST)	MW	7	-
WHB	MW	38	-
Steam fired heater	MW	87	-
Pump	MW	0	-
Total	MW	**141**	**40**

(1) Taniguchi et al., 2015

Table 16 Exergy destruction of the methanol synthesis unit.

	Unit	Case B	Case C
Feed preheater (HT3)	MW	2.9	2.0
Additional preheater HT8	MW	-	5.7
Recycle compressor (RC)	MW	-	2.4
Methanol turbine (MT)	MW	-	2.4
Methanol reactor (MR)	MW	22	22
Syngas compressor (SGC)	MW	2.6	2.6
Separator drum (DM2)	MW	1.0	1.0
Total	MW	29	38

4.8 References

Iandoli CL and Kjelstrup S, “Exergy analysis of a GTL process based on low temperature slurry FT reactor technology with a cobalt catalyst”, *Energy and Fuels*, vol. 21, pp. 2317-2324, 2007.

Blumberg T, Morosuk T, and Tsatsaronis G, 2016, “Exergy-based evaluation of methanol production from natural gas”, *Research Gate*, conference paper, https://www.researchgate.net/publication/320271856_Exergy-based_evaluation_of_methanol_production_from_natural_gas [accessed 7 Aug 2022].

Fu C and Gundersen T, “Using exergy analysis to reduce power consumption in air separation units for oxy-combustion processes”, *Energy*, vol. 44, pp. 60-68, 2012.

Ramireddy V, 2012, “An overview of combined cycle power plant”, *Electrical Engineering Portal*, https://electrical-engineering-portal.com/an-overview-of-combined-cycle-power-plant [accessed 21 September 2022].

Khan MN, Cloete S and Amini S, “Efficient Production of Clean Power and Hydrogen Through Synergistic Integration of Chemical Looping Combustion and Reforming”, *Energies*, vol. 13, pp. 3443, 2020.

Matzen M, Alhajji M and Demirel Y, “Technoeconomics and Sustainability of Renewable Methanol and Ammonia Productions Using Wind Power-based Hydrogen”, *Journal of Advanced Chemical Engineering*, vol. 5 pp. 128, 2015.

Stanbridge S, 2016, “Teaching an old plant new tricks: The rise of the methanol plant revamp”, *Hydrocarbon Processing*, https://www.hydrocarbonprocessing.com/magazine/2016/july-2016/special-report-

refinery-of-the-future/teaching-an-old-plant-new-tricks-the-rise-of-the-methanol-plant-revamp [accessed 1 September 2022].

Langston LS, “Aspects of Gas Turbine Thermal Efficiency”, *ASME, Mechanical Engineering*, 2020, vol. 142, pp. 54–55.

Kajaste R, Hurme M and Oinas P, “Methanol-Managing greenhouse gas emissions in the production chain by optimizing the resource base”, *AIMS Energy*, vol. 6, pp. 1074-1102, 2018.

Taniguchi M, Asaoka H and Ayuhara T, “Energy saving air-separation plant based on exergy analysis”, KEBELCO Technology Review No. 33, *Shinko Air Water Cryoplant, Ltd.,* 2015.

Dong L, Wei S, Tan S, & Zhang H, “GTL or LNG: Which is the best way to monetize “stranded” natural gas?”, *Petroleum Science*, pp. 388-394, 2008.

Ring TA, 2020, “Equipment costing CAPEX”, *University of Utah*, https://my.che.utah.edu/~ring/Design%20II/Lecture%20Ppts/L2-Equipment%20Costing.ppt [accessed 15 February 2023].

Chapter 5 Conclusions and Recommendations

This work investigated opportunities and methods to improve the conventional natural gas to methanol process. The literature review identified that current industrial GTL processes suffer large exergy losses due to inadequate process heat integration and recovery, mainly in the syngas and oxygen production units. The ITM oxygen technology was found to have the potential to replace the conventional cryogenic air separation and reduce the large power demands associated with oxygen production.

Three flow sheet cases were identified, namely case A, B and C. Case A was defined as the conventional case. Case B focused on the integration of the ITM oxygen technology. Case C was a further modification of case B which focused on heat recovery in the methanol loop to produce more power. Energy, exergy and pinch analysis methods were applied. Benefits of replacing the conventional cryogenic ASU with the novel ITM oxygen technology were investigated. Power cycles were integrated to produce power from process heat. A new and improved flow sheet, case C, was successfully developed. In the development of the new flow sheet, the process intent was maintained. This can be seen from the process LHV and carbon efficiencies which remained the same in all cases.

The pinch analysis results showed that the process contains enough heat to achieve all its heating requirements, however, several practical challenges limit achieving minimum energy requirements. From the analysis, it was found that large temperature driving forces exist in the conventional case, with a ΔT_{min} of 200 °C. Integrating the ITM oxygen reduced this ΔT_{min} to 15 °C. Utility requirements were also lower than in the conventional case.

Replacing the cryogenic ASU with ITM and integrating ITM oxygen into the ATR process is a more efficient method to recover the high temperature syngas heat with

reduced exergy losses. The ITM oxygen unit integrated with power cycles resulted in 47% more power production compared to the conventional case A. The exergy analysis results showed a decrease in overall exergy losses by 21% in this new flow sheet. The ITM oxygen power cycle was found to produce enough power to drive its own compressors and with excess power of 28 MW. The cryogenic ASU in the conventional case has a power demand of 33 MW. This work shows that lower cost production of oxygen may be the feasible solution to reduce the high costs of large-scale syngas manufacture. The ITM oxygen presents such opportunities by substituting the energy intensive cryogenic ASU and combining oxygen, syngas and power production into a single thermally integrated unit.

This work demonstrated that the methanol loop has sufficient process heat for combined heat and power production to satisfy the syngas compressor power requirements. It was found that configuring the methanol process into a power production cycle in case C results in an increase in the overall plant excess power to 32 MW. This is an overall 68% power production improvement compared to the conventional case. However, two challenges were identified from the methanol process power cycle, namely reduced methanol production caused by lower flash pressures and inadequate process heat for feed preheat. These challenges can be mitigated, however, at an additional cost. Feasibility of increasing power production and thermal efficiency in the methanol process power cycle vs cost implications of the required additional utility systems should be further investigated.

Thermal efficiencies of heat engines as well as combined heat and power systems in each case were analyzed to understand how the thermal efficiency performance changes from one flow sheet case to another. Breaking down the thermal efficiencies into the various plant sections and analyzing them separately was found to be an effective method which can be used for the analysis of the plant's performance. This

method enables prioritized and focused flow sheet improvement. A thermal efficiency of 40% was achieved from the combined ITM oxygen power cycle producing power and steam. Thermal efficiencies of the MP and HP Rankine cycles were found to be slightly low at 14% and 23%, respectively and lower than typical efficiencies reported in literature. The air-standard model for power cycles can be used to identify parameters to be investigated, such as turbine inlet temperature and compressor pressure ratio, to improve the thermal efficiencies.

A decrease in the consumption of natural gas as fuel in the utility systems was observed. As a result, the new flow sheet specific gas efficiency improved by 6% compared to the conventional case. This is a significant improvement especially for large-scale plants. A 40% decrease in CO_2 emissions was also observed as a results of reduced usage of fired heaters.

The overall thermal efficiencies of the cases were not optimized as this was not part of the study objectives. A further study can be conducted to investigate improving the thermal efficiencies of the power cycles in each case by performing a sensitivity analysis to impact parameters such as turbine and compressor inlet temperature and pressure ratio. The specific parameters to assess can be determined from the air-standard model equation for a Brayton power cycle. The thermal efficiency improvement can result in higher power production and reduced equipment duties which is a benefit to both capital and operating costs.

Appendix A Flow diagrams and mass balance

Case A PFD and Mass balance table

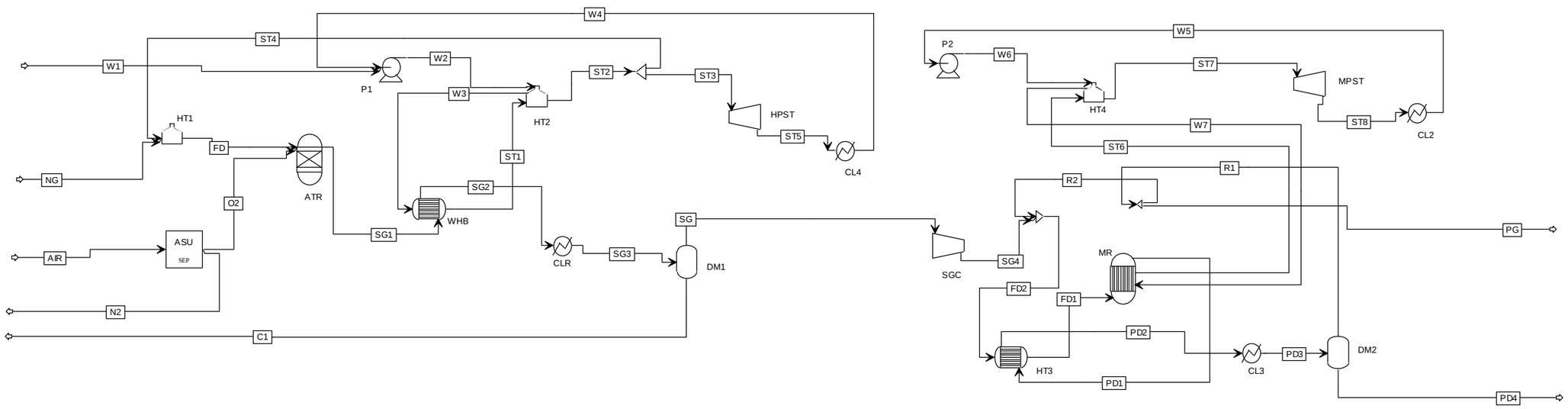

	Units	C1	FD	FD1	FD2	NG	O2	PD1	PD3	PD4	PG	R1	R2	SG	SG1	SG2	SG4	ST3	ST5	ST6	ST7	ST8	W1	W4	W5
Temperature	C	30	605	250	95	30	150	280	30	30	30	30	30	30	1033	537	30	437	102	180	229	102	25	102	102
Pressure	kPa	2400	2400	9000	9000	2400	2400	9000	9000	9000	9000	9000	9000	2400	2400	2400	2400	4000	100	1000	1000	100	100	100	100
Vapor Fraction	wt/wt	0.00	1.00	1.00	1.00	1.00	1.00	1.00	0.62	0.00	1.00	1.00	1.00	1.00	1.00	1.00	0.74	1.00	0.97	0.88	1.00	0.94	0.00	0.00	0.00
Mass Density	kg/cum	989	5.7	24	34	17	22	31	67	801	43	43	43	11	2.8	4.6	15	13	0.6	5.7	4.5	0.6	994	917	917
Enthalpy Flow	MW	-413	-427	-760	-835	-161	4	-922	-1106	-555	-19	-551	-532	-333	-423	-556	-746	-931	-982	-1136	-1106	-1137	-429	-1150	-1324
Exergy	MW	1	1836	3412	3388	1765	15	3334	3287	1389	66	1897	1831	1534	1702	1607	1539	99	41	70	80	46	1	6	7
Mass Entropy	J/kg-K	-9250	-2232	308	-604	-6280	-499	-1199	-3647	-7173	-1535	-1535	-1535	448	3301	2021	-2061	-2497	-2174	-3336	-2566	-2398	-9324	-8285	-8285
Mass Flows	kg/hr	92957	224508	659427	659427	127908	135027	659427	659427	252332	14248	407095	392846	266578	359535	359535	359535	265000	265000	305000	305000	305000	96600	265000	305000
Mole Flows	kmol/hr	5160	12962	54682	54682	7600	4220	41146	41146	7957	1162	33189	32028	22655	27815	27815	27815	14710	14710	16930	16930	16930	5362	14710	16930
Mole Fractions																									
O2		0.00	0.00	0.00	0.00	0.00	1.00	0.00	0.00	0.00	0.00	0.00	0.00	0.00	0.00	0.00	0.00	0.00	0.00	0.00	0.00	0.00	0.00	0.00	0.00
CH4		0.00	0.56	0.00	0.00	0.95	0.00	0.00	0.00	0.00	0.00	0.00	0.00	0.01	0.01	0.01	0.01	0.00	0.00	0.00	0.00	0.00	0.00	0.00	0.00
C2H6		0.00	0.02	0.00	0.00	0.03	0.00	0.00	0.00	0.00	0.00	0.00	0.00	0.00	0.00	0.00	0.00	0.00	0.00	0.00	0.00	0.00	0.00	0.00	0.00
N2		0.00	0.01	0.06	0.06	0.02	0.00	0.07	0.07	0.00	0.09	0.09	0.09	0.01	0.00	0.00	0.00	0.00	0.00	0.00	0.00	0.00	0.00	0.00	0.00
CO2		0.00	0.00	0.09	0.09	0.01	0.00	0.10	0.10	0.06	0.12	0.12	0.12	0.05	0.04	0.04	0.04	0.00	0.00	0.00	0.00	0.00	0.00	0.00	0.00
CO		0.00	0.00	0.18	0.18	0.00	0.00	0.09	0.09	0.00	0.11	0.11	0.11	0.28	0.22	0.22	0.22	0.00	0.00	0.00	0.00	0.00	0.00	0.00	0.00
H2		0.00	0.00	0.67	0.67	0.00	0.00	0.55	0.55	0.00	0.68	0.68	0.68	0.65	0.53	0.53	0.53	0.00	0.00	0.00	0.00	0.00	0.00	0.00	0.00
H2O		1.00	0.41	0.00	0.00	0.00	0.00	0.01	0.01	0.06	0.00	0.00	0.00	0.00	0.19	0.19	0.19	1.00	1.00	1.00	1.00	1.00	1.00	1.00	1.00
CH3OH		0.00	0.00	0.00	0.00	0.00	0.00	0.17	0.17	0.87	0.00	0.00	0.00	0.00	0.00	0.00	0.00	0.00	0.00	0.00	0.00	0.00	0.00	0.00	0.00

Utilities	Units	Cooling water	Natural gas	Air
Temperature	C	20	30	25
Pressure	bar	8	24	1
Flow	t/h	40056	17	435

Case B PFD and Mass balance table

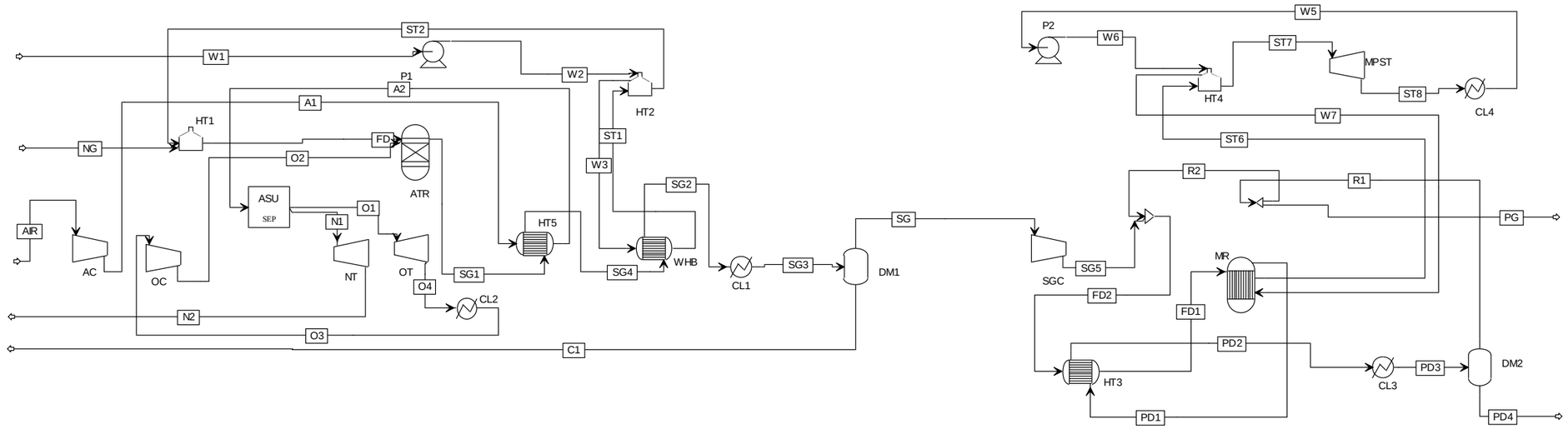

	Units	A2	AIR	C1	FD	FD1	FD2	N2	NG	O2	O4	PD1	PD4	PD5	PG	R1	SG	SG1	SG3	SG4	SG5	ST6	ST7	ST8	W1	W5
Temperatur	C	900	25	30	600	250	94	337	30	153	363	280	30	280	30	30	30	1034	349	537	189	180	229	102	25	102
Pressure	kPa	2400	101	2400	2400	9000	9000	100	2400	2400	100	9000	9000	9000	9000	9000	2400	2400	2400	2400	9000	1000	1000	100	101	100
Vapor Fraction	wt./wt.	1.00	1.00	0.00	1.00	1.00	1.00	1.00	1.00	1.00	1.00	1.00	0.00	1.00	1.00	1.00	1.00	1.00	1.00	1.00	1.00	0.88	1.00	0.94	0.00	0.00
Mass Densi	kg/cum	7.09	1.18	989	5.73	24.5	34.9	0.55	16.9	21.7	0.60	31.2	801	31.2	43.8	43.8	11.1	2.85	5.98	4.58	26.7	5.73	4.48	0.62	994	917
Enthalpy Flo	MW	154	0	-413	-427	-760	-835	41	-161	4	12	-922	-555	-922	-19	-551	-333	-423	-604	-556	-303	-1136	-1106	-1137	-429	-1324
Exergy	MW	128	1	1	1836	3413	3388	16	1765	15	9	3334	1388	3334	66	1898	1534	1702	1579	1607	1562	70	80	46	1	7
Mass Entro	J/kg-K	710	161	-9250	-2232	308	-605	769	-6280	-491	733	-1199	-7173	-1199	-1536	-1536	449	3303	1355	2025	585	-3333	-2563	-2395	-9324	-8285
Mass Flows	kg/hr	584987	584987	93257	224508	674375	674375	449254	127908	135733	135733	674375	252234	674375	14775	422141	266984	360241	360241	360241	266984	305000	305000	305000	96600	305000
Mole Flows	kmol/hr	20200	20200	5176	12962	55146	55146	15956	7600	4244	4244	41620	7953	41620	1178	33668	22658	27835	27835	27835	22658	16930	16930	16930	5362	16930
Mole Fractions																										
O2		0.21	0.21	0.00	0.00	0.00	0.00	0.00	0.00	1.00	1.00	0.00	0.00	0.00	0.00	0.00	0.00	0.00	0.00	0.00	0.00	0.00	0.00	0.00	0.00	0.00
CH4		0.00	0.00	0.00	0.56	0.00	0.00	0.00	0.95	0.00	0.00	0.00	0.00	0.00	0.00	0.00	0.01	0.01	0.01	0.01	0.01	0.00	0.00	0.00	0.00	0.00
C2H6		0.00	0.00	0.00	0.02	0.00	0.00	0.00	0.03	0.00	0.00	0.00	0.00	0.00	0.00	0.00	0.00	0.00	0.00	0.00	0.00	0.00	0.00	0.00	0.00	0.00
N2		0.78	0.78	0.00	0.01	0.06	0.06	0.99	0.02	0.00	0.00	0.08	0.00	0.08	0.10	0.10	0.01	0.00	0.00	0.00	0.01	0.00	0.00	0.00	0.00	0.00
CO2		0.00	0.00	0.00	0.00	0.09	0.09	0.00	0.01	0.00	0.00	0.10	0.06	0.10	0.12	0.12	0.05	0.04	0.04	0.04	0.05	0.00	0.00	0.00	0.00	0.00
CO		0.00	0.00	0.00	0.00	0.18	0.18	0.00	0.00	0.00	0.00	0.09	0.00	0.09	0.11	0.11	0.28	0.22	0.22	0.22	0.28	0.00	0.00	0.00	0.00	0.00
H2		0.00	0.00	0.00	0.00	0.66	0.66	0.00	0.00	0.00	0.00	0.54	0.00	0.54	0.67	0.67	0.65	0.53	0.53	0.53	0.65	0.00	0.00	0.00	0.00	0.00
H2O		0.00	0.00	1.00	0.41	0.00	0.00	0.00	0.00	0.00	0.00	0.01	0.06	0.01	0.00	0.00	0.00	0.19	0.19	0.19	0.00	1.00	1.00	1.00	1.00	1.00

Utilities	Units	Cooling water	Natural gas	Air
Temperature	C	20	30	25
Pressure	bar	8	24	1
Flow	t/h	29858	6.8	215

Case C PFD and Mass balance table

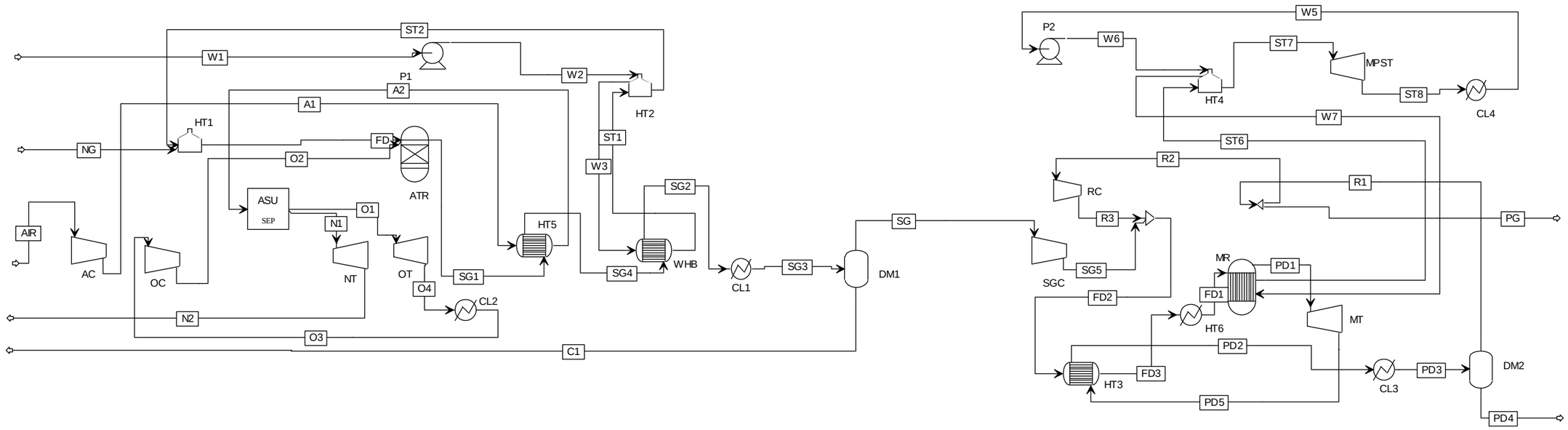

	Units	A2	AIR	C1	FD	FD2	FD1	N2	NG	O2	O4	PD1	PD4	PD5	PG	R1	SG	SG1	SG3	SG4	SG5	ST6	ST7	ST8	W1	W5
Temperature	C	900	25	30	600	98	250	337	30	153	363	280	30	253	30	30	30	1037	351	539	189	180	228	102	25	102
Pressure	kPa	2400	101	2400	2400	9000	9000	100	2400	2400	100	9000	7000	7000	7000	7000	2400	2400	2400	2400	9000	1000	1000	100	101	100
Vapor Fraction	wt/wt	1.00	1.00	0.00	1.00	1.00	1.00	1.00	1.00	1.00	1.00	1.00	0.00	1.00	1.00	1.00	1.00	1.00	1.00	1.00	1.00	0.88	1.00	0.94	0.00	0.00
Mass Density	kg/cum	7.1	1.18	989	5.7	36.2	25.7	0.55	16.9	21.7	0.60	32.7	801	26.9	37.1	37.1	11.14	2.84	5.96	4.57	26.67	5.74	4.50	0.62	994	917
Enthalpy Flow	MW	154	0.0	-413	-427	-906	-840	41	-161	4	12	-994	-551	-1006	-22	-628	-333	-423	-604	-556	-303	-1137	-1107	-1137	-429	-1324
Exergy	MW	128	0.6	1.4	1836	3374	3395	16	1765	15	9	3320	1386	3307	66	1879	1534	1703	1580	1607	1562	105	120	84	1.3	7.5
Mass Entropy	J/kg-K	710	161	-9250	-2232	-506	264	769	-6280	-491	733	-1088	-7214	-1069	-1193	-1193	449	3303	1355	2025	585	-3350	-2579	-2411	-9324	-8285
Mass Flows	kg/hr	586435	586435	93525	224508	711621	711621	450366	127908	136069	136069	711621	250491	711621	16140	461130	267052	360577	360577	360577	267052	305000	305000	305000	96600	305000
Mole Flows	kmol/hr	20250	20250	5191	12962	55517	55517	15996	7600	4254	4254	41973	7911	41973	1192	34062	22660	27852	27852	27852	22660	16930	16930	16930	5362	16930
Mole Fractions																										
O2		0.21	0.21	0.00	0.00	0.00	0.00	0.00	0.00	1.00	1.00	0.00	0.00	0.00	0.00	0.00	0.00	0.00	0.00	0.00	0.00	0.00	0.00	0.00	0.00	0.00
CH4		0.00	0.00	0.00	0.56	0.00	0.00	0.00	0.95	0.00	0.00	0.00	0.00	0.00	0.00	0.00	0.01	0.01	0.01	0.01	0.01	0.00	0.00	0.00	0.00	0.00
C2H6		0.00	0.00	0.00	0.02	0.00	0.00	0.00	0.03	0.00	0.00	0.00	0.00	0.00	0.00	0.00	0.00	0.00	0.00	0.00	0.00	0.00	0.00	0.00	0.00	0.00
N2		0.78	0.78	0.00	0.01	0.06	0.06	0.99	0.02	0.00	0.00	0.08	0.00	0.08	0.10	0.10	0.01	0.00	0.00	0.00	0.01	0.00	0.00	0.00	0.00	0.00
CO2		0.00	0.00	0.00	0.00	0.10	0.10	0.00	0.01	0.00	0.00	0.12	0.05	0.12	0.13	0.13	0.05	0.04	0.04	0.04	0.05	0.00	0.00	0.00	0.00	0.00
CO		0.00	0.00	0.00	0.00	0.18	0.18	0.00	0.00	0.00	0.00	0.10	0.00	0.10	0.12	0.12	0.28	0.22	0.22	0.22	0.28	0.00	0.00	0.00	0.00	0.00
H2		0.00	0.00	0.00	0.00	0.65	0.65	0.00	0.00	0.00	0.00	0.52	0.00	0.52	0.64	0.64	0.65	0.53	0.53	0.53	0.65	0.00	0.00	0.00	0.00	0.00
H2O		0.00	0.00	1.00	0.41	0.00	0.00	0.00	0.00	0.00	0.00	0.01	0.07	0.01	0.00	0.00	0.00	0.19	0.19	0.19	0.00	1.00	1.00	1.00	1.00	1.00
CH3OH		0.00	0.00	0.00	0.00	0.00	0.00	0.00	0.00	0.00	0.00	0.17	0.88	0.17	0.00	0.00	0.00	0.00	0.00	0.00	0.00	0.00	0.00	0.00	0.00	0.00

Utilities	**Units**	**Cooling water**	**Natural gas**	**Air**
Temperature	C	20	30	25
Pressure	bar	8	24	1
Flow	t/h	29813	6.8	237

Appendix B Pinch analysis models

Case A ATR process pinch analysis model

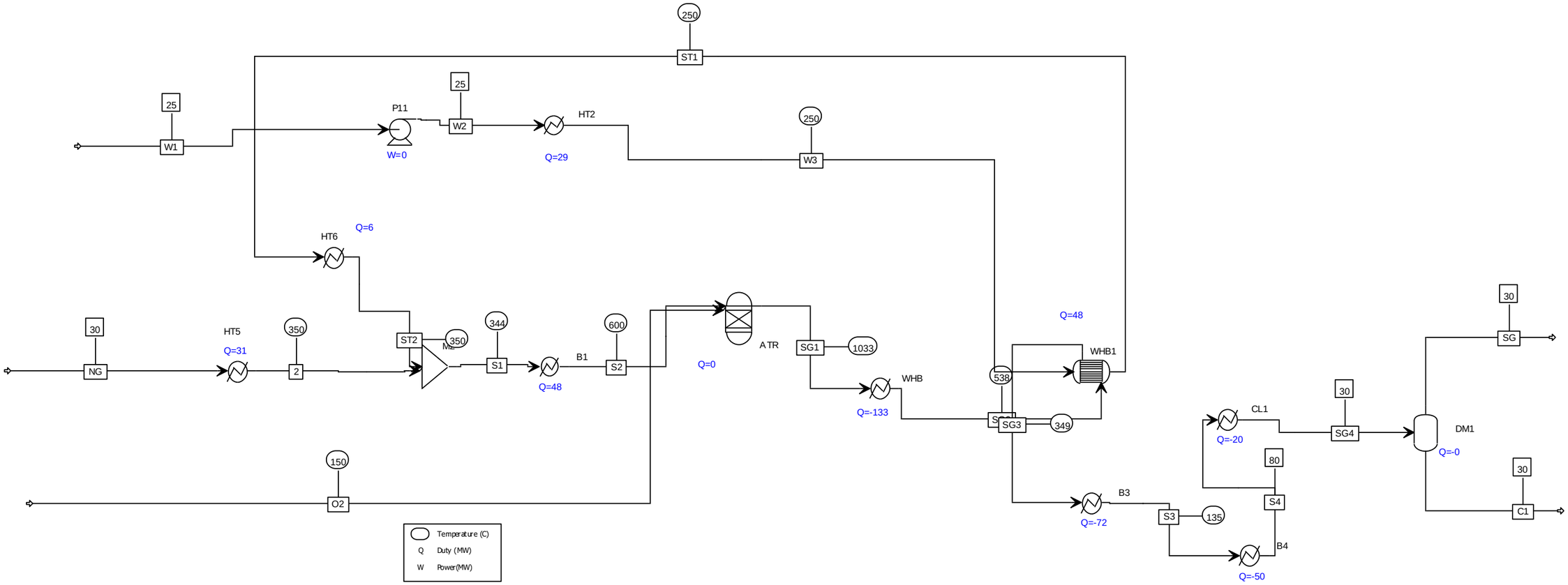

Table 17 Case A pinch analysis mass balance

	Units	2	C1	NG	O2	S1	S2	S3	S4	SG	SG1	SG2	SG3	SG4	ST1	ST2	W1	W2	W3
From		HT5	DM1			M2	B1	B3	B4	DM1	ATR	WHB	WHB1	CL1	WHB1	HT6		P11	HT2
To		M2		HT5	ATR	B1	ATR	B4	CL1		WHB	WHB1	B3	DM1	HT6	M2	P11	HT2	WHB1
Phase		Vapor Phase	Liquid Phase	Vapor Phase	Vapor Phase	Vapor Phase	Vapor Phase			Vapor Phase	Vapor Phase	Vapor Phase	Vapor Phase		Vapor Phase	Vapor Phase	Liquid Phase	Liquid Phase	Liquid Phase
Temperature	C	350	30	30	150	344	600	135	80	30	1033	538	349	30	250	350	25	25	250
Pressure	kPa	2400	2400	2400	2400	2400	2400	2400	2400	2400	2400	2400	2400	2400	4000	4000	100	4000	4000
Molar Vapor Fraction		1.0	0.0	1.0	1.0	1.0	1.0	0.9	0.8	1.0	1.0	1.0	1.0	0.8	1.0	1.0	0.0	0.0	0.0
Molar Liquid Fraction		0.0	1.0	0.0	0.0	0.0	0.0	0.1	0.2	0.0	0.0	0.0	0.0	0.2	0.0	0.0	1.0	1.0	1.0
Molar Solid Fraction		0.0	0.0	0.0	0.0	0.0	0.0	0.0	0.0	0.0	0.0	0.0	0.0	0.0	0.0	0.0	0.0	0.0	0.0
Mass Vapor Fraction		1.0	0.0	1.0	1.0	1.0	1.0	0.9	0.8	1.0	1.0	1.0	1.0	0.7	1.0	1.0	0.0	0.0	0.0
Mass Liquid Fraction		0.0	1.0	0.0	0.0	0.0	0.0	0.1	0.2	0.0	0.0	0.0	0.0	0.3	0.0	0.0	1.0	1.0	1.0
Mass Solid Fraction		0.0	0.0	0.0	0.0	0.0	0.0	0.0	0.0	0.0	0.0	0.0	0.0	0.0	0.0	0.0	0.0	0.0	0.0
Molar Enthalpy	**kJ/kmol**	**-61670**	**-287295**	**-76401**	**3611**	**-132066**	**-118682**	**-87407**	**-93911**	**-52970**	**-54733**	**-71939**	**-78112**	**-96519**	**-236023**	**-231840**	**-287741**	**-287640**	**-268056**
Mass Enthalpy	kJ/kg	-3664	-15947	-4540	113	-7625	-6852	-6754	-7256	-4495	-4229	-5559	-6036	-7458	-13101	-12869	-15972	-15966	-14879
Molar Entropy	J/kmol-K	-73242	-166647	-105697	-15958	-56767	-38708	-1875	-18765	5269	42704	26197	17534	-26681	-58251	-50928	-167974	-167911	-119488
Mass Entropy	J/kg-K	-4352	-9250	-6280	-499	-3277	-2235	-145	-1450	447	3300	2024	1355	-2062	-3233	-2827	-9324	-9321	-6633
Molar Density	kmol/cum	0	55	1	1	0	0	1	1	1	0	0	0	1	1	1	55	55	41
Mass Density	kg/cum	8	989	17	22	8	6	10	13	11	3	5	6	15	19	15	994	994	734
Enthalpy Flow	MW	-130	-413	-161	4	-476	-427	-676	-726	-333	-423	-556	-604	-746	-352	-345	-429	-428	-399
Average MW		17	18	17	32	17	17	13	13	12	13	13	13	13	18	18	18	18	18
Mole Flows	kmol/hr	7600	5172	7600	4240	12962	12962	27827	27827	22655	27827	27827	27827	27827	5362	5362	5362	5362	5362
Mole Fractions																			
O2		0.0	0.0	0.0	1.0	0.0	0.0	0.0	0.0	0.0	0.0	0.0	0.0	0.0	0.0	0.0	0.0	0.0	0.0
CH4		0.9	0.0	0.9	0.0	0.6	0.6	0.0	0.0	0.0	0.0	0.0	0.0	0.0	0.0	0.0	0.0	0.0	0.0
C2H6		0.0	0.0	0.0	0.0	0.0	0.0	0.0	0.0	0.0	0.0	0.0	0.0	0.0	0.0	0.0	0.0	0.0	0.0
N2		0.0	0.0	0.0	0.0	0.0	0.0	0.0	0.0	0.0	0.0	0.0	0.0	0.0	0.0	0.0	0.0	0.0	0.0
CO2		0.0	0.0	0.0	0.0	0.0	0.0	0.0	0.0	0.1	0.0	0.0	0.0	0.0	0.0	0.0	0.0	0.0	0.0
CO		0.0	0.0	0.0	0.0	0.0	0.0	0.2	0.2	0.3	0.2	0.2	0.2	0.2	0.0	0.0	0.0	0.0	0.0
H2		0.0	0.0	0.0	0.0	0.0	0.0	0.5	0.5	0.7	0.5	0.5	0.5	0.5	0.0	0.0	0.0	0.0	0.0
H2O		0.0	1.0	0.0	0.0	0.4	0.4	0.2	0.2	0.0	0.2	0.2	0.2	0.2	1.0	1.0	1.0	1.0	1.0
CH3OH		0.0	0.0	0.0	0.0	0.0	0.0	0.0	0.0	0.0	0.0	0.0	0.0	0.0	0.0	0.0	0.0	0.0	0.0
AR		0.0	0.0	0.0	0.0	0.0	0.0	0.0	0.0	0.0	0.0	0.0	0.0	0.0	0.0	0.0	0.0	0.0	0.0
Mass Flows	kg/hr	127908	93169	127908	135619	224508	224508	360127	360127	266958	360127	360127	360127	360127	96600	96600	96600	96600	96600
Volume Flow	cum/hr	16443	94	7580	6206	27305	39179	36987	28520	23960	126381	78562	60233	24054	4964	6382	97	97	132

Table 18 Case A Aspen Energy Analyzer heat exchanger summary

Heat exchanger	Duty (MW)	Cost (USD)	Area (m2)	Shells	LMTD (°C)	Overall U (kJ/h-m2-°C)	FFactor
CL1	20	202768	798	2	24	4060	0.93
WHB	133	198109	774	2	491	1260	1.00
B4	50	957340	4011	9	66	640	0.97
HT6	6	143475	504	2	233	208	0.91
HT2	29	176326	664	2	473	391	0.86
WHB1	48	280159	1100	3	177	885	1.00
B3	72	735903	3062	7	189	517	0.99
HT5	31	387322	1554	4	433	206	0.83
B1	48	100000	6816	15	175	178	0.83

Case B ATR process pinch analysis model

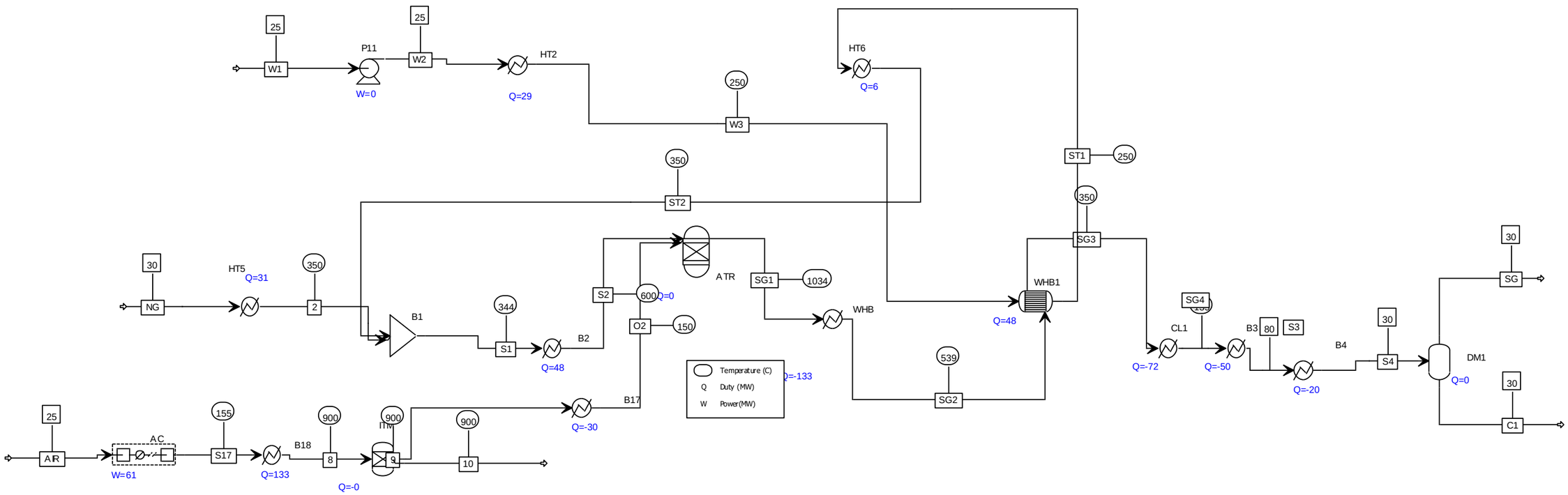

Table 19 Case B pinch analysis mass balance

	Units	2	8	9	10	AIR	C1	NG	O2	S1	S2	S3	S4	S17	SG	SG1	SG2	SG3	SG4	ST1	ST2	W1	W2	W3
From		HT5	B18	ITM	ITM		DM1		B17	B1	B2	B3	B4	AC	DM1	ATR	WHB	WHB1	CL1	WHB1	HT6		P11	HT2
To		B1	ITM	B17		AC		HT5	ATR	B2	ATR	B4	DM1	B18		WHB	WHB1	CL1	B3	HT6	B1	P11	HT2	WHB1
Phase		Vapor Phase	Vapor Phase	Vapor Phase	Vapor Phase	Vapor Phase	Liquid Phase	Vapor Phase	Vapor Phase	Vapor Phase	Vapor Phase			Vapor Phase	Vapor Phase	Vapor Phase	Vapor Phase	Vapor Phase		Vapor Phase	Vapor Phase	Liquid Phase	Liquid Phase	Liquid Phase
Temperature	C	350	900	900	900	25	30	30	150	344	600	80	30	155	30	1034	539	350	135	250	350	25	25	250
Pressure	kPa	2400	2400	2400	2400	101	2400	2400	2400	2400	2400	2400	2400	2400	2400	2400	2400	2400	2400	4000	4000	100	4000	4000
Molar Vapor Fraction		1.0	1.0	1.0	1.0	1.0	0.0	1.0	1.0	1.0	1.0	0.8	0.8	1.0	1.0	1.0	1.0	1.0	0.9	1.0	1.0	0.0	0.0	0.0
Molar Liquid Fraction		0.0	0.0	0.0	0.0	0.0	1.0	0.0	0.0	0.0	0.0	0.2	0.2	0.0	0.0	0.0	0.0	0.0	0.1	0.0	0.0	1.0	1.0	1.0
Molar Solid Fraction		0.0	0.0	0.0	0.0	0.0	0.0	0.0	0.0	0.0	0.0	0.0	0.0	0.0	0.0	0.0	0.0	0.0	0.0	0.0	0.0	0.0	0.0	0.0
Mass Vapor Fraction		1.0	1.0	1.0	1.0	1.0	0.0	1.0	1.0	1.0	1.0	0.8	0.7	1.0	1.0	1.0	1.0	1.0	0.9	1.0	1.0	0.0	0.0	0.0
Mass Liquid Fraction		0.0	0.0	0.0	0.0	0.0	1.0	0.0	0.0	0.0	0.0	0.2	0.3	0.0	0.0	0.0	0.0	0.0	0.1	0.0	0.0	1.0	1.0	1.0
Mass Solid Fraction		0.0	0.0	0.0	0.0	0.0	0.0	0.0	0.0	0.0	0.0	0.0	0.0	0.0	0.0	0.0	0.0	0.0	0.0	0.0	0.0	0.0	0.0	0.0
Molar Enthalpy	kJ/kmol	-61670	27502	28821	27151	-8	-287295	-76401	3611	-132066	-118682	-93936	-96544	3732	-52962	-54720	-71923	-78094	-87433	-236023	-231840	-287741	-287640	-268056
Mass Enthalpy	kJ/kg	-3664	950	901	964	0	-15947	-4540	113	-7625	-6852	-7258	-7459	129	-4494	-4228	-5557	-6034	-6755	-13101	-12869	-15972	-15966	-14879
Molar Entropy	J/kmol-K	-73242	20558	17897	15933	4666	-166647	-105697	-15955	-56767	-38708	-18771	-26688	-11243	5289	42735	26248	17602	-1883	-58251	-50928	-167974	-167911	-119488
Mass Entropy	J/kg-K	-4352	710	560	566	161	-9250	-6280	-499	-3277	-2235	-1450	-2062	-388	449	3302	2028	1360	-145	-3233	-2827	-9324	-9321	-6633
Molar Density	kmol/cum	0	0	0	0	0	55	1	1	0	0	1	1	1	1	0	0	0	1	1	1	55	55	41
Mass Density	kg/cum	8	7	8	7	1	989	17	22	8	6	13	15	19	11	3	5	6	10	19	15	994	994	734
Enthalpy Flow	MW	-130	154	34	120	0	-413	-161	4	-476	-427	-726	-746	21	-333	-423	-556	-604	-676	-352	-345	-429	-428	-399
Average MW		17	29	32	28	29	18	17	32	17	17	13	13	29	12	13	13	13	13	18	18	18	18	18
Mole Flows	kmol/hr	7600	20200	4244	15956	20200	5177	7600	4244	12962	12962	27833	27833	20200	22657	27833	27833	27833	27833	5362	5362	5362	5362	5362
Mole Fractions																								
O2		0.0	0.2	1.0	0.0	0.2	0.0	0.0	1.0	0.0	0.0	0.0	0.0	0.2	0.0	0.0	0.0	0.0	0.0	0.0	0.0	0.0	0.0	0.0
CH4		0.9	0.0	0.0	0.0	0.0	0.0	0.9	0.0	0.6	0.6	0.0	0.0	0.0	0.0	0.0	0.0	0.0	0.0	0.0	0.0	0.0	0.0	0.0
C2H6		0.0	0.0	0.0	0.0	0.0	0.0	0.0	0.0	0.0	0.0	0.0	0.0	0.0	0.0	0.0	0.0	0.0	0.0	0.0	0.0	0.0	0.0	0.0
N2		0.0	0.8	0.0	1.0	0.8	0.0	0.0	0.0	0.0	0.0	0.0	0.0	0.8	0.0	0.0	0.0	0.0	0.0	0.0	0.0	0.0	0.0	0.0
CO2		0.0	0.0	0.0	0.0	0.0	0.0	0.0	0.0	0.0	0.0	0.0	0.0	0.0	0.1	0.0	0.0	0.0	0.0	0.0	0.0	0.0	0.0	0.0
CO		0.0	0.0	0.0	0.0	0.0	0.0	0.0	0.0	0.0	0.0	0.2	0.2	0.0	0.3	0.2	0.2	0.2	0.2	0.0	0.0	0.0	0.0	0.0
H2		0.0	0.0	0.0	0.0	0.0	0.0	0.0	0.0	0.0	0.0	0.5	0.5	0.0	0.7	0.5	0.5	0.5	0.5	0.0	0.0	0.0	0.0	0.0
H2O		0.0	0.0	0.0	0.0	0.0	1.0	0.0	0.0	0.4	0.4	0.2	0.2	0.0	0.0	0.2	0.2	0.2	0.2	1.0	1.0	1.0	1.0	1.0
CH3OH		0.0	0.0	0.0	0.0	0.0	0.0	0.0	0.0	0.0	0.0	0.0	0.0	0.0	0.0	0.0	0.0	0.0	0.0	0.0	0.0	0.0	0.0	0.0
AR		0.0	0.0	0.0	0.0	0.0	0.0	0.0	0.0	0.0	0.0	0.0	0.0	0.0	0.0	0.0	0.0	0.0	0.0	0.0	0.0	0.0	0.0	0.0
Mass Flows	kg/hr	127908	584987	135739	449248	584987	93259	127908	135739	224508	224508	360247	360247	584987	266988	360247	360247	360247	360247	96600	96600	96600	96600	96600
Volume Flow	cum/hr	16443	82557	17325	65229	493924	94	7580	6211	27305	39179	28522	24056	30104	23961	126501	78687	60360	36989	4964	6382	97	97	132

Table 20 Case B Aspen Energy Analyzer heat exchanger summary

Heat exchanger	Duty (MW)	Cost (USD)	Area (m2)	Shells	LMTD (°C)	(kJ/h-m2-°C)	FFactor
CL1	72	737611	3071	7	190	518	0.99
WHB	133	197636	772	2	492	1261	1.00
B4	20	202756	798	2	24	4061	0.93
HT6	6	143475	504	2	233	208	0.91
HT2	29	176326	664	2	473	391	0.86
WHB1	48	278557	1092	3	178	885	1.00
B3	50	957428	4011	9	66	640	0.97
HT5	31	387322	1554	4	433	206	0.83
B2	48	5676558	6816	15	175	178	0.83
B18	133	9242176	39509	84	121	135	0.79
B17	30	303333	1135	4	379	247	0.99

Appendix C Exergy Analysis

Table 21 Molar chemical exergy of components.

Component	Phase	Molar exergy (kJ/kmol)
H_2	g	236100
O_2	g	3970
N_2	g	720
CO	g	275100
CO_2	g	19870
H_2O	g	9500
H_2O	l	900
CH_4	g	831650
C_2H_6	g	1495840
CH_3OH	g	722300
CH_3OH	l	718000